universität wien

MASTERARBEIT | MASTER'S THESIS

Titel | Title

Topological Insertion Probabilities in Two-Dimensional Self-Avoiding Ring Polymers

verfasst von | submitted by

Dominik Schramm BSc

angestrebter akademischer Grad | in partial fulfilment of the requirements for the degree of

Master of Science (MSc)

Wien | Vienna, 2024

Studienkennzahl lt. Studienblatt | Degree programme code as it appears on the student record sheet:	UA 066 876
Studienrichtung lt. Studienblatt | Degree programme as it appears on the student record sheet:	Masterstudium Physics
Betreut von | Supervisor:	Univ.-Prof. Dipl.-Ing. Dr. Christos Likos

Acknowledgements

I want to express my gratitude towards my patient supervisor Christos for always sharing his knowledge and intuitions and especially for letting me play unnecessarily long with ideas which were not initially within the scope of this thesis.

Abstract

A two dimensional, ideal ring polymer's probability distribution of being entangled with a single pole has been determined in full analyticity by A. Grosberg and H.Frisch in 2003 [GF03]. This thesis strives to complement this result with the corresponding quantities for rigid and self-avoiding rings. Both polymer types are being investigated for one as well as two poles. Primary goal of this thesis is the determination of the probability density distribution $p_2(D)$ of the distance D between two poles for both the rigid and the self-avoiding polymer. While the rigid case is treated in full analyticity, the self-avoiding ring is simulated with a Monte–Carlo technique, determining the densities numerically. Furthermore, a model is proposed to find the density $p_2(D)$ semi-analytically. The system of a planar self-avoiding ring with two topological poles is reminiscent of a ring that is a constituent of a polycatenane, where the poles represent the places where the neighboring rings poke through the 'plane' of the ring in question.

$p_2(D)$ is obtained successfully which gives rise to an average pole-distance of $\langle D \rangle \approx \langle R_g \rangle$. Furthermore, it is determined that the entropic pole-pole pair potential is attractive on all length scales. Additionally, the model reproduces the center of mass distance of two neighboring rings in a polycatenane almost exactly as well as it predicts the elastic properties of a catenane under tension on ring level, where a novel stress-softening phase has been observed.

Kurzfassung

Die Wahrscheinlichkeitsdichtefunktion eines zweidimensionalen, idealen Ring Polymers einen einzelnen Pol zu umschlingen wurde analytisch von A. Grosberg und H. Frisch im Jahr 2003 berechnet [GF03]. Diese Masterarbeit versucht die eben genannten Ergebnisse mit den entsprechenden Größen von starren, sowie flexiblen, selbstvermeidenden Ringen zu ergänzen. Letztere beiden Polymertypen werden für den Fall eines Pols sowie den Fall zweier Pole betrachtet. Das Hauptziel dieser Arbeit ist die Bestimmung der Wahrscheinlichkeitsdichte $p_2(D)$ des Abstands D zwischen den beiden Polen für den starren Ring und das flexible, selbstvermeidende Ringpolymer. Während der starre Fall analytisch behandelt wird, wird der selbstvermeidende mit einer Monte–Carlo Technik simuliert, um die Wahrscheinlichkeitsdichten numerisch zu bestimmen. Des Weiteren wird ein Modell erstellt, um die Dichte $p_2(D)$ halb-analytisch zu finden. Das System des planaren, selbstvermeidenden Rings mit zwei topologischen Polen im Inneren erinnert an einen Ring, der ein Teil eines Polycatenans ist, wobei die beiden Pole diejenigen Stellen markieren, an denen die benachbarten Ringe die Ebene des beobachteten Ringes durchstoßen.

$p_2(D)$ wird erfolgreich berechnet, mit dessen Hilfe der Mittelwert $\langle D\rangle \approx \langle R_g\rangle$ bestimmt werden kann, wobei R_g der Gyrationsradius des Rings beschreibt. Des weiteren wird herausgearbeitet, dass das entropische Paarpotential der beiden Pole anziehend auf allen Längenskalen ist. Zuletzt wird die Korrespondenz des Modells mit dreidimensionalen Polycatenanen getestet. Es stellt sich heraus, dass der mittlere Schwerpunktsabstand zwischen zwei benachbarten Ringen im Polycatenan mit dem vorliegenden Modell gut angenähert werden kann und dass außerdem Aussagen über die elastischen Eigenschaften von Polycatenanen auf Ring Ebene getroffen werden können. Hierbei wird eine neuartige Phase vorhergesagt, in welcher Polycatenane weicher werden unter Zugspannung.

Contents

List of Tables

List of Figures

1. Introduction

Topological materials are a broad class of materials which are to some extend restricted by topological interactions. Topology is the study of global properties of an object which do not change under continuous deformation. This entails, in particular, that the topological properties of the system are independent of its exact geometry. To put this abstract idea into a more tangible picture, let us consider a piece of cloth. We may deform the cloth as we like, as long as we abstain from cutting into it, or somehow molding some threads together (for instance, if it is made of a synthetic material), its form, i.e., its geometry, may change, but the number of stitches and the type of weave pattern with which it was produced, will remain unaltered. These properties of *how things are arranged* without reference to a specific shape are what we mean with topology. This contrasts other properties which are unaltered, for instance the material out of which the cloth was woven, which has no implication for topology [TAB+24, pp. 5-6].

This has curious consequences. Since we are not interested in the geometrical details, the exact form of our object, a cup with a handle and a doughnut are famously topologically the same object. Both display exactly one hole (which we may not close with our deformation) and may thus be continuously transformed into each other. It is noteworthy that the part of the cup which contains the coffee is not considered a hole, as it is not something one could look through. It is for this reason that it is topologically unimportant. Despite the topological equivalence of cups and doughnuts, it is not recommended to use them interchangeably during breakfast.

In polymer physics, topology arises often in the form of connecting ends of linear polymers such that they form circular shapes. It is counterintuitive at first that much would change when going from a melt of linear polymers to ring polymers, but in fact, some of the most fundamental properties are altered. One of them is the scaling relation, which is the connection of the polymerization number of a polymer with its average spacial extension [HLG+11]. Furthermore, even new properties emerge. Under the constraint that topology may not change, ring polymers, even ideal ones, display a special excluded volume interaction entirely due to not being allowed to form knots (which would be a change in topology and are hence forbidden). This is something the topologically simplest form of polymers, the linear polymers, can never achieve [Deu99].

Of course said excluded volume interaction drastically changes the behaviour of the rings even though it was the most primitive change of topology possible, namely merely connecting the two ends of a linear polymer.

The natural and logical question of course is ‘what else could be done with topology?’ and unsurprisingly this is exactly what is being investigated momentarily in dozens of institutions across the globe. Of high interest due to their novelty are more complex topological structures. Assembling such, one is confronted with endless possibilities.

In principle, one could change the topology of one species of macromolecule itself in a virtually infinite amount of ways, merely delimited by the molecular discretization itself. On top of that one can combine any number of topologically different or similar polymers to manipulate the properties of the total system. There have been promising ideas of using topological materials to construct devices like molecular motors, mechanophores and transmembrane ion channels [KL08] [ZDB20] [ABC$^+$20].

Lastly, for non-trivial topologies of the constituents, it is also thinkable to concatenate multiple polymers and create one super molecule with mostly unknown, possibly drastically different properties [FADLE24] [C$^+$23].

These three ways of meddling with topology open up a universe of possibilities. This is of course true in the active sense, meaning scientists may devise new materials on the grounds of actively creating novel materials, but also in an exploratory sense, referring to the vast amount of options such objects can naturally occur. It turns out that in biological systems topologically non-trivial objects do occur in the form of rings, rendering their study essential to the understanding of said systems [KRFH$^+$20] [KSD20].

In this thesis, we shall consider a special case of concatenated macro molecules: the polycatenane. More precicely a poly[n]catenane consists of n concatenated ring polymer units constituting an object strongly reminiscent of a chain. Recently, the creation of polycatenanes has been proven to be increasingly feasible, rendering them potentially more relevant and making them a contender of a material with real-world application [LRR$^+$22].

This inspired further research regarding their behaviour and this thesis is no exception. The study of such objects is drastically impaired by the sheer size of them; depending on the exact parameters, a single polycatenane can easily envelop many hundreds to several thousand degrees of freedom, that is, monomeric units. The simulation of such gargantuan objects is taxed by the computational cost they invoke. The simulation cost of the excluded volume interaction in principle goes like $\mathcal{O}(\mathcal{N}^2)$, where $\mathcal{N}$ is the total number of monomers in the system, rendering the algorithms incredibly slow. Even reducing the order of computional cost down to $\mathcal{O}(\mathcal{N}^{5/3})$ with methods like Verlet-lists, the computational effort is immense. Also, the relaxation time of a large object is substantially larger than the relaxation times of its constituents. This means the simulation is not just slow to advance in time because of the vast amount of degrees of freedom, but it would need to run disproportionately longer as the relaxation times of the super-molecules become immense.

It is for this reason that this thesis chooses to go down a different route. We would like to understand the most fundamental interaction of the system: the topological one. We say it is the most essential interaction since allowing rings to diffuse through one another would result in a system having little in common with the chain-like, interlocked arrangement of rings found in a catenane. The focus on the topological interaction allows for us to make three simplification in order to manage the vast amount of degrees of freedom.

Firstly, we only consider the tiniest unit of the whole chain, which still encapsulates the topological behaviour – a single ring with the strands of the neighboring rings poking

through. With this, we neglect the global behaviour of the chain, as two rings which are not direct neighbours may interact with each other any time in the full catenane system. Treating a single ring with strands in three dimensions would still be a highly non-trivial task, as one would need to take into account different orientations of the strands relative to one another and to the ring, as well as make sure that the ring and the strands do not disentangle. It is for these difficulties that we **secondly**, consider a two-dimensional ring. This relieves much of the computational effort, since now the neighboring rings only appear as two specks within the ring that the ring may not penetrate, which renders the tracking of the orientational degrees of freedom unnecessary and also naturally disallows these insertion points to leave the ring. Multiple 'in-and-out'-threadings of the same ring through another is consequently forbidden, as well. **Thirdly**, we choose to consider point-like insertions. This is not as drastic of a measure and relaxing it would not notably increase the computational cost. But considering real, monomeric insertions would result in the data absorbing excluded volume effects, and the mission of this thesis is to isolate the impact of topological interactions.

The first two of the simplifications seem massive at first glance but they are somewhat justifiable. Concatenated chains of rings which are not too big tend to be orthogonal to each other. If rigidity is added, this property is consolidated. This assures, that the places of insertion are actually circularly shaped when seen in the 'plane' of the ring, and that torsion effects are of minor importance. Furthermore, the gyration tensor of moderately sized rings has one eigenvalue which is an order of magnitude lower than the other two [LZWZ21b]; this points to negligible out-of-plane fluctuations and the ring being approximately planar. This makes two-dimensional rings a reasonable proxy for the $3d$ case.

Casting the system into two dimensions makes it a close relative of entanglement problems of $2d$ walkers, and in fact such work has been conducted on the ideal walk fully analytically by Grosberg and Frisch [GF03]. It seems logical to extend this work to the self-avoiding case, which is what this thesis aims to do, albeit with computational methods.

2. Polymer Models

In order to determine the insertion probabilities for a ring polymer, we need to precisely define its properties. We shall here consider three different polymer models; the ideal ring, the rigid ring and finally the self-avoiding ring. The rigid case and the ideal case both constitute extreme cases of zero and infinite temperature, respectively. Their properties should give some idea as to how the intermediate case, a self-avoiding polymer with non-vanishing excluded volume interactions, might behave.

2.1. Ideal Polymer

An ideal polymer is defined as a polymer with no excluded volume interactions which obeys the statistics of a true random walk.

For such polymers, we know the scaling of the mean value of the end-to-end distance to be equal to

$$R_{ee}^2 \sim N. \tag{2.1}$$

This is easily seen by considering the end-to-end distance for an ideal, linear polymer chain consisting of N monomers

$$\mathbf{R}_{ee} = \sum_{i=1}^{N} \mathbf{s}_i, \tag{2.2}$$

where $\mathbf{s}_i$ are the bond vectors pointing from the ith monomer to its neighbor, the $i+1$th monomer. Squaring equation (2.2) and taking the ensemble average gives

$$\langle R_{ee}^2 \rangle = \langle (\sum_{i=1}^{N} \mathbf{s}_i)^2 \rangle \tag{2.3}$$

$$= \sum_{i=j} \langle \mathbf{s}_i^2 \rangle + \sum_{i \neq j} \langle \mathbf{s}_i \cdot \mathbf{s}_j \rangle \tag{2.4}$$

$$= b^2 N + b^2 \sum_{i \neq j} \langle \cos \theta_{ij} \rangle, \tag{2.5}$$

where $\mathbf{s}_i = b\hat{\mathbf{n}}_i$ with the bond length b and the unit vector $\hat{\mathbf{n}}$. θ_{ij} is evidently the angle between the bond vectors $\mathbf{s}_i$ and $\mathbf{s}_j$. Since by definition of a true random walk the bond vectors are independent of each other, the distribution of the angles θ_{ij} is completely isotropic, and hence the average of the cosine vanishes. This leaves us with the desired relation

$$\langle R^2 \rangle = b^2 N, \tag{2.6}$$

which agrees with what was stated above in relation (2.1). This is an elementary but central result which can be found in virtually any polymer physics textbook, for instance in [KGP94, p.2].

Furthermore, the probability density distribution of end-to-end vectors is particularly conveniently a Gaussian distribution. The ideal polymer is one of the few cases where we are able to derive this quantity analytically. We shall briefly review the derivation of this property for the d-dimensional ideal walker. The most elegant and direct way to obtain this result is through the central limit theorem. In essence it states that a sum of independent, identically distributed (iid) variables is approximately distributed according to a Gaussian, provided, we sum enough instances of the iid variables. In the case of the ideal random walker, every step of fixed step size b can go in every direction with equal probability and the individual steps are completely independent from one another as the definition of the ideal walk dictates. The quantity of interest being the end-to-end vector $\mathbf{R}_{ee} = \sum_{i=0}^{N} \mathbf{s}_i$ where each component of the vector evidently constitutes a sum of iid variables hence the theorem is applicable. Thus, for $N \gg 1$, our distribution converges to a Gaussian according to

$$p(\mathbf{R}_{ee}) = \left(2\pi b^2 N/d\right)^{-d/2} \exp[-d\mathbf{R}^2/(2b^2N)], \tag{2.7}$$

with d being the number of dimensions [KGP94, p.15].

We do not expect the scaling behaviour of the polymer to change, once we keep its ends together to make it a ring. In this scenario we may simply consider a random walk of length $N/2$ which of course obeys the same, albeit properly scaled, distributions. The probability density for an ideal walker with a closed trajectory to have an end-to-end vector $\mathbf{R}_{N/2}$ after $N/2$ steps is simply

$$p_{loop}(\mathbf{R}) = \frac{\Omega_{N/2}(\mathbf{R})\Omega_{N/2}(-\mathbf{R})}{\Omega_N(0)} \tag{2.8}$$

$$= \frac{\Omega^2_{N/2}(\mathbf{R})}{\Omega_N(0)}, \tag{2.9}$$

where $\Omega_N(\mathbf{R})$ denotes the number of configurations producing an end-to-end vector $\mathbf{R}$ after N steps. Since every individual step is equally likely, $\Omega_{N/2}(\mathbf{R}) = \Omega_{N/2}(-\mathbf{R})$, which was used in the last step. The reader can convince themselves easily that there is a one to one mapping from the set of configurations with end-to-end vector $\mathbf{R}$ to the set with $-\mathbf{R}$ trivially by putting a minus sign in front of each bond vector. Evidently, $\Omega_N(0)$ counts the amount of configurations leading to a closed loop, where $\mathbf{R} = \mathbf{0}$. Subsequently we can harness the fact that our linear chain probability density

$$p_{N/2}(\mathbf{R}) \propto \Omega_{N/2}(\mathbf{R}) \tag{2.10}$$

and hence, using equation (2.7), we know that $\Omega_{N/2}(\mathbf{R})$ must be proportional to a Gaussian as well. Hence,

$$p_{loop}(\mathbf{R}) \propto p^2_{N/2}(\mathbf{R}) \propto \exp[-2d\mathbf{R}^2/(2b^2N/2)], \tag{2.11}$$

which is again a Gaussian distribution with some scaled variance. Probably the most interesting quantity of a polymer to consider is the radius of gyration R_g. It is defined according to

$$R_g^2 = \frac{1}{2N^2}\sum_{i,j}^{N}(\mathbf{r}_{ij})^2 \tag{2.12}$$

and is a measure for the size of the system in question. The vector $\mathbf{r}_{ij}$ is the vector pointing from the i-th to the j-th bead of the polymer chain. Since none of the beads interact in any way, the quantity $\mathbf{r}_i$ can be thought of as the end-to-end distance of an ideal polymer chain with $|i-j|$ monomers. This is a direct manifestation of self-similarity in an ideal polymer chain. However, we know how a polymer chain with $|i-j|$ beads behaves and consequently we are capable of computing the average value of R_g which we shall briefly demonstrate in the following. Let

$$\langle R_g^2\rangle = \frac{1}{2N^2}\left\langle\sum_{i,j}^{N}\mathbf{r}_{ij}^2\right\rangle \tag{2.13}$$

$$= \frac{1}{2N^2}\sum_{i,j}^{N}\langle\mathbf{r}_{ij}^2\rangle. \tag{2.14}$$

The summand $\langle\mathbf{r}_{ij}^2\rangle = |i-j|b^2$ according to (2.6) and hence

$$\langle R_g^2\rangle = \frac{b^2}{2N^2}\sum_{i,j}^{N}|i-j| \tag{2.15}$$

$$= \frac{b^2}{2N^2}2\sum_{i=1}^{N}\sum_{j=1}^{i}(i-j) \tag{2.16}$$

$$= \frac{b}{L^2}\sum_{i=1}^{N}\sum_{j=1}^{i}(bi-bj)\frac{L}{N}\frac{L}{N} \tag{2.17}$$

$$= \frac{b}{L^2}\sum_{x=0}^{L}\sum_{y=0}^{x}(x-y)\Delta x\Delta y \tag{2.18}$$

$$\approx \frac{b}{L^2}\int_0^L \mathrm{d}s\int_0^s \mathrm{d}t(s-t) \tag{2.19}$$

$$= \frac{bL}{6} = \frac{b^2N}{6} = \frac{\langle R_{ee}^2\rangle}{6}, \tag{2.20}$$

where the change from summation to integration is only valid for $N \gg 1$. In three dimensions we would need to be weary of topological exclusion effects. There, if we wished to conserve the topological class of our polymer, an excluded volume effect would appear due to possible knot-forming in $3d$. In two dimensions, knots cannot form and hence the scaling of the radius of gyration is the same for the ring as for the linear chain [WTH+11]. We have now determined the essential statistical quantities of the ideal random walker and shall now proceed to consider a rigid ring.

2.2. Rigid Ring

The case of the rigid polymer is trivial here. Being confined to a circular conformation, the probability distribution of its end-to-end distance vector simply constitutes a delta function

$$p(\mathbf{R}) = 1/\Omega_d \; \delta(|\mathbf{R}| - 2R_c), \tag{2.21}$$

where we denoted the radius of the circle with R_c and the d-dimensional solid angle with Ω_d. With end-to-end distance, we mean the distance between the initial point and the point after half of the length of the entire polymer. Trivially, the average value of the mean squared end-to-end distance amounts to

$$\langle \mathbf{R}^2 \rangle = 4R_c^2. \tag{2.22}$$

Again, usually the more useful quantity is radius of gyration, whose average of course amounts to

$$\langle R_g^2 \rangle = R_c^2 \tag{2.23}$$

2.3. Self-Avoiding Ring

Unfortunately in the case of a self-avoiding ring, we are not able to analytically calculate its behaviour, due to which we have to resort to computational methods. We choose a Monte-Carlo simulation with hard spheres of diameter d_s connected by a thread to their neighbours and topologically arranged in a ring. Let the maximal extension of the thread be l . This translates into a pair-potential of the monomers which can be written as

$$U(r_{ij}) = \begin{cases} \infty & \text{if } r_{ij} < d_s \\ 0 & \text{if } d_s \leq r_{ij} \leq l \\ \infty & \text{if } r_{ij} > l \end{cases}, \tag{2.24}$$

where r_{ij} is the distance between monomer i and j. This is of course just an infinite well potential. The monomers are forbidden to overlap or break the thread and otherwise feel no potential acting on them. This method, featuring infinite energies, is particularly convenient for the Monte–Carlo method, as all the Boltzmann factors either vanish or reduce to unity, diminishing computational load significantly – Instead of measuring the energy of each configuration, then assessing its probability and discarding it if necessary to assure correct sampling, we simply accept each Monte–Carlo step, provided the resulting configuration is legitimate. Also the model completely neglects the chemistry of our polymer; none of the bonds may be broken or reconnected which follows directly from the potential (2.24). So to speak, the hard spheres are a coarse grained model of a true polymer which forgot all of the atomic and/or molecular details of its monomeric units.

After having produced a sizable amount of configurations via the Monte Carlo technique, we proceed by inspecting their statistical behaviour and whether it matches with theoretical predictions. One of the most easily accessible tests to check this is to examine the statistics of the radius of gyration of the sample. We now wish to know, how the radius of gyration

of our ring polymer scales with the amount of monomers in it. To this end, let us quickly recapitulate Flory theory of a self avoiding polymer chain and derive the the scaling law of the radius of gyration.

2.3.1. Flory theory

Flory theory is one of the simplest models which still predicts key features of polymer statistics to an often satisfactory extent. Due to a fortuitous cancellation in two of the simplifications in Flory theory, it turns out to be exact in one and two dimensions [DS87]. Since this thesis is about a two dimensional ring polymer, we are fortunate to have an analytical benchmark to be comparing our results with. Even though the calculations of Flory are strictly speaking not correct, we will present them anyways, since they are –compared to the correct field theoretical considerations– easy to understand and give the reader an intuition about the system at hand.

In Flory theory it is attempted to construct a free energy F_{Flory} from an entropic and a steric free Energy contribution.

$$F_{\text{Flory}} = F_{\text{steric}} + F_{\text{entropic}} \tag{2.25}$$

These give rise to two statistical forces which counteract each other. The steric force is prone to maximize the extension of the chain to minimize volume interactions of the monomers and the entropic contribution captures the loss of possible conformations and thereby the loss of entropy if a chain is being stretched. For the steric interaction we assume a gas of free, non-correlated, homogeneously distributed monomers in a volume R^2, where R is the length scale of the extension of our ring polymer. One monomer in this gas has an interaction probability proportional to $\sim \frac{N}{R^2}$ in two dimensions and hence taking the interaction possibilities of all the monomers into account, we arrive at

$$p_{\text{steric}} \sim \frac{N^2}{R^2} \sim \frac{F_{\text{steric}}}{k_{\text{B}}T}. \tag{2.26}$$

For the entropic contribution, we simply take the energy of an entropic spring of an ideal polymer. This energy is most easily obtained using the end-to-end vector distribution of an ideal chain (2.7) and realizing that the entropy of the system is the logarithm of the latter up to a negligible constant.

$$S = k_{\text{B}} \log p(\mathbf{R}_{ee}) \tag{2.27}$$

and since

$$F_{\text{entropic}} = U - TS, \tag{2.28}$$

we obtain, using (2.7) and that $U = 0$

$$F_{\text{entropic}} = k_{\text{B}}T \frac{R^2}{b^2 N}, \tag{2.29}$$

where b is again the bond length.

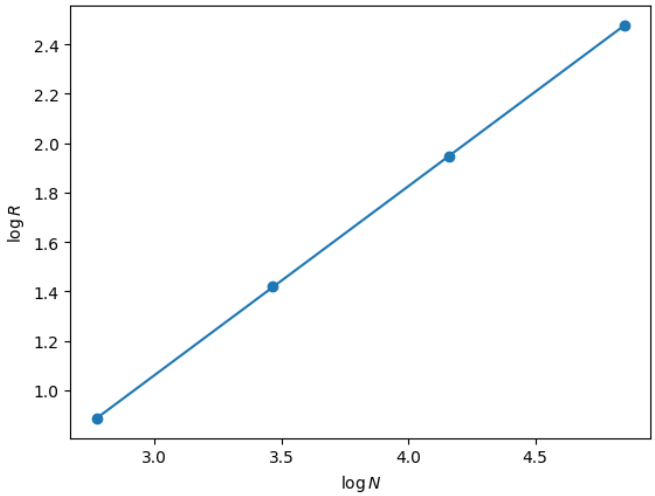

Figure 2.1.: log-log plot of the scaling law of the radius of gyration of two dimensional self avoiding ring polymers.

The complete expression of the Flory free energy is obtained combining equations (2.25) (2.29) and (2.26) to

$$F_{\text{Flory}} \sim k_{\text{B}}T \left(\frac{R^2}{b^2 N} + \frac{N^2}{R^2} \right). \tag{2.30}$$

Minimizing this energy with respect to R, we finally are left with

$$R \sim N^{\frac{3}{4}}, \tag{2.31}$$

which is the desired result.

To inquire whether our data is reasonable, we the investigate the scaling of our average radius of gyration R_g with the monomer number N. In the below plot 2.1 one can see the values obtained from decorrelated rings obtained from the Monte-Carlo simulation. The logarithm of both sides has been taken such that

$$R_g = bN^{\nu} \tag{2.32}$$

$$\log R_g = \log b + \nu \log N \tag{2.33}$$

and the scaling law reveals itself in the slope of the fitted line.

We determined the slope of our fit to be $\nu = 0.76 \pm 0.01$ which is in good agreement with the theory in two dimensions. The exponent ν is in principle dependent on the number of dimensions d but we shall omit the general derivation here.

2.3.2. Distribution of the Gyration Radius

The behaviour of the average gyration radii seems to be meeting our expectations satisfactorily. This enables us to go into more depth and investigate the behaviour of the

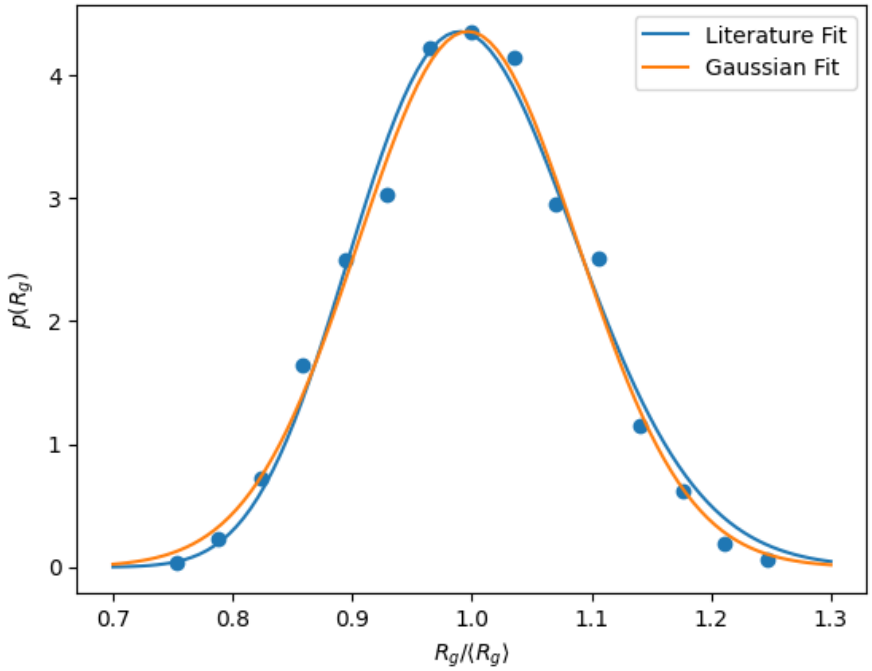

Figure 2.2.: R_g distribution and two fits. The blue line resembles the fit proposed by literature, the orange line a Gaussian. Exemplary we display the results for $N = 32$.

R_g-distribution. According to [VL90] it should follow the form

$$p(R) = C \exp\left(-A\left(\frac{R}{N^\nu}\right)^{\alpha d} - B\left(\frac{N^\nu}{R}\right)^{\delta}\right) \tag{2.34}$$

in a good solvent. Since our monomer-monomer potential $\beta U_{i,j}$ is independent of $k_\mathrm{B}T$, we expect the behaviour of an athermal solvent which is congruent with the above in the right regime. Here, d is the number of dimensions, ν is the Flory-exponent, α and δ are the quantities

$$\delta = \frac{1}{1-\nu} \tag{2.35}$$

$$\alpha = \frac{1}{\nu d - 1}. \tag{2.36}$$

Furthermore, A and B are fit parameters, and C is the normalization. Fitting the above function to our histogrammed data, we obtain what is displayed in figure 2.2. The figure includes a Gaussian fit as well as the above mentioned more sophisticated way. It is striking, how little difference there is between the two fits; for practical purposes the Gaussian fit might be a good enough approximation. The advantages lay in its

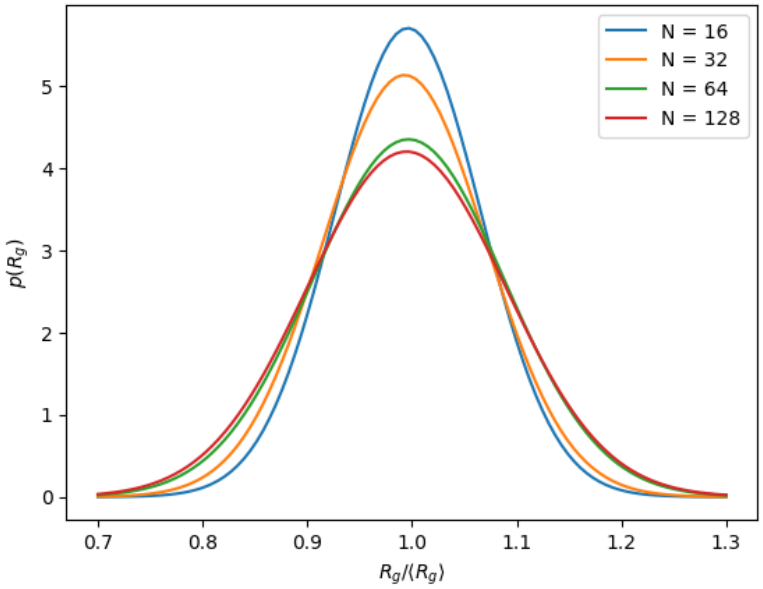

Figure 2.3.: All Gaussian fits for all polymerization numbers considered. One can see emerging universality as converging to some limiting curve around $N = 64$.

simplicity; it contains a parameter less and is comparably easy to work with analytically and computationally.

Furthermore, we want to make sure our system displays universality for large N. To be more precise, we expect that the normalized probability density functions will decreasingly change with growing N and approach some limiting shape which will never be crossed by increasing N even further. This is a reasonable assumption as the system is discretized, but apart from that, every ring should behave the same. It is easy to understand this, if we imagine we had not discretized space and were still in a continuous model. We would rid ourselves of any granularity and then every ring would look the same if we looked at it from the right distance, i.e., if we scaled the axes correctly. This of course is exactly what we do when comparing the discrete rings by regarding everything relative to their respective length-scale.

Hence, scaled correctly, highly polymerized rings of different polymerization numbers behave the same, while small-N-rings can display different dynamics because they still experience appreciable discretization effects; the length scale of the entire ring and the length scale of one monomer and its bonds are simply still too similar. As $d/R_g \to 0$, universality appears as one can see from figure 2.3; with increasing polymerization, the curves seem too approach some limit. While the differences between the distribution for $N = 16$, $N = 32$ and $N = 64$ are appreciable, the distributions of $N = 64$ and $N = 128$ are barely distinguishable anymore.

In table 2.1 we see the average values of the radius of gyration for every degree of polymerization considered.

N	16	32	64	128
$\langle R_g \rangle$	2.43 ± 0.02	4.14 ± 0.06	7.0 ± 0.1	11.9 ± 0.2

Table 2.1.: $\langle R_g \rangle$ for all polymerization numbers

2.3.3. Decorrelation

In this section we want inspect the decorrelation behaviour of our system. We intuitively understand that if only a little time has passed between two Monte-Carlo 'snapshots', the configurations must be more similar, than when the time interval between the two is greater. Fluctuations will surely have nullified any potential order for sufficiently large time intervals and conversely will not have changed the coarse shape of the polymer significantly if not much time has passed. This behaviour is not straightforward to quantify since it means somehow quantifying 'similarity' of two configurations which is not a quantity easily molded into a mathematical expression. However, if we focus on only one degree of freedom, we are capable of tracking how this degree of freedom changes over time. For instance, we might be tracking orientation and see how the polymer orients itself over time and compare it to the incident configuration. To this end, we might define a quantity which is positive, if the incident polymer and the later version are oriented similarly, vanishes, when they are orthogonal and negative if their orientations are roughly antiparallel. First, configurations will evolve away from there starting point, but of course may incidentally return to a similar orientation. This will lead to an erratically oscillating behaviour in the defined quantity if we only consider one pair of configurations. Hence, we can only reasonably asked, 'how much are they similar on average?' after a certain time. So we average the value of this quantity over all configuration pairs with the same amount of Monte-Carlo time between them and should see a decaying trend. After a certain amount of time, all information of the initial configuration is lost and all orientations are equally likely and average themselves out. In this sense, we say the system has *decorrelated*.

Of course, in reality we have only observed that the property of *orientation* has relaxed. There could be other degrees of freedom which are harder to decorrelate and that need more time to lose memory of the starting conditions. In this sense, we cannot know which degree of freedom takes the longest to relax before we have run the simulation and calculated it. Since the system at hand is not very complex, luckily there are not too many candidates. The property needs to be a macroscopical one, since the largest lengthscales typically need the most time to relax, so there are only two possibilities: the orientational degree of freedom and the translational one. We have treated both and shall present their behaviour briefly.

First, we want to consider the translational degree of freedom and postulate that when the system has moved enough through space, we can regard it as decorrelated. The relevant length scale has to be of the order of the rings radius of gyration as it is the largest length-scale present. So we track the movement of the center of mass of the ring and when it has moved a distance roughly equal to the radius of gyration, we consider

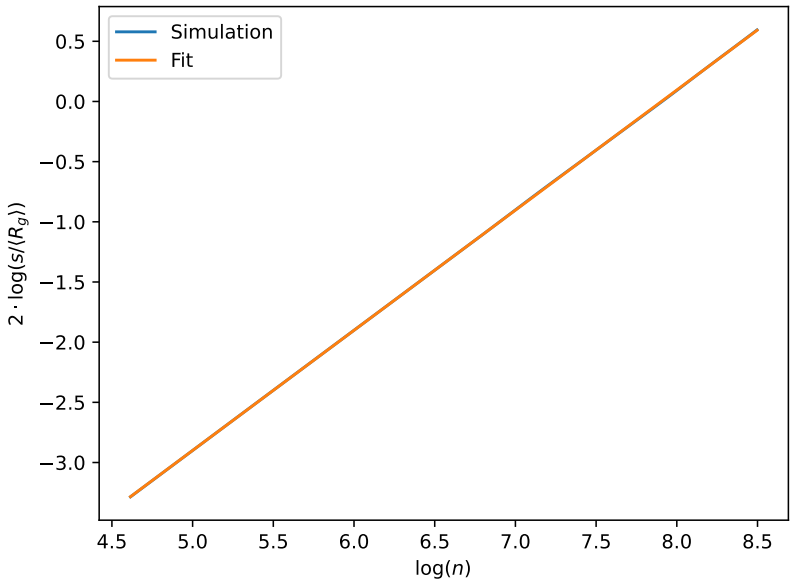

Figure 2.4.: A log-log plot of s, the distance to the origin, in terms of n, the number of center-of-mass steps. The overlapping well confirms the expected random-walk behaviour. In this example a ring with $N = 32$ was used.

it as decorrelated. Heuristically, this makes sense; when the center of mass has moved roughly a length of the order of R_g away from the origin, the new conformation has little overlap with the original one and should hence be sufficiently different on average. The movement of the center of mass is not anymore self-avoiding and pleasingly we know the statistics of a true random walk and may check the validity of our code for free. A true random walker with a randomly varying step size s will, after N steps on average have moved away from its starting point a distance

$$R = \sqrt{\langle s^2 \rangle}\sqrt{N}. \tag{2.37}$$

From this follows that

$$\log R^2 = C + \log N \tag{2.38}$$

To show that our system follows a random walk, we fit the log of the square of the distances overcome by the random walker with the linear function (2.38), as seen in figure 2.4.

Figure 2.4 makes a strong case for the expected behaviour, so we fit the data to the original function (2.37) after how many steps the walker has on average traversed a distance of the order of the radius of gyration. In figure 2.5 we see exemplarily how much distance is covered by the walker for a monomer number of $N = 32$. Around $n \approx 3000$ a distance of $\sim R_g$ has been covered on average. .

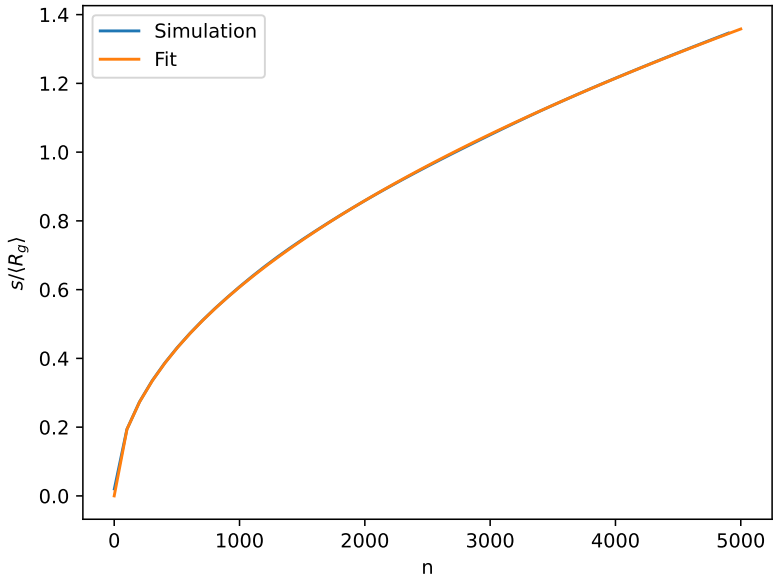

Figure 2.5.: Here, the actual distance s travelled after n center-of-mass steps is presented. We see that a distance of R_g from the origin has on average been achieved around $n \approx 3000$ for a ring of polymerization $N = 32$.

Our second method involves defining a different quantity which we relax to measure correlation. The quantity $q_{t_0,t}$ of choice is

$$q_{t_0,t} = \frac{2}{N} \sum_{i=1}^{\frac{N}{2}} \frac{\mathbf{r}_{i,t_0} \cdot \mathbf{r}_{i,t}}{\mathbf{r}_{i,t_0}^2}, \tag{2.39}$$

where $\mathbf{r}_{i,t} = \mathbf{r}_{i+\frac{N}{2}} - \mathbf{r}_i$ at time t and where $\mathbf{r}_i$ is the position vector of the i-th monomer and N the total amount of monomers in the ring. By t we mean the ongoing numeration of Monte-Carlo configurations of which we may think in terms of a time. The quantity $q_{t_0,t}$ is evidently connected to the orientation of the polymer. It is maximal when the vectors $\mathbf{r}_{i,t_0}$ and $\mathbf{r}_{i,t}$ are mostly aligned, it vanishes when they are orthogonal and it becomes negative when they point in opposite directions.

Now, we expect the quantity $q_{t_0,t}$ to erratically oscillate with time; however, its average should tend to zero. The further the configurations are apart in time, the less likely it is, they are oriented in a preferred way. With this knowledge, we define our correlation function

$$\Gamma_{t_0,t} = \langle q_{t_0,t} \rangle, \tag{2.40}$$

where $\langle . \rangle$ denotes the ensemble average. We expect the correlation function to roughly follow an exponential and shall give a slightly incorrect, yet insightful argument (many systems follow power law decorrelation at criticality. Also systems with multiple length scales, such as micells, have multiple different characteristic relaxation times [FSBK03]). Let us consider the system in equilibrium. At a specific time t_0, we take a snapshot of our ring. Now we let a time Δt pass and take another snapshot at $t_1 = t_0 + \Delta t$ and a third at $t_2 = t_1 + \Delta t$. We repeat the process many times for many different t_0 and are now able to compute our correlation function Γ_{t_0,t_1} as the average correlation between the set of configurations at t_0 and t_1. Let it evaluate to

$$\Gamma_{t_0,t_1} = 1 - \varepsilon, \text{ where } 0 \leq \varepsilon \leq 1. \tag{2.41}$$

Since we are in equilibrium, all of the configurations are equally valid and no specific point in time is preferred, the equilibrated system obeys time translational symmetry. This means that only the distance between two points in time matters, due to which we are able to write

$$\Gamma_{t_0,t_1} = \Gamma_{t_1,t_2} = \Gamma(\Delta t). \tag{2.42}$$

As a matter of a fact, our correlation function is, by construction, time translationally invariant; it is a consequence of averaging over all correlations between configuration pairs of the same distance in time. We now need to impose a second property on our system in order to make it exponentially decaying. Precisely we assume that

$$\Gamma(\Delta t)^2 = \Gamma(2\Delta t). \tag{2.43}$$

This property is not necessarily true; there are many examples of systems in which time translational invariance is given, but the system undergoes many different phases of

decorrelation and not every time step is equivalent. Property (2.43) implies recursively that

$$\Gamma(n\Delta t) = \Gamma(\Delta t)^n \tag{2.44}$$
$$= (1-\varepsilon)^n, \tag{2.45}$$

where of course we used our definition (2.41). We must not forget that ε takes different values for different choices of the discretization interval Δt. Hence, it must be a function of Δt and we assume it is analytical. Making use of the latter property, we expand it around $\Delta t = 0$

$$\varepsilon(\Delta t) \approx \varepsilon(0) + \frac{1}{\tau}\Delta t, \tag{2.46}$$

where we defined $\varepsilon'(0) \equiv 1/\tau$. The correlation function has to approach unity, when $\Delta t \to 0$. Setting $\Delta t = 0$ in equation (2.44), we see immediately, that $\varepsilon(0) = 0$. The latter simplifies our first order Taylor expansion to

$$\varepsilon(\Delta t) \approx \frac{1}{\tau}\Delta t. \tag{2.47}$$

Taking now a long, finite time step $t = n\Delta t$ and assembling equations(2.47) and (2.44) we finally obtain

$$\Gamma(t) = \left(1 - \frac{t}{n\tau}\right)^n \xrightarrow[n\to\infty]{} e^{-t/\tau}. \tag{2.48}$$

In figure 2.6 we see the data of $N = 32$ monomers fitted to an exponential and observe satisfactory, yet not exact correspondence. The actual correlation function seems to deviate systematically from the exponential fit; it decreases faster before the correlation length is reached and slower afterwards.

As the correlation length of the orientational degree of freedom is longer than the translational one checked above, the fit parameter τ in the exponential fit is in the following taken as the correlation time to ensure proper decorrelation.

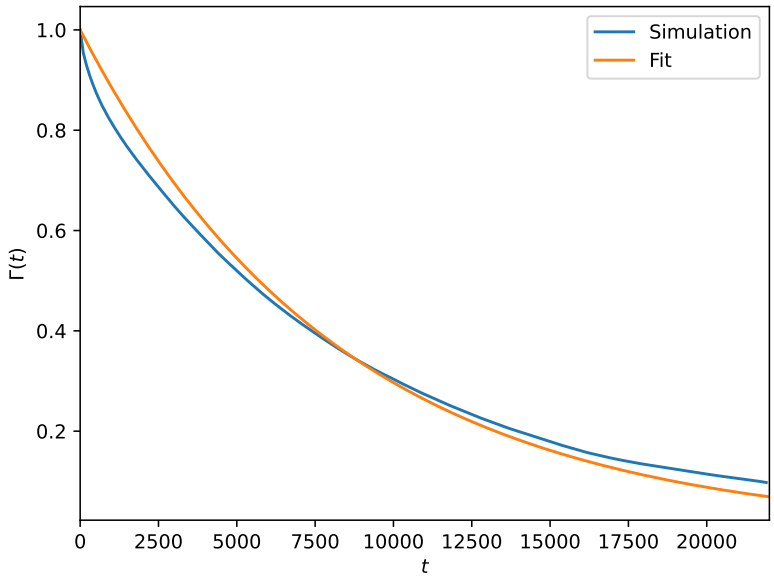

Figure 2.6.: Relaxation of the orientational degree of freedom of a ring with polymerization $N = 32$, measured by the in equation (2.40) introduced correlation function $\Gamma(t) = \langle q(t) \rangle$, where t is the number of MC configurations. The fit is an exponential as derived in equation (2.48). We consider configurations which are one correlation length τ apart to be independent. t is specific to the exact set of parameters chosen in the simulation. Here, $\tau \approx 8000$.

3. One Insertion

3.1. Bayesian Argument for one Insertion

Before we delve into simulations, we strive to understand some of the basic properties of the system at hand.

Consider an idealized two-dimensional self-avoiding polymer in a square of sidelength L. We let the polymer thermally fluctuate which leads to unsteady shape and moving center of mass-position. We shall proceed with discretizing space inside the square by subdividing it in $\mathcal{N}$ small but finite squares of volume $a^2 \coloneqq \Delta x \cdot \Delta y$ and casting the constraint of a fixed center of mass on the system as shown in figure 3.1. This constraint does not change anything about the internal dynamics of the ring since relaxing it only adds a constant term $S_0 = k_B \log \mathcal{N}$ to the entropy which can be neglected.

We are now interested in finding the probability of the pole being at position $\mathbf{r}$ relative to some reference monomer of the ring under the condition that the pole lies on the inside of the ring. According to Bayes' theorem on probabilities this can be expressed as

$$P_1(\mathbf{r}|\text{in}) = P_1(\text{in}|\mathbf{r})P(\mathbf{r})/P_1(\text{in}). \tag{3.1}$$

Throwing poles on random lattice sites inside the square while assuming a uniform probability distribution, every lattice site i, which corresponds to a vector $\mathbf{r}$ pointing to it has a probability of hosting a pole according to

$$P(\mathbf{r}) = 1/\mathcal{N}. \tag{3.2}$$

Under this assumption, the probability of the pole landing inside the polymer simply reduces to

$$P_1(\text{in}) = \frac{\langle \mathcal{A} \rangle}{A}, \tag{3.3}$$

after taking the ensemble average (denoted by the $\langle \, . \, \rangle$) of the fluctuating area $\mathcal{A}$ encircled by the polymer. A simply denotes the area of the square we embedded the polymer in. We can write by definition

$$A = \mathcal{N} \cdot \Delta x \Delta y \tag{3.4}$$

and combining eqs.(3.1) (3.2), (3.3) and (3.4) we obtain

$$P_1(\mathbf{r}|\text{in}) = \frac{P_1(\text{in}|\mathbf{r})}{\langle \mathcal{A} \rangle} \Delta x \Delta y. \tag{3.5}$$

We notice that the final expression in eq. (3.5) does not depend on the volume of the square, as it should be – the internal dynamics of the ring cannot depend on empty space it never explores.

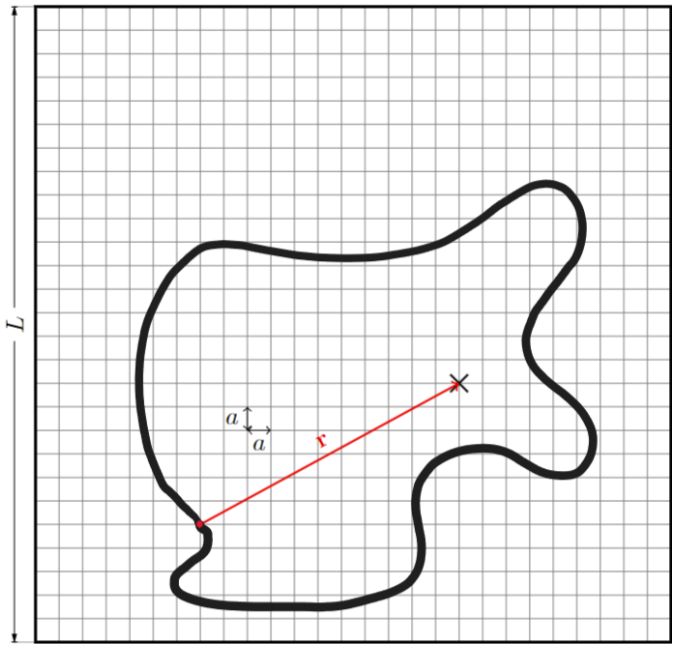

Figure 3.1.: A pole is thrown on a general, fluctuating polymer on a grid.

We can now go back to the continuous space by taking the limit to infinitesimal discretization lengths $\Delta x, \Delta y \to \mathrm{d}x, \mathrm{d}y$ which leaves us with

$$P_1(\mathbf{r}|\mathrm{in}) = \frac{P_1(\mathrm{in}|\mathbf{r})}{\langle \mathcal{A} \rangle} \mathrm{d}^2 r \tag{3.6}$$

whereby we mean with $\mathrm{d}^2 r = \mathrm{d}x\mathrm{d}y = r \cdot \mathrm{d}r\mathrm{d}\varphi$.

Equation (3.6) suggests that we can think of the quantity

$$p_1(\mathbf{r}|\mathrm{in}) = \frac{P_1(\mathrm{in}|\mathbf{r})}{\langle \mathcal{A} \rangle} \tag{3.7}$$

as the probability density that a point lies inside the polymer separated by a vector $\mathbf{r}$ from a reference point on the polymer, i.e. from an arbitrary monomer.

This is a central result since the probability $p_1(\mathbf{r}|\mathrm{in})$ is cumbersome to compute directly. With the knowledge of relation (3.7), we can resort to finding the much more readily available $P_1(\mathrm{in}|\mathbf{r})$ instead and use that it is proportional to the desired probability density.

The problem of a self-avoiding fluctuating ring-polymer seems to be an insurmountable task for analytical treatment. However, theoretical analysis of a system at hand is usually crucial to acquire an intuition for the dynamics of the like. Consequently, we shall approach the system by analyzing the two extreme cases of our problem -the zero temperature limit and the infinite temperature limit. At zero temperature, all fluctuations are being nullified and the ring freezes into a fixed position. Considering a flexible ring with infinitesimal bending energy and gradually cooling it (or equivalently, increasing

rigidity much beyond k_BT) the polymer will settle in a position of minimal bending energy. This of course is achieved by the circular arrangement of the monomers, hence in our first analysis we shall consider a rigid ring as the object to subject to insertions. The infinite temperature limit physically amounts to nullifying all repulsive, here, steric forces, provided, they are finite. Our system technically does not display finite energies. We allow ourselves to be a bit sloppy and still treat the ideal case as the infinite temperature case of our system. Put more precisely, infinite temperature levels out any energy landscape laid out by the system and replaces it with a uniform energy, the gradient of which vanishes and hence we cannot observe any forces in the system. This is equivalent to considering a true, non-self-avoiding, random walk. This will be our second preliminary analysis, before dealing with the complexity and the rich behaviour of our self-avoiding or finite-temperature system.

3.2. True Random Walk

This thesis was inspired in part by a paper of Grosberg and Frisch [GF03]. There, the behaviour of a true random walker which is subject to a topological constraint is analyzed in several different scenarios.

Amongst them is the case of an ideal ring-polymer's entanglement with a point-like obstacle. The authors strive to find the entanglement probability for such a system. The leading question of this thesis is similar in nature. However, we intended to study the properties of a *self-avoiding* ring-polymer when it wraps itself around one *or two* poles. Thus, we attempt to extend the analysis from an ideal chain to a self-avoiding one, as well as to cover the case of two insertions. However, the paper gives us a glimpse of how our system behaves in the infinite temperature limit. The ideal ring can be thought of as a closed random walker. We notice that there is a fundamental difference between a true random walk and a self avoiding one; the true random walker can encircle an obstacle multiple times, in the continuous limit even infinitely many times, as discussed later. Spitzer already derived the winding angle distribution for an open random walker in 1958 [Spi58]. Letting a random walker start from a point other than the origin, and letting it walk for a time t, it will cover some angle θ with some object at the origin after a time t. Spitzer showed that the quantity $x = \frac{2\theta(t)}{\log t}$ is asymptotically Cauchy-distributed as $t \to \infty$ and therefore reads

$$W(\theta) = \frac{1}{\pi}\frac{1}{1+x^2};\ x = \frac{2\theta(t)}{\log t}. \tag{3.8}$$

Here, we would like to remind the reader that the statistics of an ideal random walk and the ideal polymer have a one-to-one correspondence. Going from the polymer to the diffusion picture, the product at plays the role of bN and is the contour length of the walk (which bN is for the polymer). The bond length b is mapped to the diffusion constant a, as it is a measure of how fast the walker is going (the polymer is growing) with t (N). It is well known that the Cauchy distribution has diverging or undefined moments. For example the mean reads

$$\langle x \rangle = \frac{1}{\pi} \int_{-\infty}^{\infty} \frac{x'}{1+x'^2} \mathrm{d}x' \tag{3.9}$$

$$= \frac{1}{2\pi} \log |1+x^2| \Big|_{-\infty}^{\infty} \tag{3.10}$$

and is undefined. One could could intuitively object to this result and make an argument, that on symmetry grounds, the mean must evaluate to zero. And indeed, one could be tempted to formulate the integral in terms of a Cauchy principal value according to

$$\langle x \rangle = \lim_{a\to\infty} \frac{1}{\pi} \int_{-ca}^{a} \frac{x'}{1+x'^2} \mathrm{d}x' \tag{3.11}$$

$$= \lim_{a\to\infty} \frac{1}{2\pi} \log |1+x^2| \Big|_{-ca}^{a} \tag{3.12}$$

$$= \frac{1}{2\pi} \log \frac{|1+a^2|}{|1+c^2a^2|} \tag{3.13}$$

and evidently for $c = 1$ this would yield the expected $\langle x \rangle = 0$. However, we can clearly see from expression 3.11 that the integral is dependent on c which would permit the assignment of infinitely many different numbers to $\langle x \rangle$. This of course can not be the case and therefore we must resort to leaving the mean undefined. It is for this reason that we say a probability density $f(x)$ must provide that

$$\langle x^n \rangle = \int_0^{\infty} |x^n| f(x) \tag{3.14}$$

remains finite, to have a defined moment of the n-th order.

In fact, none of the higher moments converge either. At first, this seems counter intuitive, but it makes sense, since continuous walker can wrap around the point-like obstacle at infinitesimal distance and obtain a large winding number without 'using up' much of its trajectory length.

It is of course not the same as for a ring; we have a non-trivial topological difference when considering an true random walk, or a true random walk with the ends kept together, but it illustrative and shows, that true random walk-systems can host certain pathologies.

The probability of an ideal ring to be entangled n-times with a given point-like obstacle being at distance r from some reference monomer is

$$W_n(\xi) = 2e^{-\xi} \int_0^{\infty} \cos(2\pi n\mu) I_\mu(\xi) \mathrm{d}\mu, \tag{3.15}$$

where $\xi = \frac{2r^2}{b^2 N}$ and $I_\mu(\xi)$ is the modified Bessel-function. We think of b as the bond length and N as the monomer number in the ring, such that $R_{ee} = b^2 N$ is the end-to-end distance of the walker.

For a ring it is not very natural to keep one monomer at a distance r from the pole since all monomers are equivalent. Therefore it is logical to define the quantity

$$\sigma_n(N) = \int_0^\infty 2\pi r \; W_n(\xi) \; \mathrm{d}r = \frac{\pi b^2 N}{2} \int_0^\infty W_n(\xi) \; \mathrm{d}\xi \; . \tag{3.16}$$

σ_n has the dimensions of an area and can be understood in the following way. Let an ideal polymer fluctuate freely within some large area A which is much larger than the extend of the polymer so that the ring is not affected by the boundaries of the area A. Then σ_n/A is the probability that the ring-polymer makes an n-fold link with the obstacle. The integral

$$\int_0^\infty e^{-\xi} I_\mu(\xi) \mathrm{d}\xi, \tag{3.17}$$

obtained by setting $n = 0$, diverges. And not unreasonably so; we set $n = 0$ to represent the unentangled case. But σ_0 has to diverge; an unentangled polymer is free to move away arbitrarily far from the obstacle and hence making σ_0 approach the overall area A. Unless we explicitly take a volume restriction into account, the integral diverges. Hence the authors introduce an additional parameter in order to perform the integration. They write

$$\int_0^\infty e^{-\alpha\xi} I_\mu(\xi) \mathrm{d}\xi = \frac{1}{\sqrt{\alpha^2 - 1}\left(\alpha + \sqrt{\alpha^2 - 1}\right)^\mu}, \tag{3.18}$$

solving the integral. Integration with respect to μ yields the result

$$\sigma_n(t, \alpha) = \frac{\pi N b^2 \log(\alpha + \sqrt{\alpha^2 - 1})}{\sqrt{\alpha^2 - 1}\left[(2\pi n)^2 + \left(\log(\alpha + \sqrt{\alpha^2 - 1})\right)^2\right]}. \tag{3.19}$$

Now, the limit $\alpha \to 1$ can be taken without any complications and we arrive at

$$\sigma_n(N) = \frac{1}{4\pi} \frac{b^2 N}{n^2}. \tag{3.20}$$

Thus we are provided with a closed-form expression which is directly proportional to the probability of our polymer winding itself around a pole n-times.

In the paper the quantity $\langle r_n^2 \rangle$, the distance to some reference monomer in the ring, given a winding number n, is investigated. It has been obtained by realizing that taking the derivative with respect to α of expression (3.19), we essentially perform the average over r_n^2 for some winding number n. Straightforward calculation yields

$$\langle r_n^2 \rangle = \frac{b^2 N}{6} \left[1 + \frac{3}{2\pi n^2}\right]. \tag{3.21}$$

Equation (3.21) is an interesting result; firstly, of course, it diverges for $n = 0$ which reflects the fact that the ring is unentangled and is able to explore the entire extend of

the arbitrarily large area A . Secondly, it is noteworthy, that for an infinite number of windings, i.e., taking the limit $n \to \infty$ of equation (3.21), the mean squared distance does not actually vanish. This implies that the bulk amount of windings is performed only by a small section of the rings trajectory and the rest of the ring fluctuates freely. This is related to the aforementioned pathologies of infinite windings in the asymptotic Spitzer formula (3.8).

3.3. Rigid Ring

We choose an arbitrary reference point c on a circle $S^1(0, R)$ of radius R around the origin and throw poles in a random directions and at distance r such that the poles are uniformly distributed in space. The vector connecting the point c on the circle and the pole shall be called $\mathbf{r}$, accordingly.

Now, for a given vector $\mathbf{r}$, a given reference point on a circle c, and a given circle, there is no probabilistic element to be found; the pole will land simply inside or outside, depending on the configuration. This is why we need to loosen one of these constraints and let either c vary, that is, choose it randomly and uniformly, while leaving the circle and the vector constant, or we fixate c and $\mathbf{r}$ and draw the orientation of the circle around c randomly, or we simply rotate the vector while keeping the reference point and the circle still. All three approaches are equivalent and will yield the same result, here however, it is most convenient to use the latter version as it entails an intuitive geometric meaning. In chapter 4, we will explain in depth as to why all three methods are valid.

Figure 3.2 is a sketch of the above described. We strive to find the probability of the pole landing inside the circle, given a fixed circle, a fixed point c and random orientation of $\mathbf{r}$ such that the pole distribution is uniform (we particularly note that $r = |\mathbf{r}|$ is not uniformly distributed).

For a uniformly distributed set of poles, i.e., every single vector $\mathbf{r}$ being equally likely, we can simply consider a circle $S^1(c, r)$ with radius r and center at the reference point c and compare the length of the section of $S^1(c, r)$ that lays within the large circle with its total circumference. Let $\sigma(r)$ be the arc length of the inside section, then

$$P_1(\text{in}|\mathbf{r}) = \frac{\sigma(r)}{2\pi r}. \tag{3.22}$$

Since $\sigma(r)$ is a circular arc, it is proportional to the radius r and can be written as

$$\sigma(r) = \theta r, \tag{3.23}$$

where θ is the angular section of $S^1(c, r)$ which lays inside $S^1(0, R)$.

Hence, combining eqs. (3.22) and (3.23),

$$P_1(\text{in}|\mathbf{r}) = \frac{\theta}{2\pi}. \tag{3.24}$$

We hereby find that our task has now reduced to finding the angle θ.

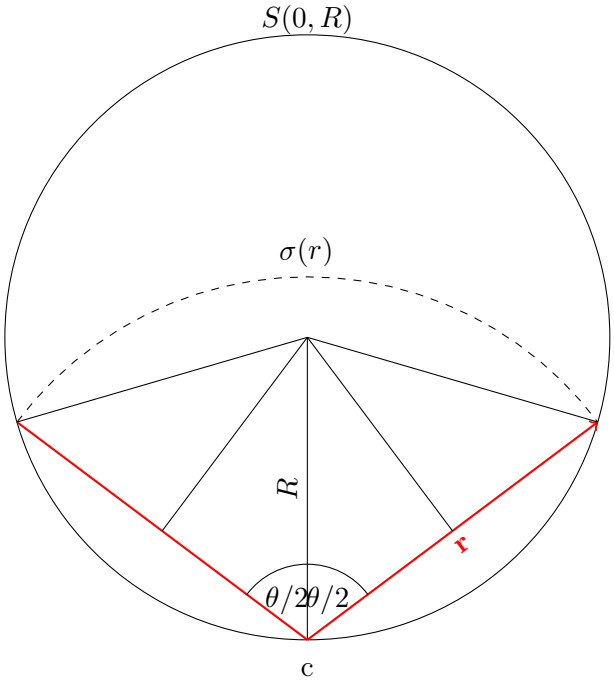

Figure 3.2.: The insertion probability of a single pole thrown a distance r from point c, can be obtained by finding the arc $\sigma(r)$ of the circle $S^1(c,r)$ which lays inside the solid line circle $S^1(0,R)$.

Just considering the anatomy of the system we immediately see that $\theta \to \pi$ in the limit of small r since for very small r the curvature of the circle effectively vanishes. This reduces the problem further to the question of which angular portion of $S^1(c,r)$ circle lays in the upper and the lower half plane when we shift c to the origin. Or equivalently, whether a pole thrown from some origin will land in the upper or lower half-plane. Since all directions are axiomatically equally probable, we see that $p_1(\text{in}|\mathbf{r}) = \frac{1}{2}$ or as stated before, $\theta = \pi$.

For $r \geq 2R$ on the other hand, we note that θ vanishes because $S^1(0,R)$ fully lies inside $S^1(c,r)$. Therefore the probabilities at the extreme cases must reduce to $p_1(r \to 0) \to \frac{1}{2}$ and $p_1(r \to 2R) \to 0$, respectively.

From figure 3.2 we see immediately that

$$\cos\frac{\theta}{2} = \frac{r}{2R}. \tag{3.25}$$

The maximal value of θ has to be π in the limit of $r \to 0$. Thus, with $\theta \in [0,\pi]$, the cosine is invertible on the chosen domain and

$$\theta = 2\arccos\frac{r}{2R}, \tag{3.26}$$

which, using equation (3.24), finally leads to

$$P_1(\text{in}|\mathbf{r}) = \frac{1}{\pi} \arccos \frac{r}{2R}. \tag{3.27}$$

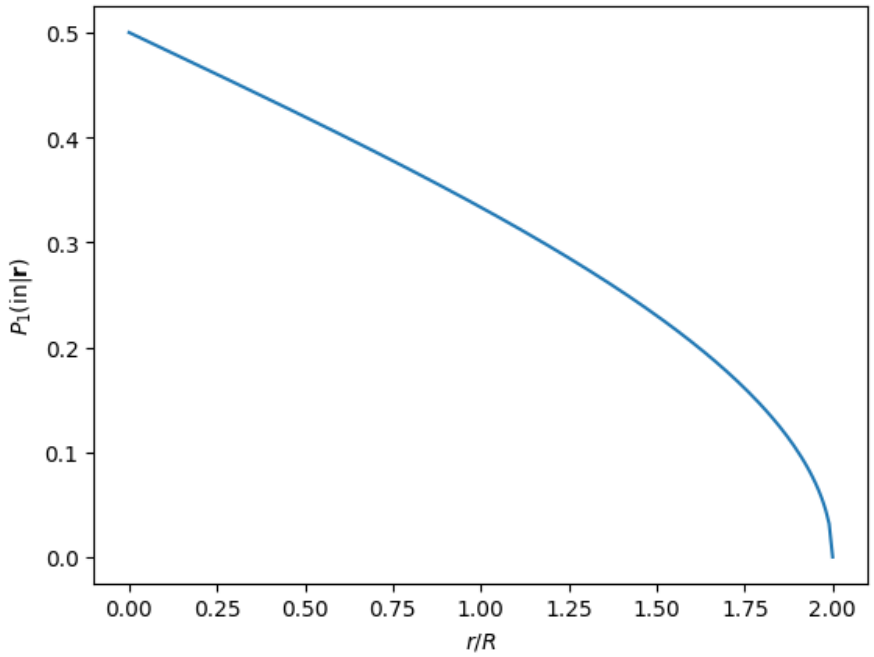

Figure 3.3.: Probability of inserting one pole at $\mathbf{r}$, averaged over the entire circle. The probability depends only on the length of the vector $r = |\mathbf{r}|$.

In figure 3.3 we see relation (3.27) graphed and that it behaves exactly as expected; for small r the argument of the arc cosine vanishes and $\arccos(0) = \frac{\pi}{2}$ implying $P_1 \to \frac{1}{2}$,whereas for $r \to 2R$ the probability vanishes since the argument of the arccosine approaches 1 and $\arccos(1) = 0$.

We almost reached our final result. Using 3.7, we can easily reverse condition and variable in our probability density and find

$$p_1(\mathbf{r}|\text{in}) = \frac{P_1(\text{in}|\mathbf{r})}{\langle \mathcal{A} \rangle} \tag{3.28}$$

$$= \frac{P_1(\text{in}|\mathbf{r})}{\pi R^2}, \tag{3.29}$$

where we used that $\langle \mathcal{A} \rangle = \pi R^2$ in the rigid case.

Finally, we are interested in finding the probability density not of the vector $\mathbf{r}$ but of the distance $r = |\mathbf{r}|$ from the reference point on the circle. This is a marginal probability, hence we transform our probability density into polar coordinates according to

$$p_1(\mathbf{r}|\text{in})\mathrm{d}x\mathrm{d}y = r p_1(\mathbf{r}|\text{in})\mathrm{d}r\mathrm{d}\phi, \tag{3.30}$$

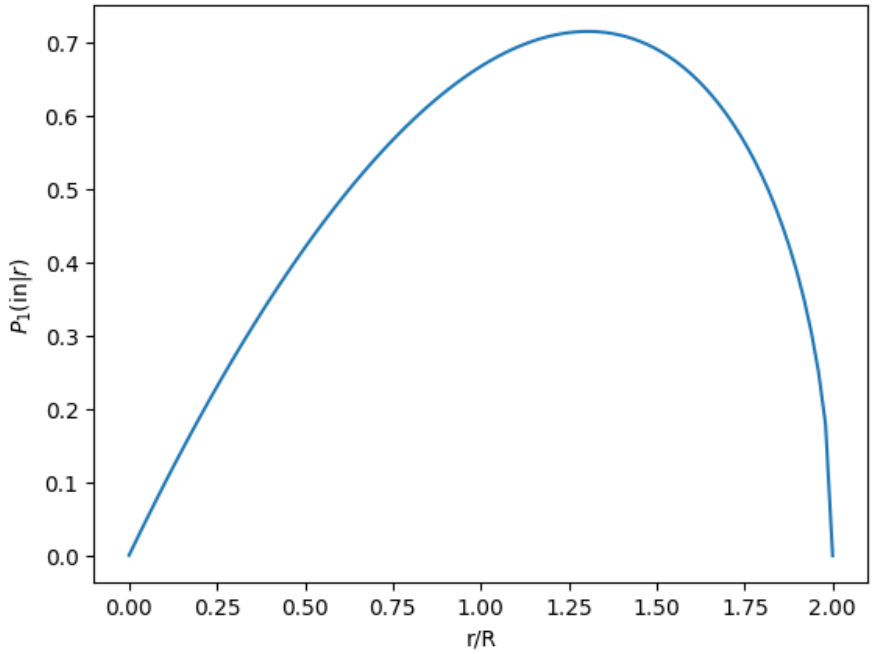

Figure 3.4.: Here we show the probability of a pole being some distance r away from its reference monomer described by equation (3.31).

and integrate out our angular variable ϕ. Since the probability does not depend on the angle, the integration is trivial and amounts to an additional factor of 2π. Corollary,

$$p_1(r = |\mathbf{r}|) = 2\pi r p_1(\mathbf{r}|\text{in}) \tag{3.31}$$

$$= \frac{2r}{\pi R^2} \arccos \frac{r}{2R}. \tag{3.32}$$

In figure 3.4, we see function (3.31) plotted. Interestingly, it is not symmetrical, the maximum is notably shifted to the right and is at $r \approx 1.3$.

This seems counter intuitive at first glance, since we have circular symmetry in the system. However, we break this symmetry as soon as we pick one point as a reference to measure r, and hence the probability density may be skewed as well, without contradiction.

3.4. Flexible Self-Avoiding Ring

Having created enough decorrelated configurations, we can now proceed with the pole insertion. We use a method in spirit of what was described in the section 3.3. First, we choose vector $\mathbf{r}$. Then we pick a reference monomer on the circle and throw the pole such, that $\mathbf{r}$ connects the monomer with the pole. Afterwards we check, whether the pole lands inside and choose the next monomer as a reference while leaving the vector fixed. When we have chosen every monomer as a reference, we move on to the next configuration to

obtain the relevant statistics. In the appendix in chapter A.1 this process is described to greater depth for the interested reader.

While unfortunately we are not capable of providing a fully analytical treatment of the self-avoiding case, we are still in the position of performing a somewhat qualitative analysis of the results. The flexible, self-avoiding ring has features of both the extreme cases. On the one hand, it is a flexible ring, implying it is capable of stretching beyond the average radius of gyration. This means, the insertion probability is non vanishing, even for distances significantly greater than $2R_g$. Of course this is a feature shared with the true random walker, but in contrast to it, the self-avoiding walker can never cross itself. This implies that it may neither wind more than one time around a pole nor separate the area enclosed by it into multiple regions, both of which are evidently a major characteristic of the true random walk. The latter two properties, however, are shared by the rigid case; the rigid case is naturally self-avoiding. Self-avoidedness will also lead to more swollen configurations; the higher the monomer-population density of one region in space, the lower the probability that another monomer will end up there. This is a somewhat unique quality of the finite temperature case; for it to make sense we require the walker to be fluctuating and at the same time having an excluded volume, where the extreme cases only feature one of these characteristics.

In figure 3.5 we see the results of the simulation. As heuristically expected, the tail is softened in comparison to the rigid case, as it does not vanish precisely at $r = 2R$ with diverging negative slope but tends to zero only around $r/\langle R_g \rangle = 3$, therefore has nontrivial contributions for an entire radius of gyration over the zero point of the rigid case.

That the probability is close to $\frac{1}{2}$ at $r = 0$, is owed to the same effect of´vanishing curvature on small length scales as explained for the rigid case; locally a (continuous) self-avoiding polymer always has the curvature of some circle, which, on even smaller length scales, vanishes. The argument only holds for continuous polymers, since the finite angles of a discrete polymer do not change below a certain length scale, therefore the graph is truncated at the very small length scales.

3.5. Comparison

To conclude this chapter, we shall now have a brief look at all the obtained probabilities of one insertion and repeat and juxtapose the results from above.

In figure 3.6 we can see, that the self-avoiding ring approaches the rigid ring probability in the low r regime. This is the expected behaviour which one can think of in a similar way as in the rigid case; even if we have a very highly curved polymer section, going to sufficiently small distances, the curvature eventually vanishes and the problem reduces again to finding a pole in the upper and the lower half-plane, as stated in chapter3.3.

On length scales below the bond length, the model is not capable of describing a continuous polymer anymore (although one would probably have to think of it the other way around; real polymers are discrete, after all) but more importantly, our insertion detection algorithm breaks down since it cannot resolve length scales below the bond

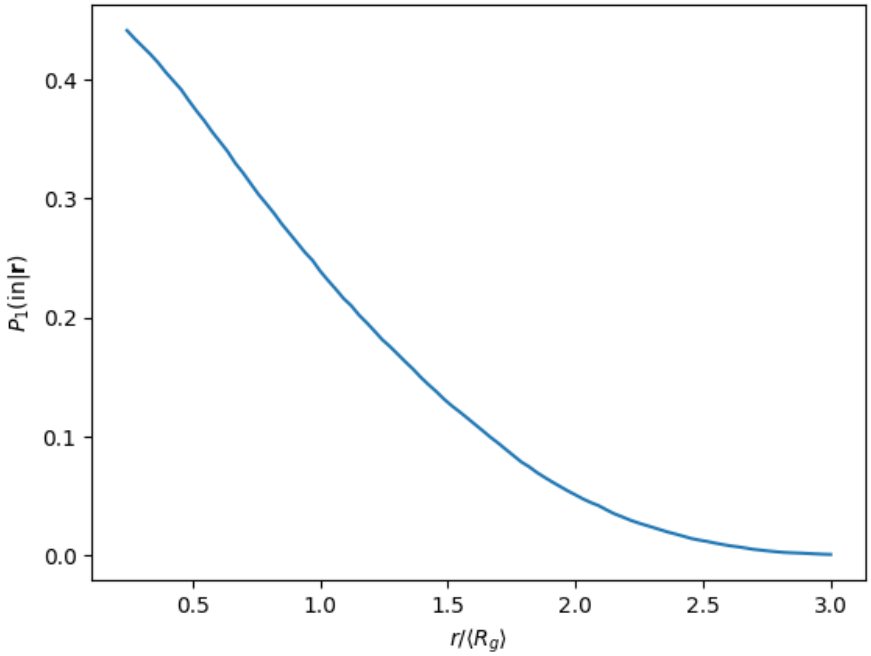

Figure 3.5.: Insertion probability of a self-avoiding ring for one pole inserted at $\mathbf{r}$, averaged over all monomers. The probability again only depends on r. Here shown for polymerization number $N = 128$.

length. Hence, the data obtained for small length-scales in the self avoiding case is not physical and omitted in the figure.

It is notable how different the ideal walker behaves from the other two in the small distance limit; the probability of finding a pole for some small vector r from a monomer on the ideal polymer is approaching unity. This can be explained by the fact that an ideal ring will be crossing itself often and most of its contour will actually lie inside its outermost portions of the contour $l_{\delta A}$ which defines the boundary of the area A encircled by it. Because this is true, for short length scales the probability of a pole landing on the inside is proportional to the ratio of the contour length l_A laying inside the area and the total contour length l_{tot}, so

$$p_1(\text{in}|0) = \frac{l_A}{l_{tot}}. \tag{3.33}$$

Of course $l_{tot} = l_A + l_{\delta A}$ must hold and combined with the fact that $l_{\delta A} \sim b\sqrt{N}$ and $l_{tot} \sim bN$, we know that for ideal walkers

$$p_1(\text{in}|0) \sim 1 - \frac{\sqrt{N}}{N} \tag{3.34}$$

and thus goes to unity for sufficiently long chains.

In the case of long distances r from the reference monomer, primarily the flexibility of the chains dictates how the insertion probability behaves. At distances $r/\langle R_g \rangle = 2$, the

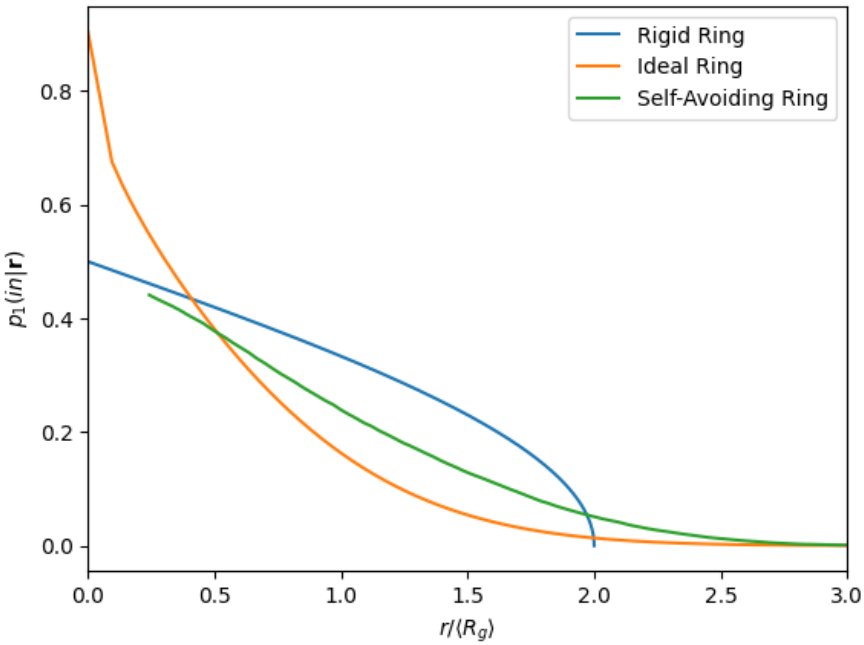

Figure 3.6.: A comparison of the one-insertion probabilities for the rigid ring (blue), the ideal ring (orange) and the self avoiding ring (green).

rigid ring probability vanishes sharply, as projected, while the other two are non-zero. This means the self-avoiding ring is now sharing properties with the ideal ring. It is notable that the insertion probability is always higher for large distances in the self-avoiding case than in the ideal case. This stems from the larger scaling exponent $\nu = \frac{3}{4}$ for the self-avoiding ring, compared to the $\nu_0 = \frac{1}{2}$ exponent for the ideal chain. Hence, the self-avoiding chain is usually more extended than the ideal chain. Of course, both probabilities eventually asymptotically decay to zero.

4. Two Insertions

4.1. Bayesian Argument for two Insertions

After understanding the system for one insertion we shall proceed to the richer case of two poles inside the ring. It is important to note that the argument given in section 3.1 is generalizable for multiple insertions. We first insert one pole at the tip of a vector $\mathbf{r}$ from an arbitrary point on the ring as done before. Subsequently, we insert a second pole associated with a vector $\mathbf{D}$ connecting the first with the second pole. The vector $\mathbf{r}$ is therefore pointing from the reference point on the circle to the first pole and vector $\mathbf{D}$ points from the first to the second pole. Also we define $r \equiv |\mathbf{r}|$ and $D \equiv |\mathbf{D}|$. The geometry of the problem is sketched in figure 4.1.

All the poles thrown are assumed to be independently and identically uniformly distributed, therefore, we can simply write

$$P_2(\mathbf{r}, \mathbf{D}|\text{in}) = P_2(\text{in}|\mathbf{r}, \mathbf{D})\ \frac{P(\mathbf{r})\ P(\mathbf{D})}{P_2(\text{in})}, \tag{4.1}$$

where the probability of two poles being inside the ring simply is

$$P_2(\text{in}) = \frac{\langle \mathcal{A} \rangle^2}{A^2} \tag{4.2}$$

and

$$P(\mathbf{r}) = P(\mathbf{D}) = \frac{\Delta x \Delta y}{A}. \tag{4.3}$$

From there, simple algebra and remembering that one $\Delta x \Delta y$ belongs to the $\mathbf{r}$ vector and the other to $\mathbf{D}$ leads us to the expression

$$P_2(\mathbf{r}, \mathbf{D}|\text{in}) = P_2(\text{in}|\mathbf{r}, \mathbf{D}) \frac{\Delta r_x \Delta r_y \Delta D_x \Delta D_y}{\langle \mathcal{A} \rangle^2}. \tag{4.4}$$

Again, this renders the quantity

$$p_2(\mathbf{r}, \mathbf{D}|\text{in}) = P_2(\text{in}|\mathbf{r}, \mathbf{D}) / \langle \mathcal{A} \rangle^2 \tag{4.5}$$

the probability density in question. It is worth stating explicitly that the probability $P_2(\text{in}|\mathbf{r}, \mathbf{D})$ was obtained averaging over all possible ring conformations while keeping the reference monomer. This restores circular symmetry in the flexible ring and hence the probability $P_2(\text{in}|\mathbf{r}, \mathbf{D})$ does not depend on the absolute angle of the vectors $\mathbf{r}$ and $\mathbf{D}$ relative to the coordinate axis, but only on the relative angle ψ between them. Hence, we may state that

$$P_2(\text{in}|\mathbf{r}, \mathbf{D}) = P_2(\text{in}|r, D, \psi). \tag{4.6}$$

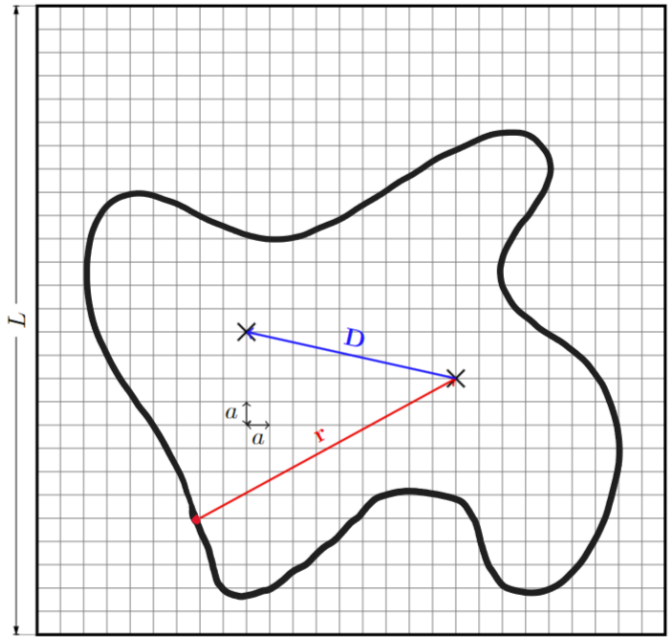

Figure 4.1.: Two poles are inserted into a fluctuating polymer on a grid.

In the following we will switch between these two notations, depending on whether we want explicitly speak of the three arguments r, D and ψ or we want to highlight that we are considering a probability of vectors rather than distances.

As done for the case of one insertion, we proceed with calculating the probability $P_2(\text{in}|\mathbf{r}, \mathbf{D})$.

4.2. Rigid Ring

After the general discussion of the flexible case, we shall focus on the derivation of the quantity $P_2(\text{in}|\mathbf{r}, \mathbf{D})$ for the rigid ring polymer. This reduces the system to what is sketched in figure 4.2.

$P_2(\text{in}|\mathbf{r}, \mathbf{D})$ resembles the probability that both poles are inside the circle, given vectors $\mathbf{r}$ and $\mathbf{D}$, and choosing the reference point on the circle randomly. From this we are able to extrapolate $p_2(\mathbf{r}, \mathbf{D}|\text{in})$ in similar fashion as in the one insertion case. This latter probability gives us information about the position of the insertions, given they are inside the ring – the two dimensional equivalent of considering one ring in a rigid polycatenane and determining its neighbours' penetration points.

In the system at hand, we have to distinguish between several cases and analyse them separately, for they might behave differently. The following sections are dedicated to single out the respective cases one after the other and derive the associated probabilities.

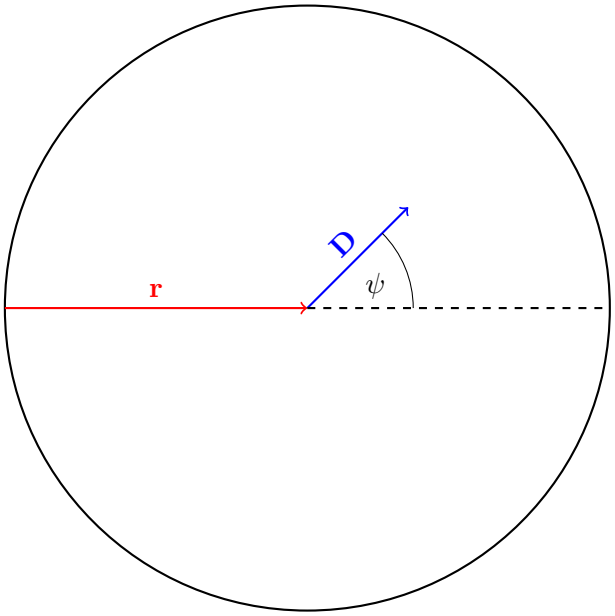

Figure 4.2.: Two insertions.

4.2.1. $r \geq D$ and $r + D \leq 2R$

We shall begin this discussion with the case $r \geq D$ as well as $r + D \leq 2R$, where R resembles the circle radius as always.

This case further splits into three distinct cases. For very small ψ the entirety of the dynamics is determined by $|\mathbf{r} + \mathbf{D}|$ and the problem reduces to the single pole problem discussed in section 3, with the corresponding probability being given by

$$P_2(\text{in}|\mathbf{r}, \mathbf{D}) = \frac{1}{\pi} \arccos \frac{|\mathbf{r} + \mathbf{D}|}{2R} \tag{4.7}$$

as shown in figure 4.3.

A quick introduction as to how to understand these figures is at order. There are three ways of conceptualizing the probabilistic element in our model. Imposing, that the length of the vectors and the size of the circle are given, whether a pole is inside or outside exclusively depends on the relative positions of the circle, the reference point on the circle as well as the direction of the vectors. This implies that we can fixate any of the three variables and let the other one vary to determine our probability. For fixated vectors $\mathbf{r}$ and $\mathbf{D}$ (fixed direction) and a fixed circle, the selection of a reference point on the circle introduces the probability. The vectors will always look in the same direction, but will be situated on different sites of the still circle.

Since our system obeys rotational symmetry, we can map this to a situation featuring a still reference point and a still circle, but a rotating vector. To see this, let us consider two cases, each with the same circle and vector as the other, but with different reference

points on the circle. We are now allowed to rotate one of the systems around their center in such a way, that the reference points on the circle coincide for both systems. However, since we rotated the entire system in one case, the vectors of the first and of the second case are no longer collinear – comparing the two cases, it looks like we have only rotated the vectors around the reference point and left the rest as is. If we do that for all possible reference points, we map these to all the possible orientations of the vectors. Thus, this corresponds to the case of a still circle and a rotating vector.

For the analysis presented here, it is most convenient to introduce a third method. From the second situation, we can equivalently rotate the circle around the reference point to counteract the rotation of the vector in a way that is reminiscent of a change of coordinate systems in classical mechanics; in one system the vector rotates around a fixated reference point, in the other the circle does.

We can now calculate the probabilities by considering those cases where either of the vector tips touches the circle, which we shall refer to a s boundary cases. This correspond to a pole being on the verge to escape the polymer, of course. If we imagine a line connecting the reference point and the center of a circle radially, and rotate the circle from one boundary case to another, that line sweeps an angle ζ which, divided by 2π, yields the desired probability. Hence the dashed lines in the figures enclose the desired angle ζ which is to be found.

If the angle ψ approaches π, $\mathbf{r}$ determines everything and we have a similar reduction to a one vector problem (see figure 4.4) with the probability given by relation (3.27). For completeness, we repeat it here

$$P_2(\text{in}|\mathbf{r},\mathbf{D}) = \frac{1}{\pi}\arccos\frac{r}{2R}. \tag{4.8}$$

The most interesting domain is therefore given by the intermediate case when neither of the extremes are in effect.

As evident from figure 4.5 the total angle ζ (and corollary the probability $P_2(\text{in}|\mathbf{r},\mathbf{D})$) which we can rotate the triangle with sides r, D, $|\mathbf{r}+\mathbf{D}|$ around the pivot on the circle such that none of its three vertices fall outside the circle is given by

$$P_2(\text{in}|\mathbf{r},\mathbf{D}) = \frac{\zeta}{2\pi} = \frac{\phi}{2\pi} + \frac{\theta}{2\pi} - \frac{\gamma}{2\pi}. \tag{4.9}$$

Since the dashed triangles are equilateral, ϕ is easily identified to be

$$\phi = \arccos\frac{r}{2R}, \tag{4.10}$$

and θ in similar fashion to be

$$\theta = \arccos\frac{|\mathbf{r}+\mathbf{D}|}{2R}. \tag{4.11}$$

To find γ we note that it is the angle between $\mathbf{r}$ and $\mathbf{r}+\mathbf{D}$ and hence

$$\gamma = \arccos\frac{\mathbf{r}\cdot(\mathbf{r}+\mathbf{D})}{|\mathbf{r}|\cdot|\mathbf{r}+\mathbf{D}|}. \tag{4.12}$$

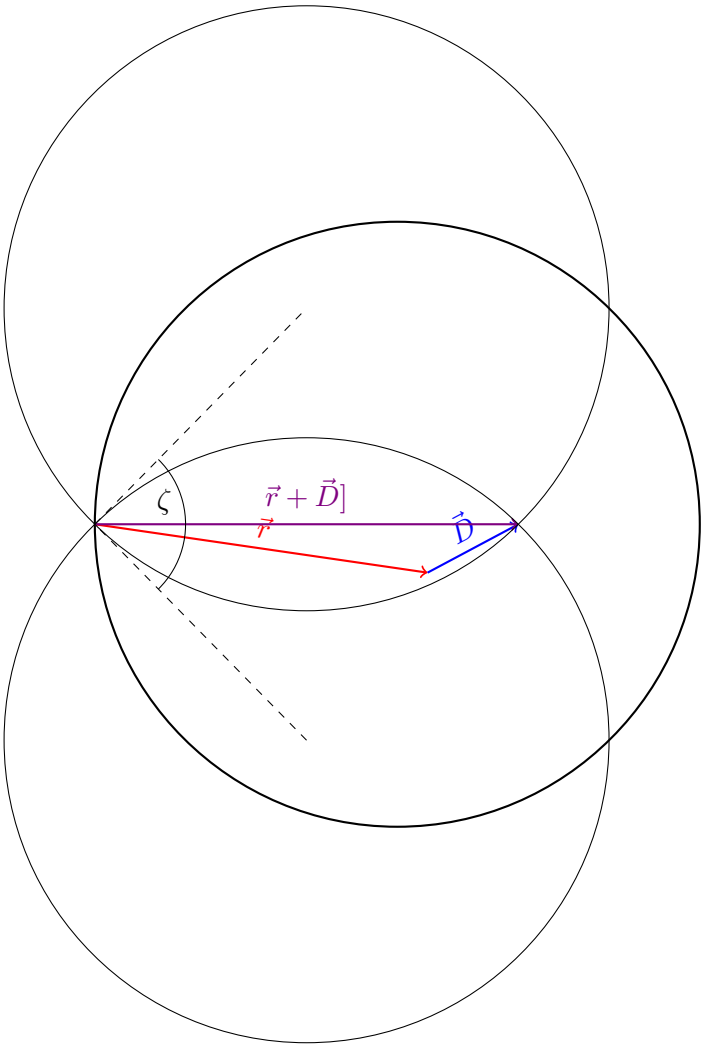

Figure 4.3.: Case A: $\psi \ll \pi/2$.

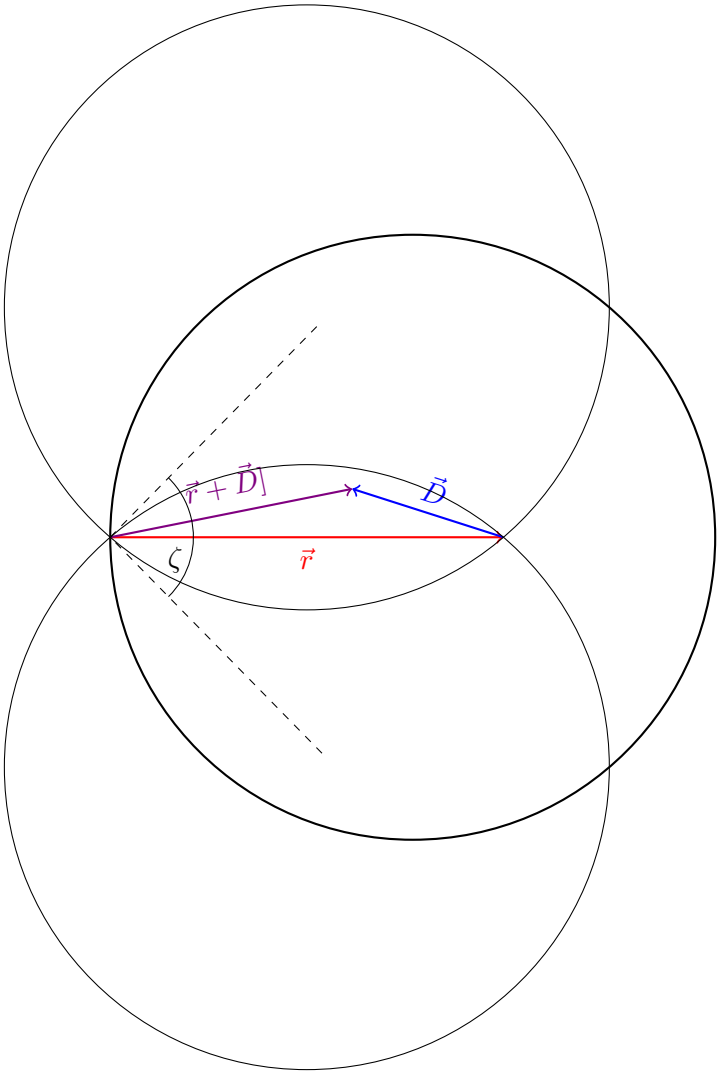

Figure 4.4.: Case B: $\psi \sim \pi$.

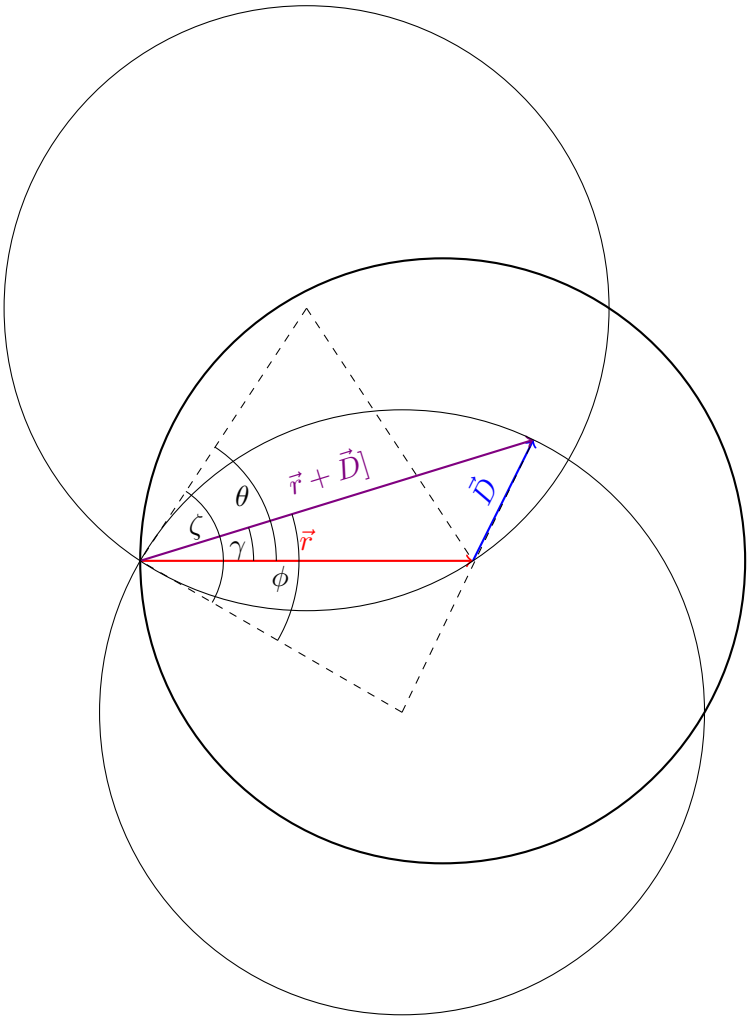

Figure 4.5.: Case C: mixed case

Putting everything together, we obtain

$$\begin{aligned} P_2(\text{in}|\mathbf{r},\mathbf{D}) =& \frac{1}{2\pi}\arccos\frac{r}{2R} + \frac{1}{2\pi}\arccos\frac{|\mathbf{r}+\mathbf{D}|}{2R} \\ & - \frac{1}{2\pi}\arccos\frac{r + D\cos\psi}{\sqrt{(r^2+D^2+2rD\cos\psi)}}. \end{aligned} \tag{4.13}$$

We have now found the desired probability. Left to determine are the boundaries of the three cases A, B and C. These cases can be differentiated between with the help of the angles $\psi_<$ and $\psi_>$ as depicted in figure 4.6.

If ψ takes the value of either of those, both poles (the one at the tip of $\mathbf{r}$ and the one at $\mathbf{r}+\mathbf{D}$) can be found *on* the circle, when we rotate the circle accordingly. At an angle smaller than $\psi_<$ everything is exclusively determined by $\mathbf{r}+\mathbf{D}$ and at an angle larger than $\psi_>$ all the dynamics only lie in $\mathbf{r}$.
The limiting angle $\psi_<$ is to be determined in terms of r and D.
Since

$$\psi_< = \pi - \xi - \phi, \tag{4.14}$$

and ξ and ϕ are given by

$$\xi = \arccos\frac{D}{2R} \qquad\qquad \phi = \arccos\frac{r}{2R}, \tag{4.15}$$

we find

$$\psi_< = \pi - \arccos\frac{D}{2R} - \arccos\frac{r}{2R}. \tag{4.16}$$

$\psi_>$ can be determined in similar fashion and amounts to

$$\psi_> = \pi - \arccos\frac{D}{2R} + \arccos\frac{r}{2R}. \tag{4.17}$$

Summarizing the above, we find that for angles $0 \le \psi \le \psi_<$ we are in region A and the expression for the probability is given by eq. (4.7).
For large angles $\psi_> \le \psi \le \pi$ we obtain eq. (3.27) being in region B.
For the mixed case to come into effect we require $\psi_< \le \psi \le \psi_>$ and obtain expression (4.13), being in region C.

4.2.2. $r \ge D$ and $r + D > 2R$

Choosing a combination of magnitudes r and D which satisfy $r \ge D$ and $r + D > 2R$, we have a similar case as in the previous chapter 4.2.1, however, now the sum of the magnitudes of the vectors $\mathbf{r}$ and $\mathbf{D}$ is greater than the largest length scale $2R$. This requires further differentiation.
Let the angle ψ_* be the angle at which $|\mathbf{r}+\mathbf{D}| = 2R$.

It can be determined by imposing the required feature on ψ and we obtain the relation:

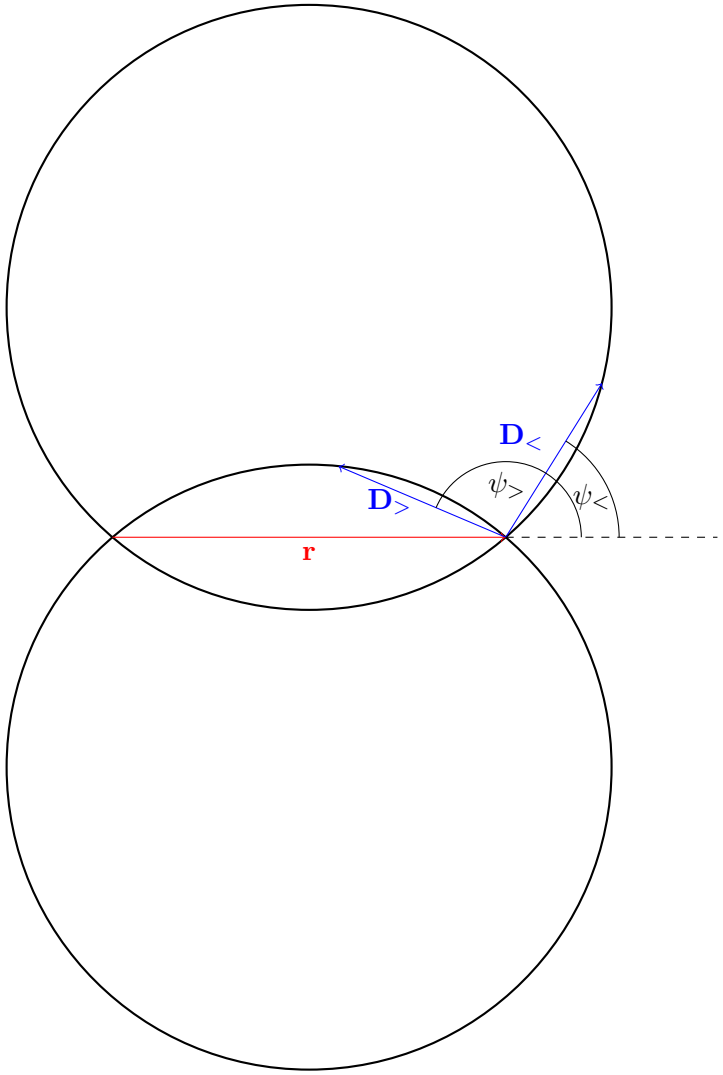

Figure 4.6.: Definition of the angles $\psi_>$ and $\psi_<$.

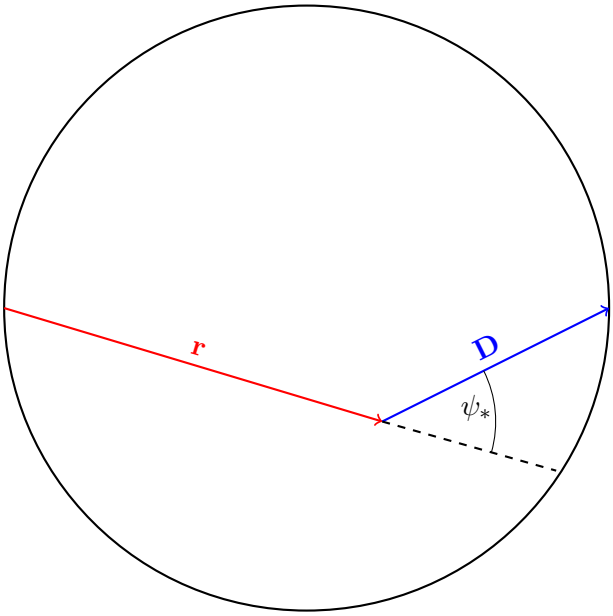

Figure 4.7.: Boundary case defining ψ_*.

$$(2R)^2 = |\mathbf{r}+\mathbf{D}|^2\Big|_{\psi=\psi_*} \tag{4.18}$$

$$= r^2 + D^2 + 2rD\cos\psi_*, \tag{4.19}$$

which leads to

$$\cos\psi_* = \frac{1-\bar{r}^2-\bar{D}^2}{2\bar{r}\bar{D}}, \tag{4.20}$$

where $\bar{r} = \frac{r}{2R}$ and similarly $\bar{D} = \frac{D}{2R}$.

Whenever $\psi = \psi_*$ we only find one legitimate configuration, namely the vector $\mathbf{r}+\mathbf{D}$ stretching over the entire circle, connecting our reference point on the circle radially with the other side of the circle, as seen in figure 4.7 .

The angle ψ_* comes into effect when $\mathbf{r}+\mathbf{D}$ touches the circle.

If $\psi_* < \frac{\pi}{2}$, we can distinguish between four cases. Since ψ_* is by definition the angle below which $|\mathbf{r}+\mathbf{D}|$ exceeds $2R$, the maximum distance inside the circle, every angle below this threshold necessarily will lead to a vanishing probability that both poles lay inside. Hence,

$$p_2(\text{in}|r, D, \psi < \psi_*) = 0. \tag{4.21}$$

If we gradually increase the angle we will eventually arrive at $\psi_<$, which is by definition the smaller of the two angles where both poles can lay on the circle. This constitutes the

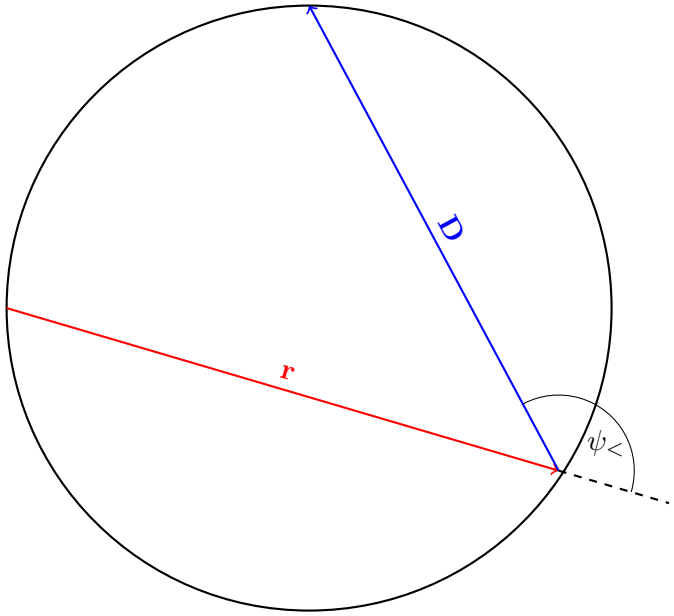

Figure 4.8.: For $\psi_* > \pi/2$ we find no valid conformation until $\psi = \psi_<$.

same situation as in the previous chapter since it simply implies that $|\mathbf{r} + \mathbf{D}|$ determines everything. Accordingly, we can use equation (4.7) in this case. Consequently, we write

$$p_2(\text{in}|r, D, \psi_* \leq \psi \leq \psi_<) = \frac{1}{\pi} \arccos \frac{|\mathbf{r} + \mathbf{D}|}{2R}. \tag{4.22}$$

Further increasing the angle, we will be in the 'mixed', 'C'-case, as depicted in figure 4.9; here, the reader can easily convince themself that

$$P_2(\text{in}|r, D, \psi_< \leq \psi \leq \psi_>) = \frac{\zeta}{2\pi} = \frac{\phi - \gamma}{2\pi}. \tag{4.23}$$

Trivially, one can obtain the angles in terms of the vector lengths and ψ again and show that the derivation from before still holds leading again to equation (4.13), so we write

$$\begin{aligned} P_2(\text{in}|r, D, \psi_< \leq \psi \leq \psi_>) = &\frac{1}{2\pi} \arccos \frac{r}{2R} + \frac{1}{2\pi} \arccos \frac{|\mathbf{r} + \mathbf{D}|}{2R} \\ &- \frac{1}{2\pi} \arccos \frac{r + D\cos\psi}{\sqrt{(r^2 + D^2 + 2rD\cos\psi)}}. \end{aligned} \tag{4.24}$$

If $\psi_* > \pi/2$ no legitimate configurations are found until $\psi = \psi_<$, where we find exactly one possible way for both poles to land inside.

Therefore the probability in this case vanishes and we may write

$$P_2(\text{in}|r, D, \psi \leq \psi_<) = 0. \tag{4.25}$$

For larger ψ we are again in the mixed realm, and the calculations from above still hold.

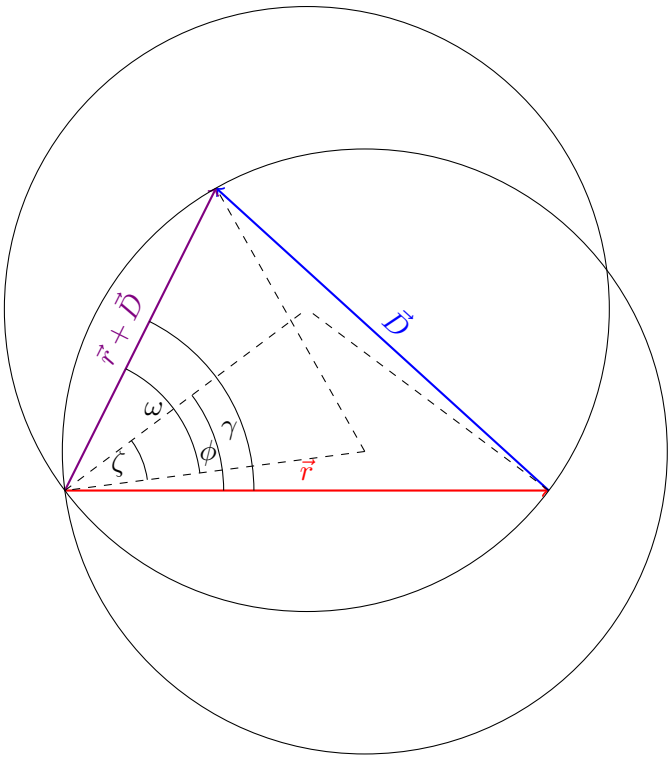

Figure 4.9.: $\psi_< < \psi < \psi_>$.

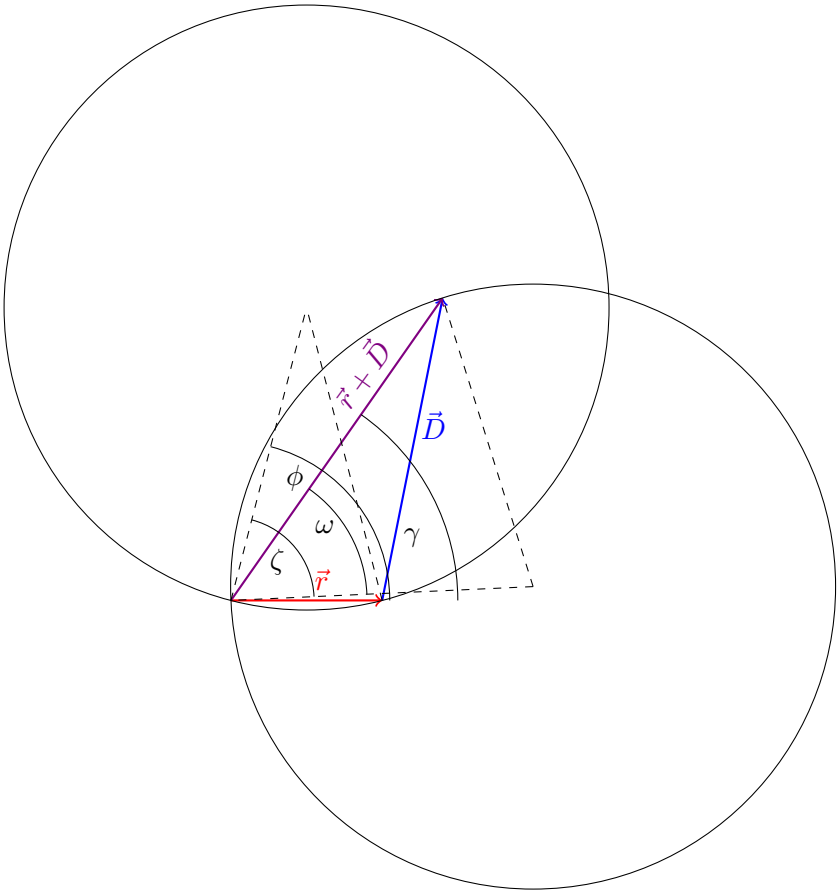

Figure 4.10.: $D > r$ and $r + D < 2R$.

And the equation (4.24) can be used to calculate the probabilities.
In the case where $\psi_> \leq \psi \leq \pi$, we simply obtain again a system where everything is governed by $\mathbf{r}$, thus we are allowed to use equation (4.8), reading

$$p_2(\text{in}|r, D, \psi_> < \psi \leq \pi) = \frac{1}{\pi} \arccos \frac{r}{2R} \tag{4.26}$$

4.2.3. $r < D$ and $D + r < 2R$

Here, for small angles, we have the same situation as in the previous cases; the probability will be solely determined by the magnitude of the sum of $\mathbf{r} + \mathbf{D}$. Hence, equation (4.7) will be in effect.

In figure 4.10 we clearly see that the amount by which the circle can be rotated around the fixation is given by angle ζ. This becomes evident if we follow the radii connected to the fixed point. This freedom of rotation is proportional of the insertion probability which we would like to find with proportionality constant of $\frac{1}{2\pi}$. According to this, the task is therefore to express ζ in terms of the quantities r, D and ψ, as done before.

We notice quickly that ζ can be written as

$$\zeta = \phi + \omega - \gamma, \tag{4.27}$$

where each of the quantities ϕ, ω and γ we can easily express as

$$\phi = \arccos \frac{r}{2R} \tag{4.28}$$

$$\omega = \arccos \frac{|\mathbf{r} + \mathbf{D}|}{2R} \tag{4.29}$$

$$\gamma = \arccos \frac{\mathbf{r} \cdot (\mathbf{r} + \mathbf{D})}{r|\mathbf{r} + \mathbf{D}|} \tag{4.30}$$

which leads to the same formula (4.13) as in previous cases.

In the third case of large angles, we can still define the quantity $\psi_>$ but it plays a different role now since the probability goes to zero at $\psi_>$ as supposed to mark a crossover to a different non-trivial regime. Thus the corresponding probability for angles $\psi \geq \psi_>$ is $P_2 = 0$.

4.2.4. $r < D$ and $r + D > 2R$

The final case we will have to consider is not much different as what is described in section 4.2.2. Again, we will have to make use of the quantity ψ_* to mark the angle at which the maximum length scale of the circle is reached, leading to a new case. As in chapter 4.2.2 we also have to be aware of the fact that the situation changes depending on the size of the angle ψ_*. If $\sqrt{r^2 + D^2} = 2R$ we find that $\psi_* = \frac{\pi}{2}$ and we have a right triangle which constitutes a boundary case. We will have to differentiate between the two regimes where the angle ψ_* is more obtuse or acute .

Let us first regard the regime $\sqrt{r^2 + D^2} \leq 2R$ which is the obtuse case. Trivially, paying attention to the fact that lowering the angle below ψ_* will increase the length of the vector $\mathbf{r} + \mathbf{D}$ to something larger than $2R$, the probability for this case vanishes. Increasing ψ past ψ_* we enter the case of $\psi_* \leq \psi \leq \psi_<$. We remember that at $\psi = \psi_<$ both poles can simultaniously be exactly on the circle. Again, this is the delimiting angle, below which the probabilities are entirely determined by $\mathbf{r} + \mathbf{D}$, hence again the relation

$$P_2(\text{in}|\mathbf{r}, \mathbf{D}) = \frac{1}{\pi} \arccos \frac{|\mathbf{r} + \mathbf{D}|}{2R} \tag{4.31}$$

must hold. Entering the regime of $\psi_< \leq \psi \leq \psi_>$ which we can see in figure 4.11

By the same methods used in previous cases we can find the relevant angle ζ by summing up auxiliary angles according to

$$\zeta = \phi + \omega - \gamma \tag{4.32}$$

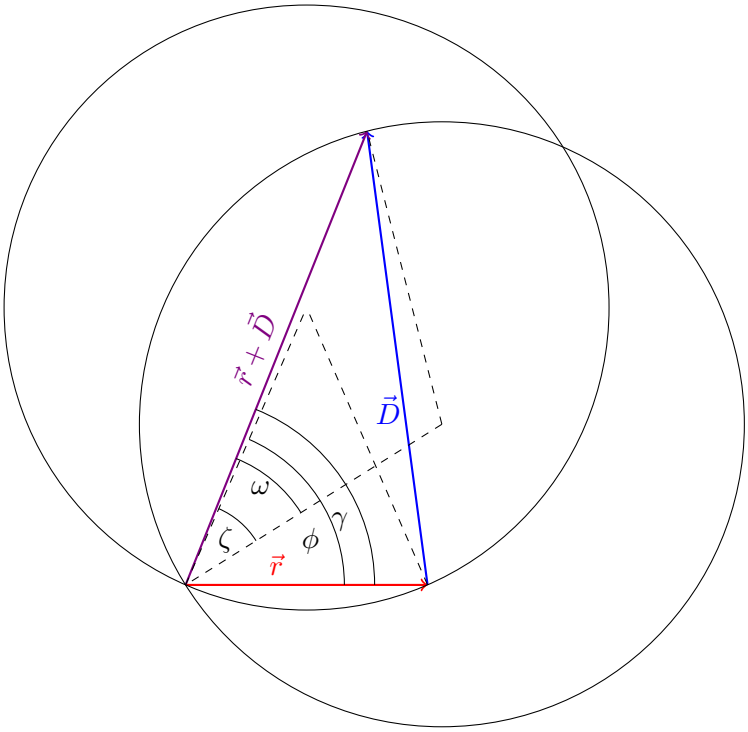

Figure 4.11.: Case $\psi_< \leq \psi \leq \psi_>$ and $\psi_* \leq \frac{\pi}{2}$.

which can be found as usual

$$\cos\phi = \frac{r}{2R} \tag{4.33}$$

$$\cos\omega = \frac{|\mathbf{r}+\mathbf{D}|}{2R} \tag{4.34}$$

$$\cos\gamma = \frac{\mathbf{r}\cdot(\mathbf{r}+\mathbf{D})}{r|\mathbf{r}+\mathbf{D}|} \tag{4.35}$$

amounting to (4.13). Since $D > r$, we must have an angle above which the probability vanishes, since, in the extreme having $\mathbf{r}$ and $\mathbf{D}$ being antiparallel, the pole at the tip of $\mathbf{D}$ will always land outside the circle. This boundary angle is $\psi_>$ and hence $P_2(\text{in}|\mathbf{r},\mathbf{D},\psi_> \leq \psi) = 0$. Our last case comes into effect when $\psi_* \geq \frac{\pi}{2}$. Here, everything with an angle below ψ_* must vanish by construction. Every case with an angle above $\psi_>$ must be affiliated with a vanishing probability as well for the same reasons as stated above. This leaves only the case $\psi_< \leq \psi \leq \psi_>$ as a contributing case.

Here, the derivation of the probability is analogous as in the previous non-trivial case, which can be easily verified by studying figure 4.12 and we obtain again relation (4.13).

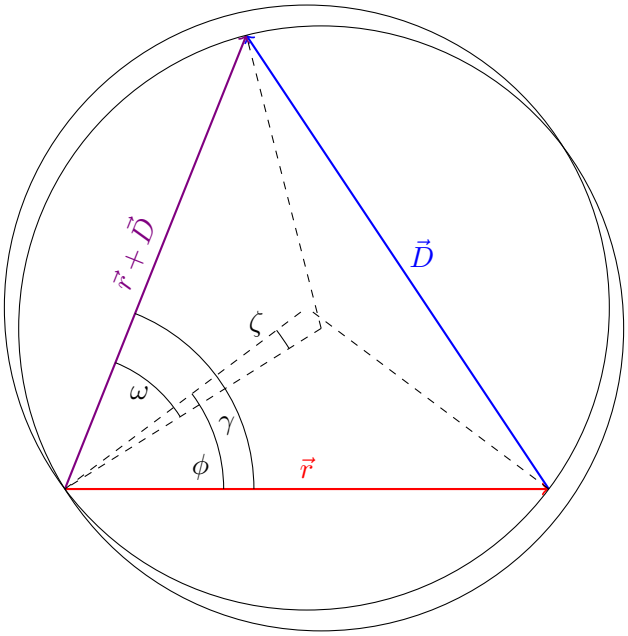

Figure 4.12.: Case $\psi_< \leq \psi \leq \psi_>$ and $\psi_* > \frac{\pi}{2}$.

4.2.5. Summary

We would like to conclude this chapter with a summary of all the above treated cases. First, we have to differentiate between $r + D < 2R$ and $r + D > 2R$. If $r + D > 2R$ we need an additional quantity

$$\psi_* = \arccos\left\{\frac{1 - \bar{r}^2 - \bar{D}^2}{2\bar{r}\bar{D}}\right\}, \tag{4.36}$$

where $\bar{r} = \frac{r}{2R}$ and $\bar{D} = \frac{D}{2R}$. Further, we need to determine the auxiliary angles $\psi_<$ and $\psi_>$. Whilst the former always amounts to

$$\psi_< = \pi - \arccos\bar{r} - \arccos\bar{D} \tag{4.37}$$

the latter is calculated with

$$\psi_> = \pi + \arccos\bar{a} - \arccos\bar{b}, \tag{4.38}$$

where $\bar{a}, \bar{b} \in \{\bar{r}, \bar{D}\}$, and $\bar{a} \geq \bar{b}$. Thus, always the arccosine of the greater value of $\bar{r}$ and $\bar{D}$ gets a plus sign, and the other a minus sign. The probability densities always assume one of four shapes. Either, trivially

$$P_2(\text{in}|r, D, \psi) = 0 \tag{4.39}$$

or

$$P_2(\text{in}|r, D, \psi) = \frac{1}{\pi}\arccos\frac{r}{2R} \tag{4.40}$$

Table 4.1.: Overview over domains, when $r + D > 2R$.

$r + D \geq 2R$			
ψ		$r > D$	$r < D$
$\psi_* \leq \pi/2$	$0 \leq \psi \leq \psi_*$	0	0
	$\psi_* \leq \psi \leq \psi_<$	(4.41)	(4.41)
	$\psi_< \leq \psi \leq \psi_>$	(4.42)	(4.42)
	$\psi_> \leq \psi \leq \pi$	(4.40)	0
$\psi_* \geq \pi/2$	$\psi \leq \psi_<$	0	0
	$\psi_< \leq \psi < \psi_>$	(4.42)	(4.42)
	$\psi_> \leq \psi \leq \pi$	(4.40)	0

or

$$P_2(\text{in}|r, D, \psi) = \frac{1}{\pi} \arccos \frac{|\mathbf{r} + \mathbf{D}|}{2R} \tag{4.41}$$

or

$$P_2(\text{in}|r, D, \psi) = \frac{1}{2\pi} \arccos \frac{r}{2R} + \frac{1}{2\pi} \arccos \frac{|\mathbf{r} + \mathbf{D}|}{2R} - \frac{1}{2\pi} \arccos \frac{\mathbf{r} \cdot (\mathbf{r} + \mathbf{D})}{r|\mathbf{r} + \mathbf{D}|}. \tag{4.42}$$

In tables 4.1 and 4.2 we give an overview in which domain, which of the formulae is used.

Table 4.2.: Overview over domains when $r + D < 2R$.

$r + D < 2R$		
ψ	$r > D$	$r < D$
$0 \leq \psi \leq \psi_<$	(4.41)	(4.41)
$\psi_< \leq \psi \leq \psi_>$	(4.42)	(4.42)
$\psi_> \leq \psi \leq \pi$	(4.40)	0

4.2.6. Results Rigid Case, two Insertions

The total functionality of the two-pole insertion function is very rich, in figures 4.13, 4.14 and 4.15 we see some cross sections of the emerging three dimensional function, fixing one of the parameters in every case.

We are now equipped to find the probability density

$$p_2(D) = \frac{2D}{(\pi R^2)^2} \int_0^\infty \mathrm{d}r\, r \int_0^\pi P_2(\text{in}|r, D, \psi)\mathrm{d}\psi. \tag{4.43}$$

Here, to somewhat ease notation, we dropped the explicit mention of the poles being inside the ring in quantity $p_2(D)$. Everything in equation (4.43) is known analytically, only the integration itself we carry out numerically and obtain what is seen in figure 4.16. The curve displays a maximum around $D/R \approx 0.82$ and vanishes at both $D/R = 0$ as well as $D/R = 2R$, which we expected for geometric reasons.

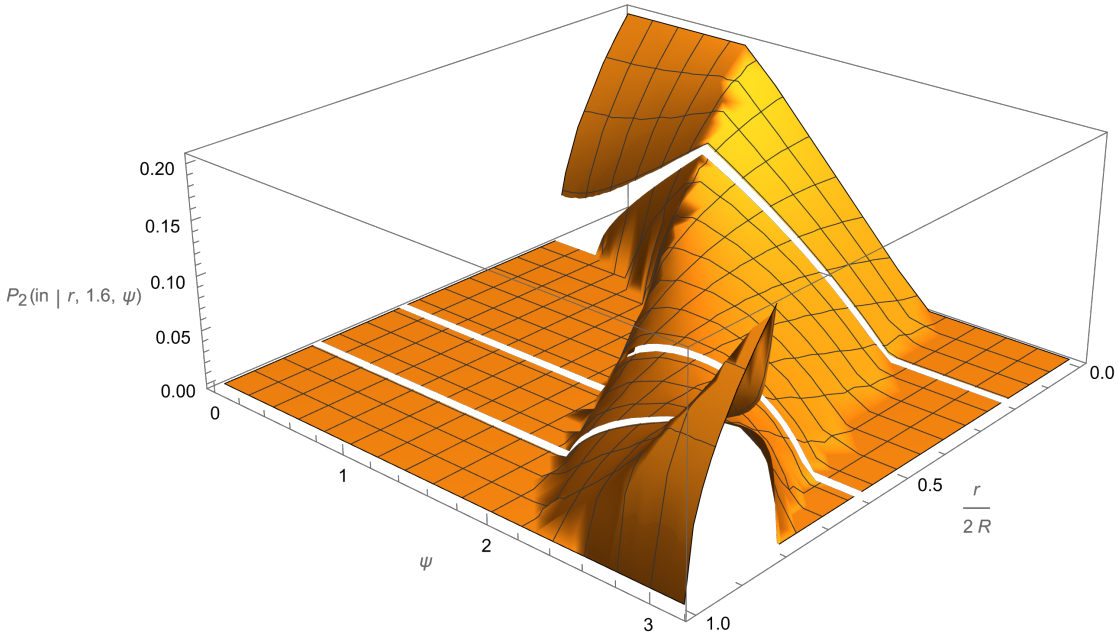

Figure 4.13.: $p_2(\text{in}|r, D, \psi)$ for $D = 1.6R$.

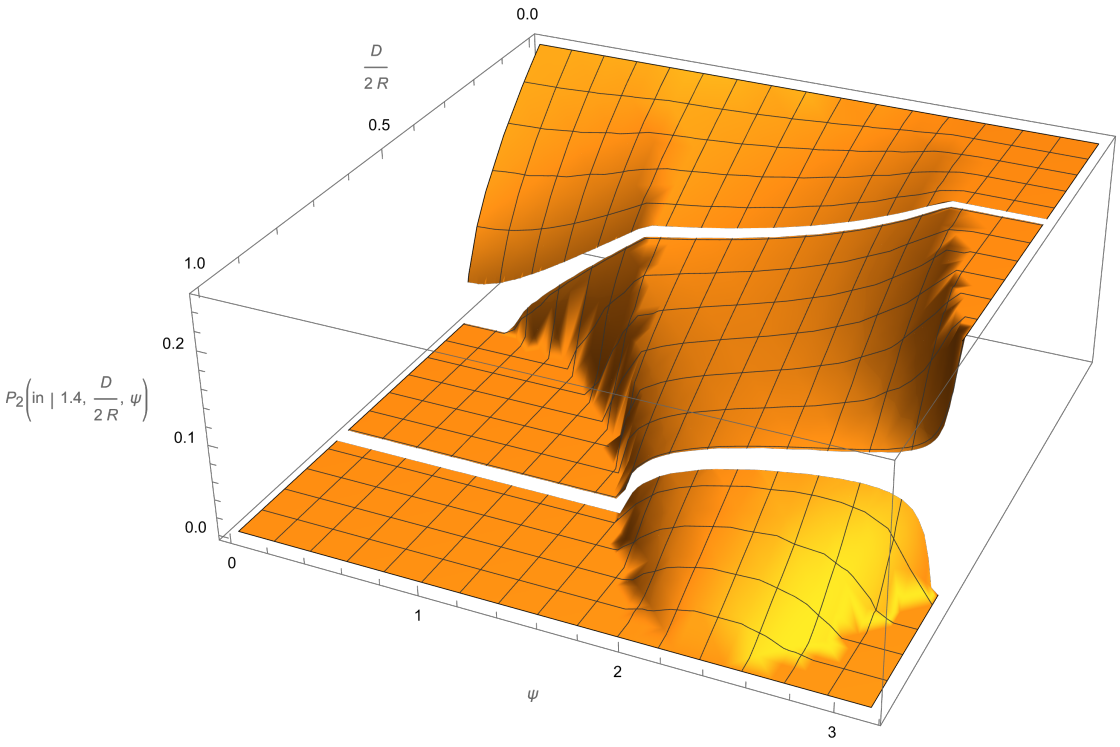

Figure 4.14.: $p_2(\text{in}|r, D, \psi)$ for $r = 1.4R$.

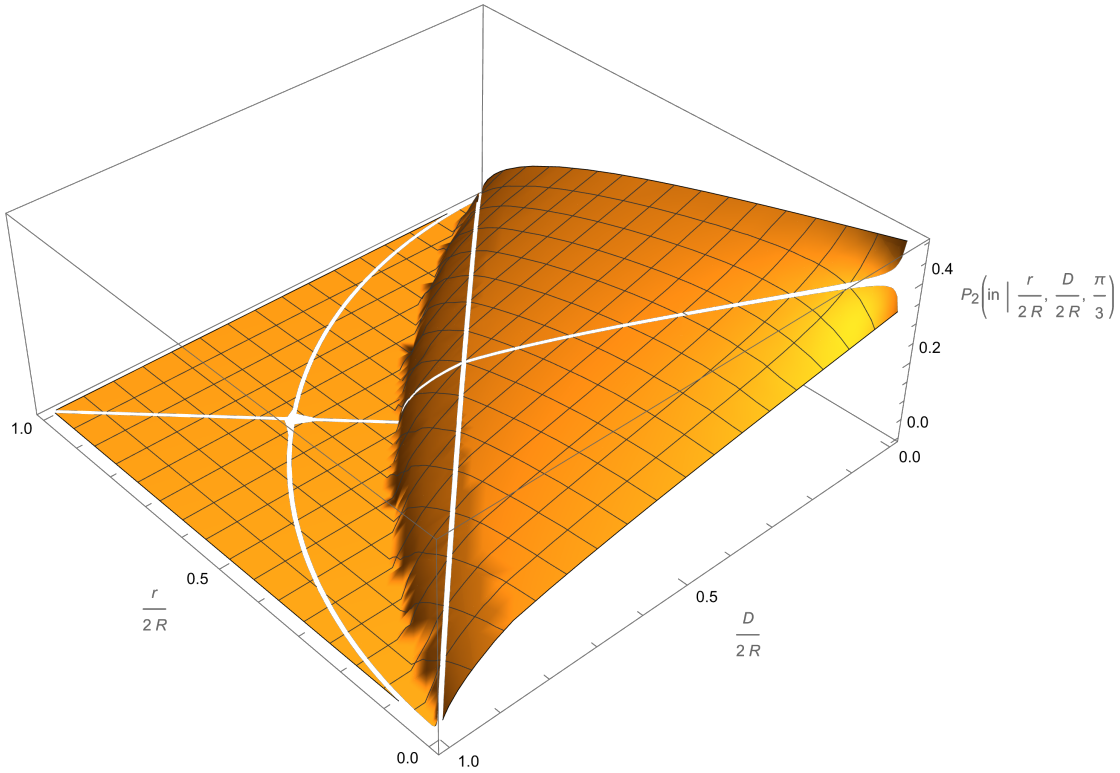

Figure 4.15.: $p_2(\text{in}|r, D, \psi)$ for $\psi = \frac{\pi}{3}$.

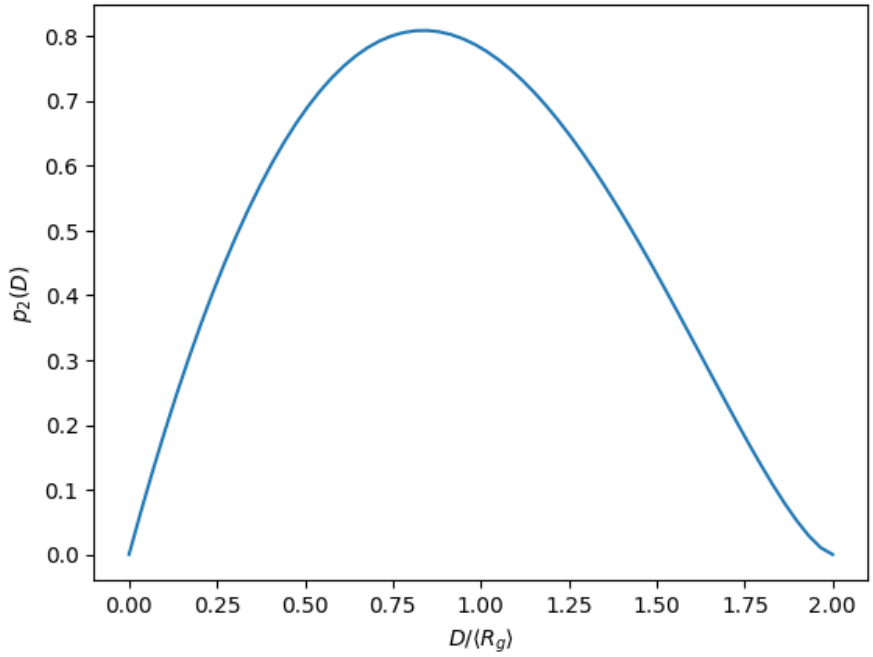

Figure 4.16.: The probability density $p_2(D)$ of the distance between the two poles.

A different quantity which is not of grave relevance for this thesis but nicely bridges the gap between the Monte–Carlo approach and molecular dynamics is $p_2(\mathbf{D})$. Mathematically, we can relate it to the previous result via

$$p_2(\mathbf{D}) \propto \frac{p_2(D)}{D}. \tag{4.44}$$

It describes not the true spacial distribution of pole distances but rather is related to the effective entropic interaction between the two poles. So, if we were to reproduce the work done here using molecular dynamics, this would be the probability density giving rise to the insertion pair potential. In figure 4.17, we see we see its graph. Interestingly, it is monotonically decreasing, which means the insertion pair potential is attractive at all times.

4.3. Self-Avoiding Ring

4.3.1. Methodology

After having thoroughly discussed the rigid case as well as the ideal case, we shall have a look at the more complex flexible, self-avoiding case. Unfortunately, we do not come far with exact, analytical methods here, due to which we resort to computational techniques. To this end we will also have to discretize the before smooth circle. We do that by constructing a ring out of some fixed number of monomers and connect them via ‘threads’.

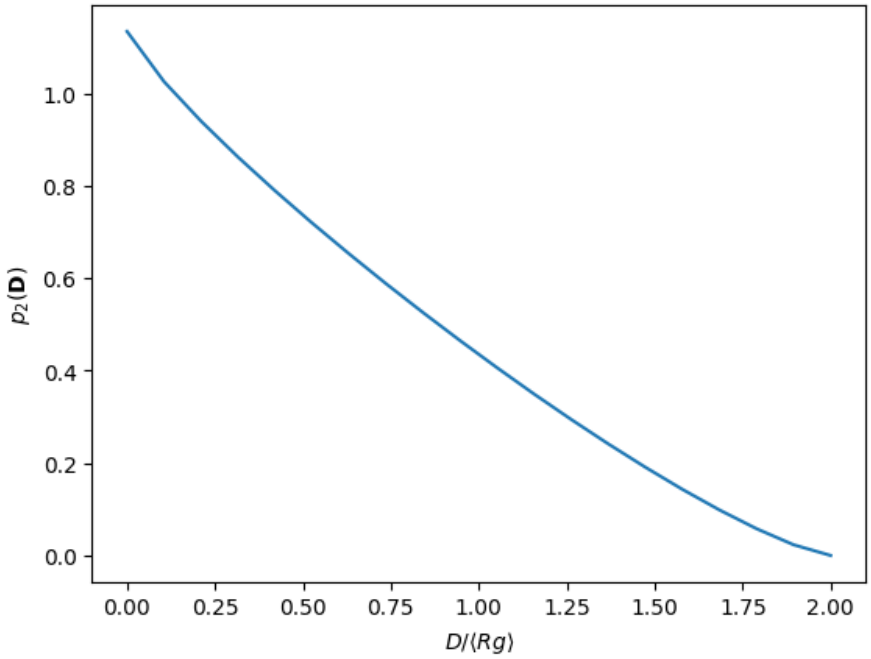

Figure 4.17.: Probability density $p_2(\mathbf{D})$ of the vector $\mathbf{D}$ connecting the two insertions.

The rules we impose on the system are simple; we allow neither the overlapping of two or more monomers (self-avoidance) nor that two neighboring monomers are too far (i.e. more than the maximal thread length) apart such that the thread would break. The thread of course represents some close ranged binding force whose details and dynamics are neglected in this thesis as we are only interested in the topological behaviour of our ring and its statistics rather than its dynamics. The chemistry we completely disregard, meaning in particular the breaking and recombination of bonds. All of our analyses are conducted while the topology of the system remains unaltered.

The approach we chose can be roughly divided into two stages: configuration creation and throwing poles.

In this thesis we chose to use a Monte-Carlo-type simulation to create the configurations without the insertions (i.e. just the 'bare' rings). In the rigid case we could trivially skip this step since by definition of a rigid circle, only one configuration was allowed, therefore the entire configuration-space was already covered by just the circle and hence regarding how the insertions behave in a circle gave us the complete statistics. In contrast to the rigid case, we are dealing with an infinite amount of possible configurations here, and we have to probe the associated configurational space such, that the set we obtain is as representative as it can be for the entire space. This is crucially important since otherwise we would introduce a bias to our data. In particular, we need to make sure that the configurations we choose are not correlated.

After having created enough configurations of the ring polymer, we advance by throwing

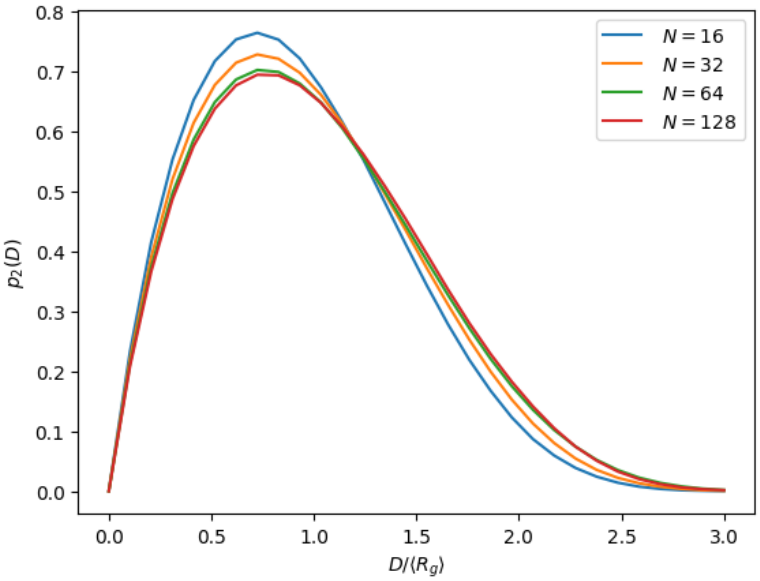

Figure 4.18.: Probability density $p_2(D)$ of two poles at distance D, normalized to the average gyration radius $\langle R_g \rangle$.

the poles into it and find their statistics. Methodologically we proceed similarly to the rigid case; we chose a reference monomer (for the rigid case, a reference point on the rigid circle), throw a first pole in some direction and distance from it and check whether it is inside the ring (as for the circle). If that is the case, we throw another pole from that first pole in similar fashion and assert whether it is inside. Both of the poles are uniformly sampled over space. From the statistics of sufficiently finely sampled poles, we then hope to extract the probabilities of two poles being a given distance D apart from each other.

4.3.2. Results

We determined the density function $p_2(D)$ of the distance of two poles being on the inside of a flexible, self avoiding ring-polymer. In figure 4.18, we see its graph for different polymerization numbers N. While at low N we see a clear difference between two subsequent curves, with increasing polymerization, the curves become more similar. The latter behaviour is of course expected as dictated by universality. We clearly see, that the results for the polymerization numbers $N = 64$ and $N = 128$ are almost identical, which leads us to the conclusion that we are close to universality. This was expected, since in chapter 2.3.2 we saw the probability densities of the radii of gyration also approach universality around $N = 64$.

The results are collected in table 4.3 .

We observe that the mean value of mean the inter-pole distance $\langle D \rangle$ is very close to $\langle R_g \rangle$ in all cases, more so for higher polymerization numbers.

Analogously to the rigid case, we would like to have a brief look at the probability

N	16	32	64	128
$\langle D \rangle$	0.93 ± 0.03	0.97 ± 0.01	1.00 ± 0.02	1.01 ± 0.01

Table 4.3.: First moment of $p_2(D)$ in the self-avoiding, flexible case.

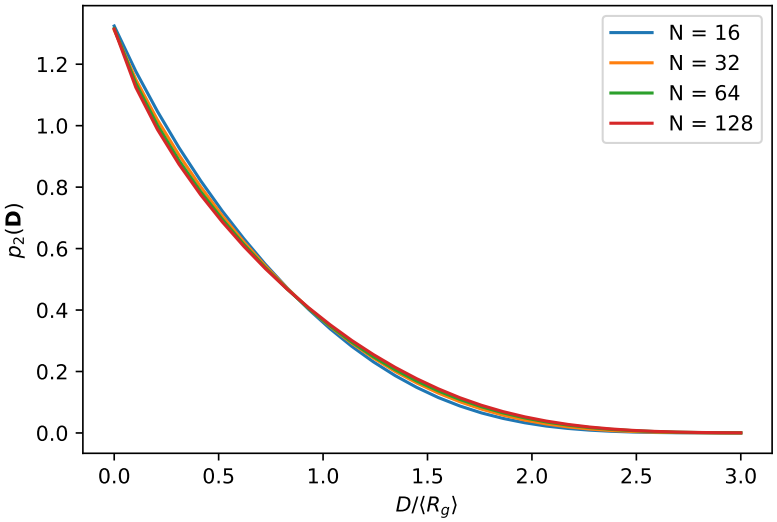

Figure 4.19.: Probability density $p_2(\mathbf{D})$ of the insertions being connected by the vector $\mathbf{D}$ for the self-avoiding, flexible ring.

density $p_2(\mathbf{D})$, as it again is closely related to the pair interaction potential one would use in a molecular dynamics simulation.

As we can see in figure 4.19, the obtained density is closely related to what we saw in figure4.17. Of course in the flexible case, the density exactly vanishes at $D/\langle R_g \rangle = 2$ while here the tail is softened again. Interestingly, the curves for different N almost collapse into one, much more than the graphs in figure 4.18 would suggest, even though the probabilities are closely related according to

$$p_2(D) \propto D p_2(\mathbf{D}). \tag{4.45}$$

We also notice, that even though the rigid density is compressed to a smaller interval, the maximal value at $D = 0$ is smaller than what we see in the self avoiding case. We hypothesize that this favoring of small length scales stems from the fact that a fractal object like the ring polymer at hand penalizes insertion probabilities exceeding a certain distance D, as its fractal structure takes away some of the area in which one could accommodate both poles. At very short length scales however, we are below the scale at which the fractality of the object plays a role and only the ratio of the contour length of the polymer and its area determine the probability densities.

5. Semi-Analytical Approaches

We shall now try to approach the insertion problem semi-analytically. There are several approaches we tried to model the final probability $p_2(D)$ of the flexible ring with varying success and domains where the approaches are valid. By endeavouring this, we hope to gain insights into how the insertion statistics arise as well as to reduce the computational effort needed.

5.1. 'Convolution' Approach

We shall call our first approach the 'convolution' approach since it is somewhat reminiscent of a convolution, even though it is not what the mathematical definition of a convolution entails. However, it is at times convenient to name things in an easily relatable way such that one can refer to them more fluently- hence, for the rest of this thesis, whenever we write 'convolution', we mean what is described in the remainder of this section.

The key idea is that it might be plausible to assume that the insertion probabilities for a flexible ring are similar to the ones of a rigid circle with a radius equal to the radius of gyration of the flexible ring. If this were approximately true, we could estimate the insertion statistics by merely knowing the distribution of the radii of gyration and using the analytical results for rigid circles.

To succeed in this, we must first regard the radius R of the rigid circle as a variable and write

$$p_2(D, R) = p_2(D|R)p(R) \tag{5.1}$$

where in all cases the probabilities are the probabilities that the insertion land on the inside of the ring. It is important to understand that $p_2(D, R)$ is equivalent to (4.43) but merely with R, which was fixed before, now treated as a variable and hence explicitly written as an argument.

From equation (5.1) we immediately see by integrating both sides that the marginal probability density $\bar{p}_2^C(D)$ can be expressed as

$$\bar{p}_2^C(D) = \int_0^\infty \mathrm{d}R \; p_2(D|R) \cdot p(R), \tag{5.2}$$

where with $p(R)$ we mean the distribution density of the radius of gyration. With the bar we explicitly denote that the probability density is an approximation. In chapter 2.3.2 we saw that the distribution of the radius of gyration follows a normal distribution to a satisfactory degree. Hence, we use the Gaussian fit to model $p(R)$ in this numerical integration, which is computationally cheaper and more convenient than using a customized fit function.

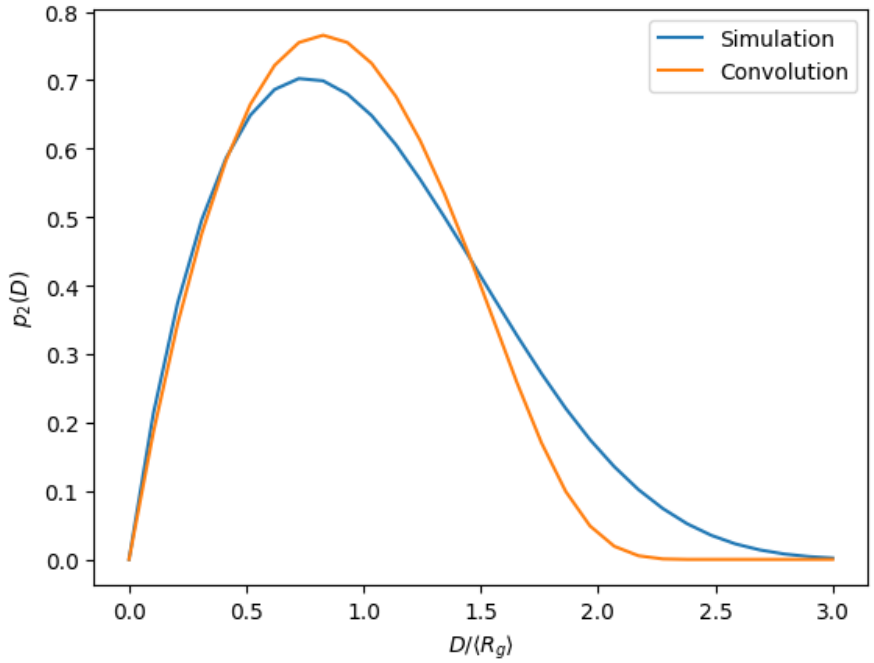

Figure 5.1.: Convolution approach compared to the results of the fully flexible simulation, shown here for $N = 64$.

Heuristically, expression (5.2) makes sense. The distribution density $p(R)$ smears out the original, analytical, rigid insertion probability $p_2(D|R)$ which is given by equation (4.43). While the analytical version sharply went to zero at $2R_g$ (see figure 4.16), the distribution density is nonzero at $R > R_g$ and therefore the probability obtained by expression (5.2) allows for bigger radii to contribute which lead to non-zero density values at $D/R_g = 2$ and higher values of D. Also, it trivially reproduces the rigid case, when the distribution of the radii simply reduces to a Dirac-delta function and we are left with the correct rigid insertion probability.

Numerical evaluation of $\bar{p}_2^C(D)$ yields what can be seen in figure 5.1. As one can see, our attempt to analytically approach the problem was not particularly successful. The model somewhat reproduces the mode of the true distribution, and even though in the low D regime, it describes the simulation to a satisfactory degree, it soon starts to deviate significantly around $D/R_g \approx 0.5$ and fails completely beyond $D/R_g = 1$. These phenomena can be readily explained; for low distances D of the pole, we approach the one insertion case. There, the quantity that mainly determines insertion success is the area $\mathcal{A}$ encircled by the polymer, as sketched in section 4. Now, there is a case to be made that for the bulk of conformations, the quantity R_g^2 can be used as a proxy for the area enclosed by our polymer. This means, that in the low D regime, the insertion statistics are actually determined mainly by R_g^2 such that correctly weighing the configurations with the probability density reproduces the insertion probability almost exactly. The

greater the distance D between the two poles gets, the more the actual shape of the polymers matters. A polymer with high radius of gyration is not necessarily a circle, but can assume a rod-like configuration, with drastically different insertion statistics. For that reason, the model ceases to be descriptive of the actual simulation somewhere between the two regimes, here around $D/R_g \approx 0.5$.

5.2. Probability Density Approach

In the following we shall elaborate on a second approach to approximate the insertion probability density of the distance $\bar{p}_2^D \approx p_2(D)$ of a flexible, self-avoiding ring. The bar again denotes approximation. We shall apply the formalism to the rigid case first which will turn out to be exact, hence no bar is added. Assuming uniform pole distribution as always done in this thesis, we know how likely it is to find a pole at distance r_1 from the center of the circle given some angular domain $\Delta\theta_1$ it fell inside. The probability is given by

$$p(r_1, \Delta\theta|R) = \frac{2r_1}{R^2}\frac{\Delta\theta_1}{2\pi}, \tag{5.3}$$

where R is the radius of the circle. The angular term determines, how likely it is that the pole lays within the domain $\Delta\theta$ and the first term describes how likely the respective distances from the center are, given radius R of the circle. For a second pole at distance r_2, we obtain the same distribution, with the respective domain. Because in the case of a rigid circle we have no angular preference and the pole-throwing-density is uniform, we can simply divide the total angle 2π into many equal parts and ignore the angular term in equation (5.3) in the continuum limit.

The total probability density of the distances only depends on relative position; hence we may always rotate the system such, that one of the angles vanishes and we only have to consider ϕ, the angle between the two vectors r_1 and r_2. Its probability density is also uniform and independent of r_1 and r_2. The connection between D and the other variables is

$$D^2(r_1, r_2, \phi) = (\mathbf{r}_1 - \mathbf{r}_2)^2 \tag{5.4}$$

$$= r_1^2 + r_2^2 - 2r_1 r_2 \cos\phi. \tag{5.5}$$

All three distributions are independent of one another which is why we can write down the density $p_2^D(D)$ as the integral

$$p_2^D(D) = \int_0^R \mathrm{d}r_1 \int_0^R \mathrm{d}r_2 \int_{-\pi}^{\pi} \mathrm{d}\phi \; p(r_1|R)\; p(r_2|R)\; p(\phi)\; \delta(D - D(r_1, r_2, \phi)) \tag{5.6}$$

$$= \int_0^R \mathrm{d}r_1 \int_0^R \mathrm{d}r_2 \int_0^{\pi} \mathrm{d}\phi \frac{2r_1}{R^2}\frac{2r_2}{R^2}\frac{1}{\pi}\delta(D - D(r_1, r_2, \phi)), \tag{5.7}$$

where we used that the integration over ϕ is symmetric and changed the boundaries accordingly.

The rules for functions within the delta-distribution permit to write

$$\delta(f(x)) = \sum_{i=0}^{n} \frac{\delta(x - x_i)}{|f'(x_i)|}, \tag{5.8}$$

where we have n roots x_i of the function $f(x)$.

We intend to integrate over ϕ first and we notice that on the interval $[0, \pi]$ there is only one root of our function $f(D, \phi, r_1, r_2) = D - \sqrt{r_1^2 + r_2^2 - 2r_1 r_2 \cos\phi}$ for given values of r_1, r_2 and D, namely

$$\phi_0 = \arccos \frac{r_1^2 + r_2^2 - D^2}{2r_1 r_2}. \tag{5.9}$$

This expression reminds us that $|r_1 - r_2| \leq D \leq r_1 + r_2$ is a condition which has to be met to find a real-valued ϕ and it stems from relation (5.4). It is easy to see, that the lower bound is given by $\phi = 0$ and the upper bound by $\phi = \pi$. The derivative of $f(D, \phi, r_1, r_2)$ with respect to ϕ amounts to

$$\left.\frac{\partial f}{\partial \phi}\right|_{\phi=\phi_0} = -\frac{r_1 r_2 \sin\phi_0}{\sqrt{r_1^2 + r_2^2 - 2r_1 r_2 \cos\phi_0}} \tag{5.10}$$

$$= -\frac{r_1 r_2}{D}\sqrt{1 - \left(\frac{r_1^2 + r_2^2 - D^2}{2r_1 r_2}\right)^2}. \tag{5.11}$$

Using relations (5.6), (5.8) and (5.10), integrating over ϕ and simplifying we obtain

$$p_2^D(D) = \frac{4D}{R^4\pi}\int_0^R \mathrm{d}r_1 \int_0^R \mathrm{d}r_2 \frac{\Theta(D - |r_1 - r_2|)\Theta(r_1 + r_2 - D)}{\sqrt{1 - \left(\frac{r_1^2 + r_2^2 - D^2}{2r_1 r_2}\right)^2}}, \tag{5.12}$$

where $\Theta(x)$ denotes the Heaviside step-function.

We see the yield of integrating (5.12) numerically in figure 5.2.

Since the two curves are congruent, the result supports our analytical considerations and suggests that they are in fact exact.

5.3. Flexible Model

The above formalism reproduces the rigid case exactly. Thus, we have achieved to compress the results of the rigid calculation and represent them in one compact double-integral. In the following, we attempt to generalize the formalism to flexible, self avoiding rings. Assume some probability distribution $p(\rho)$ of the distance ρ of a monomer to the center of mass. Let N be the number of monomers in the ring and let ρ_i be the distance of the i-th monomer to the center of mass. Now we assume the center of mass of the ring polymer to be in the origin and then sample our monomers by going in angular steps of $\Delta\theta = \frac{2\pi}{N}$. For each of the angular sections, we draw a monomer distance from the distribution $p(\rho)$.

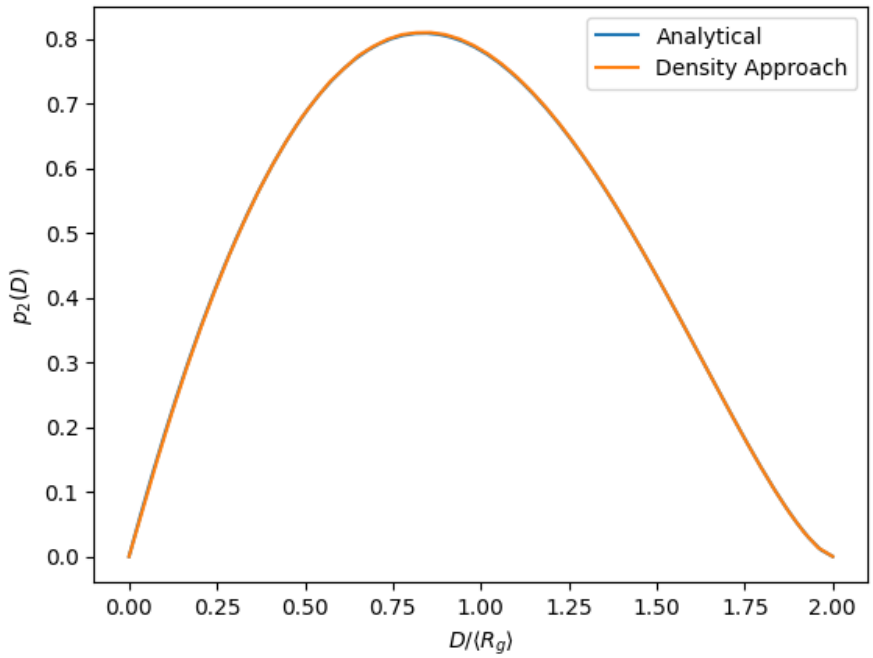

Figure 5.2.: Comparison the density approach to the integration over the all subcases sketched in section 4. The blue curve is covered up by the orange one.

Then the probability density to draw a certain sample of the monomer-center of mass-distances for the whole polymer simply amounts to

$$p(\{\rho_i\}) = \prod_{i=1}^{N} p(\rho_i). \tag{5.13}$$

We are then able to assign an area element to each monomer according to

$$\Delta A_i \approx \Delta\theta \ \rho_i^2. \tag{5.14}$$

We would like to point out that the approach at hand makes several errors; first of all the individual samples of probability density (5.13) are not representing realistic polymer rings. This is the case because we only regard the mean behaviour of every single monomer and completely disregard short range order in exchange for simplification. Put differently we completely give up connectivity; one monomer may be drawn to be at some extreme value of ρ and its neighbor at the other extreme. By doing this, we systematically underestimate the true value $p_2(D)$ at short distances; if the distance between the two poles is short and one of them is inside the ring, then they are almost always both inside, since the neighbouring monomers are connected and therefore at similar distances to the center of mass. Furthermore, in the discrete case with a finite number N of monomers, we make a slight error in the effective distribution. To understand this we need to keep in mind,

that we tacitly assumed, that the center of mass coincides with the origin, which we use to determine our monomer distances from. On *average* they are the same, but for an individual sample they may not. We can easily come to the conclusion, that the average center of mass necessarily needs to coincide with the origin by acknowledging circular symmetry; for each configuration which has a center of mass different to the origin, the mirror image of it, where the center of mass is shifted by the same amount just to the other side is equally likely. Since this is true for every possible sample, the average center of mass position needs to be at the origin. That means, with the above described method, we may draw N monomers, whose center of mass is not the origin and therefore their true, a posteriori center of mass distance is different from the assumed one. This means in turn, we draw from a slightly wrong distribution. However, taking the continuum limit $N \to \infty$ we rid ourselves of this error, because for each sample, the probability to draw a distribution with a center of mass different form the average one, tends to zero. And as stated before, the averages of the assumed center of mass and the true one are the same. A last error we make is, that with this model we forget about configurations including monomers which do not have a direct 'line of sight' with the center of mass. By that we mean that the line connecting these monomers to the center of mass crosses some part of the ring (we think of 'angular neighbours', i.e. two monomers with a difference in their angular coordinates of exactly $\Delta\theta$ as being connected by a straight line such that the entire ring resembles a closed contour). It is plausible to assume that this will not have a huge impact on the average probability density, since the 'cut off' portion of the ring will likely have a much smaller area than the bulk. And since the primary quantity to determine insertion success is closely tied to the total area encircled by the polymer, this should be an effect of negligible impact.

With these words of caution in the back of our minds, we shall now proceed to the derivation of the modified model. Since now the size of the area slices may vary, we have to take the probability of a pole falling into a certain area element explicitly into account. This leads to a modified version of equation (5.3) reading

$$\Delta p(r_1, \rho_i, i) = p(r_1|\rho_i)p(\rho_i)\frac{\Delta A_i}{A}. \tag{5.15}$$

Thus the total probability density of a pole landing in the i-th area element at distance r_1 is equal to the product of the probability that the pole landed inside this element, times the probability, that the monomer landed at the distance it did, times the probability of landing a pole at distance r_i inside this given area slice. We included figure 5.3 to compactly visualize the above described.

Writing everything in terms of ρ_i and r_1 we obtain

$$\Delta p(r_1, \rho_i, i) = \frac{2r_1}{\rho_i^2}\frac{\Delta\theta\rho_i^2}{\Delta\theta\sum_{k=1}^{N}\rho_k^2}p(\rho_i) \tag{5.16}$$

$$= \frac{2r_1\Delta\theta}{\Delta\theta\sum_{k=1}^{N}\rho_k^2}p(\rho_i) \tag{5.17}$$

$$\approx \frac{2r_1\Delta\theta}{\langle A\rangle}p(\rho_i), \tag{5.18}$$

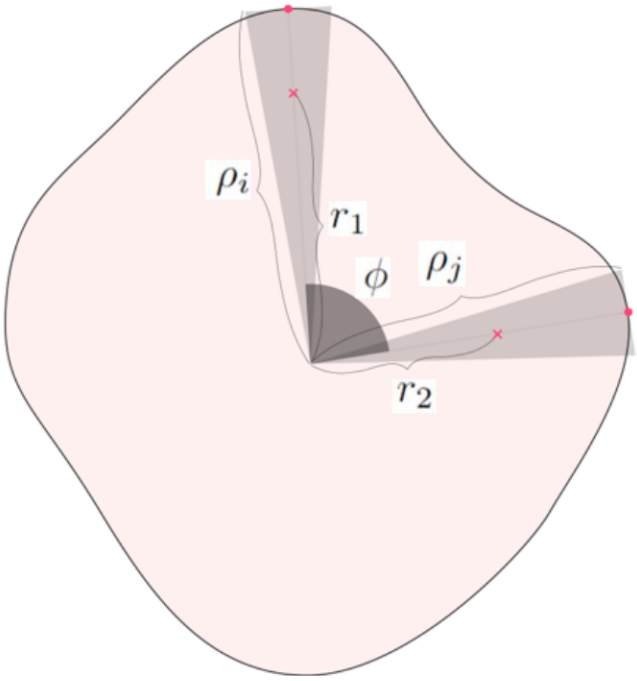

Figure 5.3.: Setup of the above described density-approach.

where $\Delta\theta = \frac{\pi}{N}$.

We replaced the sum of the area elements with the total average area $\langle A \rangle$, this step is justified in the limit of large N, where the area function will be sharply peaked at $\langle A \rangle$. This equation only refers to the densities inside a slice. Since we have infinitely many slices, it vanishes. To obtain the more useful finite version of it, we must sum over all the slices according to

$$p(r_1, \rho_1) = \sum_{i=1}^{N} \Delta p(r_1, \rho_i, i) \tag{5.19}$$

$$= \frac{2\pi r_1}{\langle A \rangle} p(\rho_1) \tag{5.20}$$

Here, by ρ_1 we mean the distance of the monomer, which is radially aligned with the first pole and the center of mass. Since the probability density (5.20) contains all the information of the monomer distribution and with $\langle A \rangle$ rendered a constant, we can conveniently integrate over ρ_i and arrive at an effective insertion probability

$$p(r_1) = \int_{r_1}^{\infty} \mathrm{d}\rho_i \; p(r_1, \rho_i, i) \tag{5.21}$$

$$= \frac{2\pi r_1}{\langle A \rangle} (1 - \mathcal{C}(r_1)), \tag{5.22}$$

where $\mathcal{C}(r_1) = \int_0^{r_1} \mathrm{d}\rho_1 \; p(\rho_1)$ is the cumulative distribution function of the monomer distribution $p(\rho_1)$ evaluated at the distance r_1 of the pole from the center of mass. Constructing the integral which gives us the desired probability density $p(D)$ we arrive at

$$\bar{p}_2^D(D) = \frac{2}{\pi} \int_0^\infty \mathrm{d}r_1 \int_0^\infty \mathrm{d}r_2 \int_0^\pi p(r_1)p(r_2)\delta(D - D(r_1, r_2, \phi)) \tag{5.23}$$

$$\propto D \int_0^\infty \mathrm{d}r_1 \int_0^\infty \mathrm{d}r_2 \; (1 - \mathcal{C}(r_1))(1 - \mathcal{C}(r_2)) \frac{\Theta(D - |r_1 - r_2|)\Theta(r_1 + r_2 - D)}{\sqrt{1 - \left(\frac{r_1^2 + r_2^2 - D^2}{2r_1 r_2}\right)^2}}. \tag{5.24}$$

We can only determine $\bar{p}_2^D(D)$ up to a proportionality factor, and have to normalize numerically as we do not know the average area $\langle A \rangle$ a priori. To get to the explicit expression (5.24) from the general one (5.23), we followed the same steps as in section 5.2 to get rid of the delta function; we find the zeros with respect to ϕ, rewrite the delta distribution with the help of relation (5.8) and integrate over ϕ. The latter integral equation is our result. Unfortunately, there is no analytical solution to it which we are aware of. However, we may now use equation (5.24) to determine an approximate model of the insertion probabilities of the flexible, self-avoiding polymer case numerically. In figure 5.4 we see the results of equation (5.23).

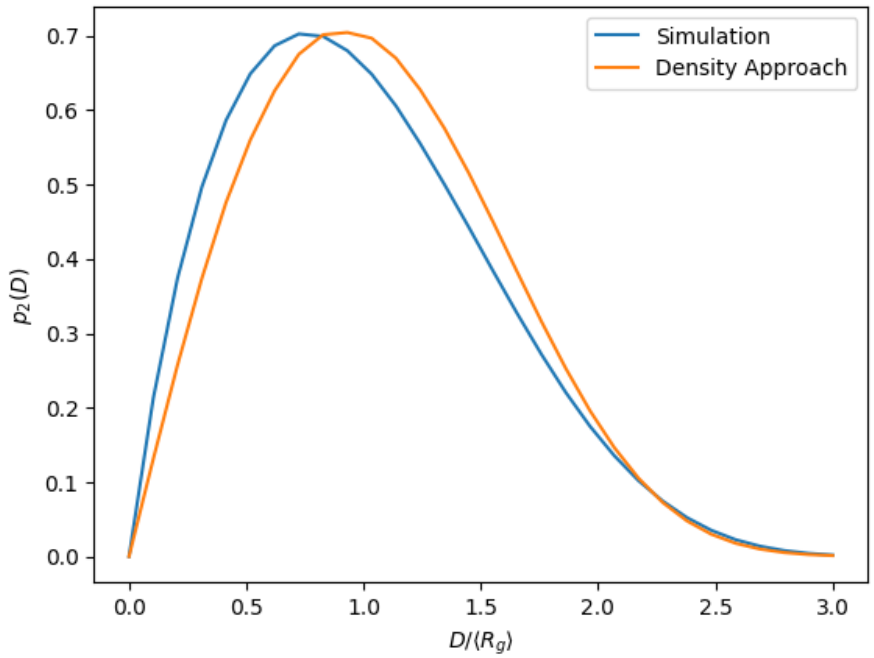

Figure 5.4.: Simulation result (blue) and the analytical 'density' approach (orange) of the two-pole insertion probability of the distances $p_2(D)$. Here, we chose the polymerization number $N = 128$.

The overlapping region of the two graphs depicted in figure 5.4 is about 94% which means the guess is reasonable and potentially applicable as a rudimentary zero-parameter approximation. However, we notice that the mode is shifted by a notable amount and that especially in the short distance regime, we systematically underestimate the true probability density. This is likely due to the connectivity error we commit which we described earlier; breaking connectivity is only legitimate if there is no correlation between the monomers. However, particularly direct neighbours are highly coupled which is not reflected in the model and hence leads to a systematic underestimation in the short distance regime, as mentioned before. As a consequence of this, we afford one parameter and try to amend this deviation. The key idea is, that disregarding the exact details, the correlation between two monomers should go exponentially to zero with their distance. This is a reasonable guess, because all monomers are equivalent as well as their relations to one another. The degree of decorrelation can therefore only depend on their distance in the chain. This is called translational invariance and it can be written down as

$$\Gamma(i,j) = \Gamma(|i-j|) \equiv \Gamma(k), \quad k = |i-j| \tag{5.25}$$

where $\Gamma(i,j)$ is our correlation function of monomers i and j. If we additionally assume that the correlation function also obeys the relation

$$\Gamma(j)\Gamma(k) = \Gamma(j+k), \tag{5.26}$$

the exponential functions are the only family that can satisfy these conditions, as shown in chapter 2.3.3. Since the correlation decays exponentially, we assume, that

$$\Gamma(x) = \frac{1}{\xi} e^{-x/\xi}, \tag{5.27}$$

where instead of an index we consider now some length x and with ξ we denote the correlation length. Now, if the correlation of the monomers dies off exponentially and the error we make is tied to the correlation between the monomers, it seems natural to assume that this error also decays exponentially. So we make the ansatz that the error distribution can be written as

$$p_{\mathrm{err}}(\mathbf{D}) = \frac{1}{\xi} e^{-D/\xi}, \tag{5.28}$$

and corollary

$$p_{\mathrm{err}}(D) = c\ D p_{\mathrm{err}}(\mathbf{D}) \tag{5.29}$$

with a normalization constant c and a free parameter ξ. Then, the corrected probability density reads

$$\tilde{p}_{\mathrm{corr}}(D) = \frac{1}{2}\Big(\bar{p}_2^D(D) + p_{\mathrm{err}}(D)\Big). \tag{5.30}$$

As we can see in figure 5.5 this ansatz was fruitful.

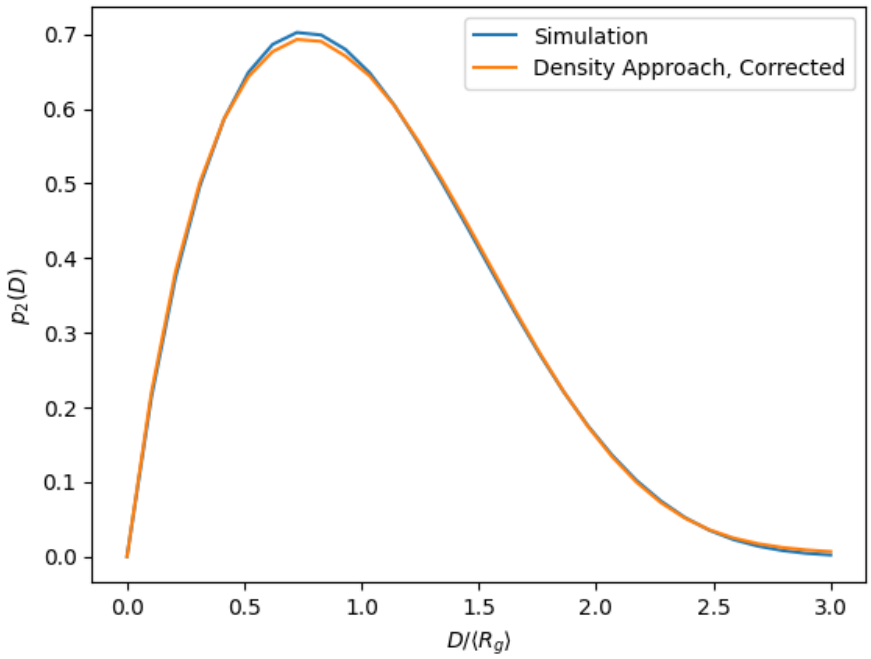

Figure 5.5.: Corrected version of the insertion density $\tilde{p}_{corr}$ approach (orange) compared with the simulation results (blue) for $N = 128$.

With an optimized parameter $\xi \approx 0.45$ the overlap between the simulation result and the model is $> 99\%$, both the short distance and the long distance regime are almost perfectly reproduced as well as the position and height of the mode. This correction works best, when we are in the higher N regime but the results for lower N are still good (depending on the demands) until $N = 32$ where most of the coarse features are still captured and the mode position still can be reproduced for a slightly different value of ξ. After that the model somewhat loses its precision; results for the lower N are found in the appendix.

6. Relation to $3d$ Polycatenanes

6.1. Center of Mass Distance

Having thoroughly discussed our $2d$ model of a ring with insertions, we shall now explore how well the model describes properties of the full, three-dimensional chain. Of course we can only reasonably attempt to make statements about local properties of the polycatenane since in our simplistic model the chain as such is not built-in. One quantity that is local and should be possible to derive from our results is the center-of-mass distance between neighbouring rings. If we assume the centers-of-mass to be on one straight line with the insertion point, as depicted in figure 6.1, we are able to calculate an estimate for the center of mass distance out of the $2d$ results.

We calculate the mean values $\langle D \rangle$ from our insertion distributions for all polymerization numbers N, as well as the average monomer distance from the center-of-mass $\langle \rho_i \rangle$.

The results of these calculations can be seen in figure 6.2. First, we confirm that the difference of topological interactions and chemical bonding manifests itself visibly in the center of mass distances. While for bonded rings, we observe an asymptotically decaying trend, for polycatenanes the distance rises and converges asymptotically. Also the absolute differences in the distances between catenanes and bonded rings is sizable and around $\langle R_g \rangle / 2$.

We can see that the values obtained from our first guess match the simulation relatively well but we do not observe an N dependence of our data. Put differently, we obtain the asymptotics already in the low N regime. This is of course unphysical and stems from the fact that for the insertion statistics, we have used point like poles, not monomeric ones with finite spacial extension. Then, apart from configurational differences, we obtain the insertion statistics with a similar mean value and thus the unnatural low N asymptotics. For the polymerization number N to play a role, we have to include the grain-size of our system, the hard-sphere monomer diameter d_s into our calculations. This granularity reintroduces gradually achieved universality, as it only ceases to matter, when scaled with

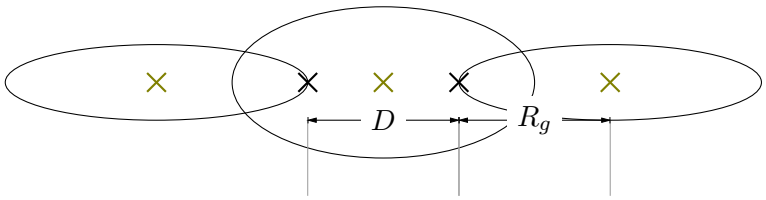

Figure 6.1.: Three rings taken from a polycatenane are assumed to have aligning centers-of-mass (olive crosses) and insertion points (black crosses).

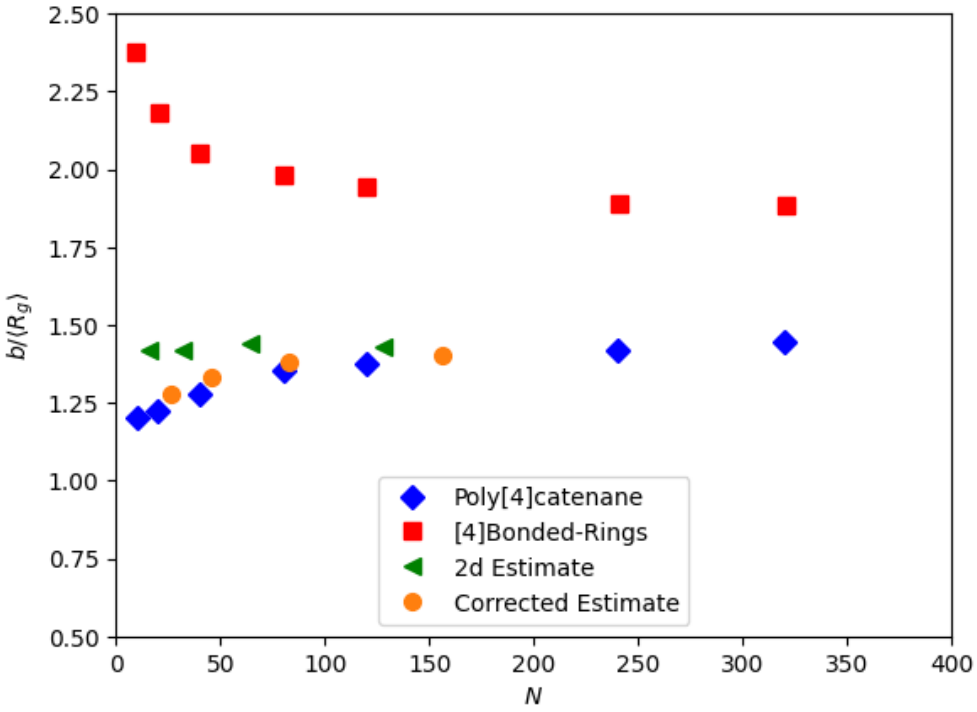

Figure 6.2.: Center of mass distances $b/\langle R_g \rangle$ between neighbouring rings in a fully $3d$ poly[4]catenane (blue) and [4]bonded-ring (red). The $3d$ data was taken from [LZWZ21a, p.4, Fig.4] and digitized. We also display are our preliminary results from the $2d$ calculations (green) and the corrected version (orange).

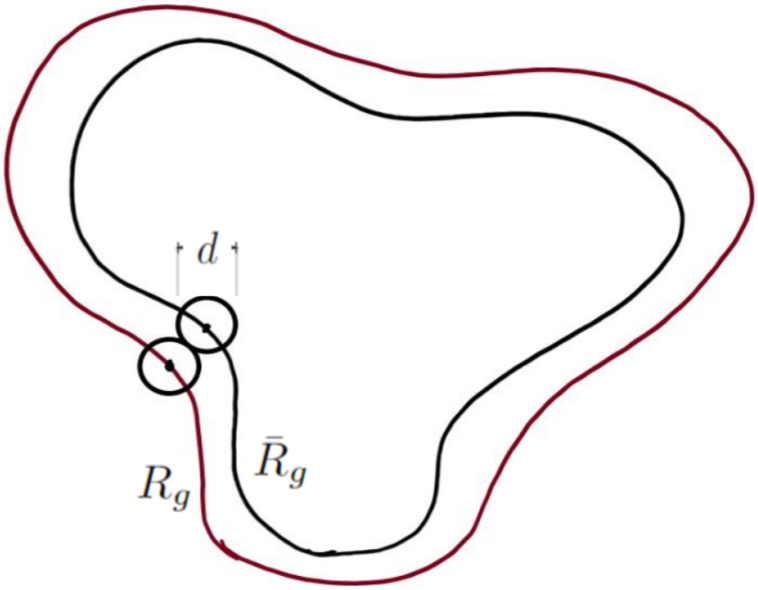

Figure 6.3.: Performing monomeric insertions in the outer ring with radius of gyration R_g, results in a smaller ring of radius of gyration $\bar{R}_g$ with point like insertions, neglecting short range interactions between the insertions.

a sufficiently large value of R_g.

6.1.1. Correction

Fortunately, there is an easy way to correct our calculations to redeem for the error made by using point insertions. If we consider a hard sphere polymer ring, with some polymerization number N, radius of gyration R_g and sphere diameter d then the spacial extension of the spheres create a forbidden zone for monomeric insertions of breadth $\sim d$ as depicted in figure 6.3. This means, we can approximately calculate the insertion probability for monomeric insertions by considering fictitious, point-like insertions in a smaller ring of the same shape but with radius of gyration $\bar{R}_g$. However, to obtain the correct behaviour, we have to scale the results of the smaller, fictitious-insertion ring with the true radius of gyration R_g of the larger ring. We keep in the back of our minds, that this correction does not account for the vanishing of probability for length scales below $D \sim d$, where the two inserted monomers would overlap. Now, in our case we have to reverse this problem; we are provided with the insertion probabilities for fictitious poles and want to deduce the statistics for real insertions. Consequently, we realize that the statistics we have calculated are the statistics for monomeric insertions of a larger ring, i.e. with a higher polymerization number N. In order to relate the two cases, we need to relate R_g and $\bar{R}_g$. Accordingly, all the distances from the monomers to the center of

mass ρ_i get shorted by an amount of the order $\sim d$ and we may write

$$\bar{R}_g^2 \approx \frac{1}{N}\sum_{i=1}^{N}(\rho_i - d)^2 \tag{6.1}$$

$$= \frac{1}{N}\sum_{i=1}^{N}(\rho_i^2 - 2\rho_i d + d^2) \tag{6.2}$$

$$= R_g^2 - 2d\langle\rho\rangle + d^2. \tag{6.3}$$

Here, ρ_i are the distances of the monomers to the center of mass of the outer ring. Now, the average distance is of the same order of magnitude as the radius of gyration

$$\langle\rho\rangle = 0.95R_g \approx R_g, \tag{6.4}$$

as obtained from the evaluation of our data. Using relation (6.4), equation (6.1) can be continued and leads to

$$\bar{R}_g \approx R_g - d. \tag{6.5}$$

We can now obtain a better estimate of the real insertion probabilities. As previously stated, we scale the statistics of the smaller ring with the gyration radius R_g of the larger ring. What we have, is the statistics of the smaller ring, scaled by its own radius of gyration $\bar{R}_g$. Consequently, we need to multiply everything by a factor $\bar{R}_g/R_g$. Now, finally we have to consider that the outer ring also has a higher polymerization number which we may calculate with Flory's scaling relation

$$\bar{R}_g + d = a(\bar{N} + \Delta N)^{\nu}, \tag{6.6}$$

where $a \approx 0.3$ is a proportionality constant we determined from our data using the considerations in chapter 2.3.1. $\bar{R}_g$, d and $\bar{N}$ are given, $\nu = \frac{3}{4}$ is the Flory exponent, so we may calculate the change in polymerization ΔN. The results of applying both considerations we can see in figure 6.2. We observe that with our simple modification, we recovered N-dependence and obtain clearly much better predictions for the $3d$-values. The error is clearly low, $\Delta b < 5\%$.

6.2. Elastic Properties

Pulling on a polycatenane by applying some force of magnitude f on both ends, we expect the chain to be stretched first on the largest length scales and then on consecutively smaller ones. This is of course due to the fact that most of the entropic contribution stems from the small length scales. Stretching the length scales one by one implies stretching regimes which are connected to different characteristic length scales and are somewhat well defined. The practical application of these considerations are captured in the notion of 'tension blobs' which are a handy tool to deriving scaling relations in soft matter physics explained in most relevant textbooks, for example in [KGP94,].

In a polycatenane the length scale which we expect to being stretched first is the one on chain level; all rings are aligned in a linear array but individually still fluctuate freely. After that we are confronted with two different degrees of freedom which are both on the length scales of the ring and thus interwoven: the moving of the insertions and the stretching of the rings. The two degrees of freedom are intimately connected to each other since it is impossible to obtain a high-distance conformation of poles without also deforming the ring in the process. We are now interested in finding the elastic properties of the polycatenane on this length scales, i.e. after already having stretched the supercoil. The central quantity characterizing the behaviour of an object under tension is the elastic modulus

$$E(F) = \frac{\mathrm{d}^2 U}{\mathrm{d}D^2}\bigg|_{D=D(F)}, \tag{6.7}$$

as it contains information on how much the object stiffens or softens with increasing force. Usually, materials tend to resist the tension and increasingly stiffen when subject to a force as long as their molecular integrity is not disturbed.

In the presented model we are inherently on ring level and can therefore only hope to recover information on stretching behaviour on this length scale or below. We would like to make the case that, on this length scale, the relevant energy $U(D)$ in equation (6.7) can be obtained from the probability density $p_2(D)$ which we determined in this thesis. The justification of our $2d$ model should be even more valid in the case of a stretched catenane; if anything, we would expect the rings of the polycatenane more orthogonal to each other. Also the rings should have an even smaller third eigenvalue of the gyration tensor indicating them to be plane like. Lastly, the effects of higher order neighbour interaction are expected to be negligible, too, as the force pulls them away from each other. All of this should increase the quality of predictions obtained by the model at hand.

Pulling on the poles, we subsequently restrict the systems mobility and thus squeeze its entropy. At moderate forces, resulting in distances on average greater than the expected value $\langle D \rangle$, we mainly restrict the orientational degree of freedom. At this stage, typical conformations still contribute to the probability density, but they preferrably fit the poles along their primary, i.e. largest axis. Since typical conformations do contribute and since they are by definition the most prevalent type of conformation obtained, their contributions will make up the bulk of successful insertions in the algorithm, even though the poles are inserted at a 'suboptimal' distance. This beautifully refelects in a $2d$ model only featuring one ring, the collective behaviour of all rings aligning with the backbone contour of the polycatenane.

At high forces, we expect a strong stretching effect; only high-R_g, rod-like, configurations will be able to contribute. These are inherently rare and additionally the poles must be align with the rod axis to fit inside. The probability to achieve high pole distances consequently vanishes. Note, how the alignment with the backbone is forced even more rigorously on the system, as the decrease of the lateral axes' size restricts orientational freedom of the pole-pair even more significantly. Since we are only interested in the stretching of the polycatenane, we shall only consider the region of $p_2(D)$ where $\frac{\mathrm{d}p_2(D)}{\mathrm{d}D} < 0$,

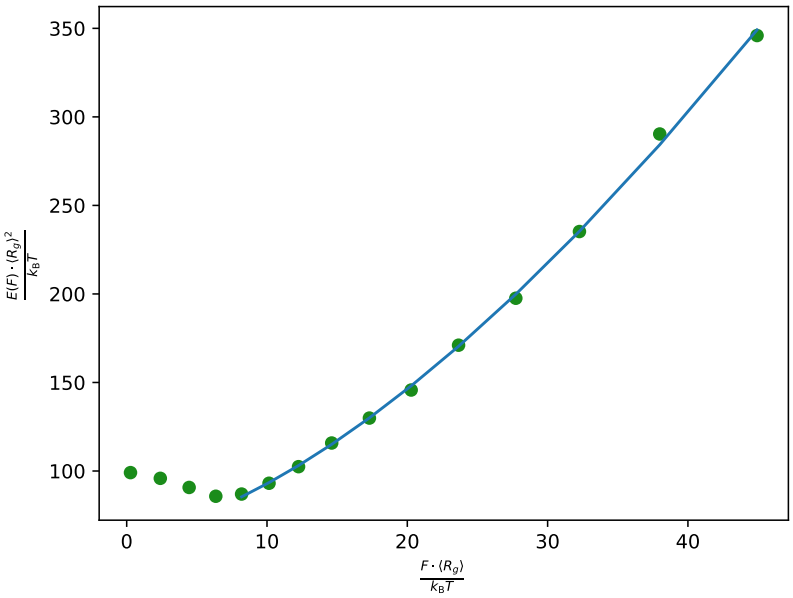

Figure 6.4.: The elastic modulus $E(F)$ of the ring in terms of the force F applied. The radius gyration $R_g \approx 7$ for $N = 64$ used here.

that is, the region to the right of the maximum. We see what we obtain for the elastic modulus in figure 6.4.

The fit is of the form

$$E(F) = cF^{\alpha}, \tag{6.8}$$

and was obtained by only fitting the ascending part of the curve. The exponent was determined to be $\alpha = 1.5 \pm 0.1$. Unfortunately, we could not find a fit function which entails both the lower and the higher force regime. Since there are only a few data points for small forces, the fitting was omitted there.

At the lower force regime, we clearly see a decrease in the elastic modulus with increasing force which suggests the existence of a stress-softening regime when stretching a polycatenane. This result is intriguing and highly uncommon; usually stress softening regimes point to material failure as observed e.g. for rubbers. However, throughout this thesis we only considered entropic effects; no reorganization and breaking of bonds is allowed. This singles out the observed stress-softening as particularly special and is likely induced by the topology of the system. Unfortunately, exploring this regime to a satisfactory extend would reach far beyond the scope of this thesis and is therefore omitted here. Hence, an explanation on the molecular level as of why the stress-softening regime emerges in the first place cannot be obtained here.

The stress-softening phase is followed by a more intuitive stiffening regime again. It should be attributable to the stretching of the rings which leads to drastic reduction of

the entropy and therefore to a steeply ascending region in the $E(F) \sim F^{3/2}$. We also expect a linear regime with constant E for very low forces $F \ll 1$. It is likely that the resolution of the presented graph is not high enough, i.e. the spacing between the data points is much greater than the extend of the Hookean regime of constant E. But we see a slight flattening of the curve close to zero which could indicate a constant elastic modulus for very low forces.

7. Outlook

This thesis raises many questions that could spark subsequent study of similar systems. One obvious generalization would be to consider additional insertions. In this document we only referred to one and two insertions into the ring, but really any number of insertions is thinkable. It is entirely unclear how the probability densities would look like. We assume that in the three insertion case each pole should have the same distance distribution to each other pole, due to circular symmetry – None of them is preferred. One could hypothesize that the modes of these distributions are shifted to lower distances, because the triangle spans an area which should increase the repulsive interaction with the ring and push everything tighter together on average. These, of course are weakly justified guesses and to achieve certainty, one would have to conduct the according simulation. Furthermore, an intriguing question would be, whether the topological forces at hand are pairwise additive. It is well known, that for many topological systems the principle of pair-wise additivity is violated. The most prominent of which likely are the Borromean rings; in figure 7.1 we can see a schematic version of them.

They display a system of three entangled rings. However, they are entangled in such a manner, that selecting any pair of the three rings and neglecting the third, one will end up with two separate rings. This means, we have an interaction which is non-additive and hence not differentiable into smaller pieces unlike many other physical forces seem to be.

However, in the system we considered here, no fundamental entanglement of the insertions is obvious, hence additivity could still be somewhat possible. The more accurate question would probably be to ask 'how non-additive are the forces at hand?'.

In this thesis, we had partial success in analytically treating the insertions' probability densities in the ring-polymer. Consequently, it would be of high interest to test the boundaries of the presented formalism. For instance, we have already shown, that in the rigid case, it reproduces exact results, because the monomer distance distribution reduces to a Dirac-delta function and is hence known exactly. For fully flexible rings of large enough size, the results where too, quite convincing. It is tempting to try and find out analytically, how the distribution of monomer distance to the center of mass changes with increasing polymerization. If this was known, we could handle everything analytically. Furthermore, the extension to flexible rings with increasing rigidity could be considered.

In principle, the model should also hold for more than two insertions. If so, one could elaborate the insertion probabilities without any further simulation; only the monomer distribution functions would be needed.

Furthermore, one could investigate how a monomer-monomer potential would modulate the probability density. One could use the non-interacting monomer density as a starting point and change it by adding a weak monomer-monomer potential, treating the two potentials as independent. Analogously, one could introduce a pole-pole interaction, which

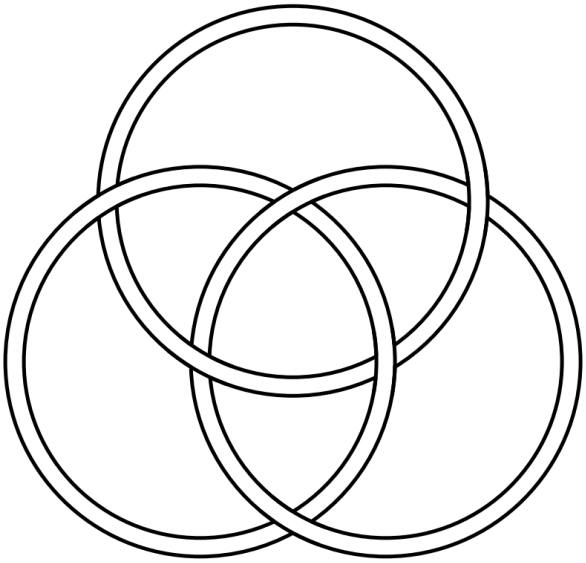

Figure 7.1.: Schematic representation of the Borromean rings taken from [CBR98].

would be another, much simpler modification, since the monomer distribution does not change.

If this were successful, one could maybe provide an approximation for the full insertion probability density for interacting systems, solely through our formalism, significantly reducing computational load.

The elastic properties were only briefly grazed in this thesis but the preliminary results bear fascinating implications and underline the impact of topological changes on a system's properties. However, further investigation is clearly needed, as the above analysis is not sufficient to explain the emergence of the stress-softening on a molecular level. To achieve this, detailed analysis of ring shape during the stress-softening regime is likely necessary. It would be intriguing to test these predictions in a fully $3d$ simulation of actual polycatenanes. Furthermore, if further computational analysis supports these claims, experimental investigation would naturally be desirable, as soon as experimentally feasible.

Bibliography

[ABC+20] David P. August, Stefan Borsley, Scott L. Cockroft, Flavio della Sala, David A. Leigh, and Simon J. Webb. Transmembrane ion channels formed by a star of david [2]catenane and a molecular pentafoil knot. *Journal of the American Chemical Society*, 142(44):18859–18865, 2020. PMID: 33084320.

[C+23] Pietro Chiarantoni et al. Linear catenanes: a computational study. 2023.

[CBR98] Peter Cromwell, Elisabetta Beltrami, and Marta Rampichini. The borromean rings. *Mathematical Intelligencer*, 20(1):53–62, 1998.

[Deu99] JM Deutsch. Equilibrium size of large ring molecules. *Physical Review E*, 59(3):R2539, 1999.

[DS87] Bertrand Duplantier and Hubert Saleur. Exact critical properties of two-dimensional dense self-avoiding walks. *Nuclear Physics B*, 290:291–326, 1987.

[FADLE24] Reyhaneh A. Farimani, Zahra Ahmadian Dehaghani, Christos N. Likos, and Mohammad Reza Ejtehadi. Effects of linking topology on the shear response of connected ring polymers: Catenanes and bonded rings flow differently. *Phys. Rev. Lett.*, 132:148101, Apr 2024.

[FSBK03] Patrick Fernandez, Simon Schrödle, Richard Buchner, and Werner Kunz. Micelle and solvent relaxation in aqueous sodium dodecylsulfate solutions. *Chemphyschem*, 4(10):1065–1072, 2003.

[GF03] Alexander Grosberg and Harry Frisch. Winding angle distribution for planar random walk, polymer ring entangled with an obstacle, and all that: Spitzer–edwards–prager–frisch model revisited. *Journal of Physics A: Mathematical and General*, 36(34):8955, 2003.

[HLG+11] Jonathan D Halverson, Won Bo Lee, Gary S Grest, Alexander Y Grosberg, and Kurt Kremer. Molecular dynamics simulation study of nonconcatenated ring polymers in a melt. i. statics. *The Journal of chemical physics*, 134(20), 2011.

[KGP94] Alexei R Khokhlov, Alexander Yu Grosberg, and Vijay S Pande. *Statistical physics of macromolecules*, volume 1. Springer, 1994.

[KL08] Euan R. Kay and David A. Leigh. Beyond switches: Rotaxane- and catenane-based synthetic molecular motors. *Pure and Applied Chemistry*, 80(1):17–29, 2008.

[KRFH+20] Richard P Koche, Elias Rodriguez-Fos, Konstantin Helmsauer, Martin Burkert, Ian C MacArthur, Jesper Maag, Rocio Chamorro, Natalia Munoz-Perez, Montserrat Puiggros, Heathcliff Dorado Garcia, et al. Extrachromosomal circular dna drives oncogenic genome remodeling in neuroblastoma. *Nature genetics*, 52(1):29–34, 2020.

[KSD20] Alexander R Klotz, Beatrice W Soh, and Patrick S Doyle. Equilibrium structure and deformation response of 2d kinetoplast sheets. *Proceedings of the National Academy of Sciences*, 117(1):121–127, 2020.

[LRR+22] Guancen Liu, Phillip M Rauscher, Benjamin W Rawe, Marissa M Tranquilli, and Stuart J Rowan. Polycatenanes: synthesis, characterization, and physical understanding. *Chemical Society Reviews*, 51(12):4928–4948, 2022.

[LZWZ21a] Huanqing Lei, Jianguo Zhang, Liming Wang, and Guojie Zhang. Dimensional and shape properties of a single linear polycatenane: Effect of catenation topology. *Polymer*, 212:123160, 2021.

[LZWZ21b] Huanqing Lei, Jianguo Zhang, Liming Wang, and Guojie Zhang. Dimensional and shape properties of a single linear polycatenane: Effect of catenation topology. *Polymer*, 212:123160, 2021.

[PF67] Stephen Prager and HL Frisch. Statistical mechanics of a simple entanglement. *The Journal of Chemical Physics*, 46(4):1475–1483, 1967.

[Spi58] F. Spitzer. *Some theorems concerning -dimensional Brownian motion.* Trans. Amer. Math. Soc. 87, 1958.

[TAB+24] Luca Tubiana, Gareth P Alexander, Agnese Barbensi, Dorothy Buck, Julyan HE Cartwright, Mateusz Chwastyk, Marek Cieplak, Ivan Coluzza, Simon Čopar, David J Craik, et al. Topology in soft and biological matter. *Physics Reports*, 1075:1–137, 2024.

[VL90] JM Victor and D Lhuillier. The gyration radius distribution of two-dimensional polymer chains in a good solvent. *The Journal of chemical physics*, 92(2):1362–1364, 1990.

[WTH+11] Y. Wang, I. Teraoka, F. Hansen, G. Peters, and O. Hassager. Mean span dimensions of ideal polymer chains containing branches and rings. *Macromolecules*, 44(2):403–412, 2011.

[ZDB20] Min Zhang and Guillaume De Bo. A catenane as a mechanical protecting group. *Journal of the American Chemical Society*, 142(11):5029–5033, 2020. PMID: 32131588.

A. Appendix

A.1. The Algorithm

Here, we shall briefly review how the algorithm of the Monte–Carlo simulations has been constructed.

A.1.1. Configurations

First, we fix the parameters of the system. We arbitrarily choose the different numbers of monomers we want to examine to be $N = 16,\ 32,\ 64,\ 128$.

We normalize the monomer diameter $d_s = 1$ and set the thread-length to $l = \sqrt{2}$ which is a convenient choice, since when choosing the step-size $s < \sqrt{2}$ small enough, the ring-polymer cannot cross itself simply by construction. This can be seen in figure A.1; if all three circles touch and the diagonally arranged ones are connected by a maximally stretched thread, i.e. they are at a distance of $\sqrt{2}$, then the minimal step-size necessary for the circle at the upper left corner to pass the two others without causing an overlap is also exactly $\sqrt{2}$. If the maximal step-size is below this threshold, we do not need to worry about special cases where the threads cross but the monomers actually never overlapped and stick to our overlap check. This significantly reduces the computational cost. With the parameters at hand, we can now construct our starting configuration. The exact coordinates of the initial configuration does not matter since we need to let it equilibrate in any case before using any configuration for our analysis. Therefore, for convenience purposes, we choose a circle-like arrangement – circle-like because we are dealing with a discrete set of points of course (the monomers) connected by straight threads, so technically we create something that looks more like a equilateral polygon of degree of the monomer number N.

From there, we repeatedly choose a random monomer in the ring and two random numbers which will become the x- and y-component of our step. The interval from which the random numbers are chosen is chosen such, that the maximal step-size does not exceed $\sqrt{2}$ for the reason described above. Then the monomer is issued to take the random step we just defined. If the configuration after the step is still legitimate, which means the moved monomer does neither overlap with any of the others, nor is it overstretching the thread connecting it to its neighbors, the configuration is accepted and the process is repeated with this new configuration as the starting point.

When every monomer has been attempted to move at least ten times, the configuration is appended to the data. Here it is important to count the *attempts* not the *moves* of the monomers since this would bias the data. The problem with this can be illustrated at a very unlikely crumpled up configuration which will naturally reject many more of

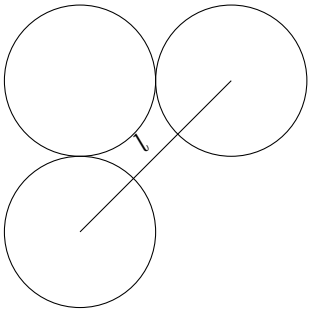

Figure A.1.: In the most extreme case, two neighboring monomers (upper right and lower left circle) are maximally stretched, such that the distance of their centers is $l = \sqrt{2}$. In that case, an intruding monomer (upper left) from a different part of the circle can never cross the line with a step of step-size smaller than $\sqrt{2}$ to reach its complementary place on the lower right. This is made use of to keep computational cost low.

the steps than a typical configuration due to overlap before accepting one and therefore needs more time to relax. However, if we count the moves instead of the attempts, the final data array would leave no trace of this, effectively distorting the amount of time the system spends in such configurations.

To speed up these simulations, it is customary to use Verlet-lists. This is necessary since the algorithms slowest part, the checking whether any monomer overlaps with any other monomer, is of the order of $\mathcal{O}(N^2)$ which is relatively slow. The usage of Verlet-lists can push this down as far as $\mathcal{O}(N^{5/3})$. We will now briefly recapitulate what a Verlet-list is and how it works. As mentioned above the overlap check is what makes the computation expensive since it goes like $\mathcal{O}(N^2)$. The idea is now, that we can reduce the number of checks by only keeping track of the neighbourhood of every monomer. First, one has to decide, how large this neighborhood is going to be. In fact, choosing the most effective size of a neighborhood is not a trivial task. It is hopeless to calculate the efficiencies of differently sized neighborhoods analytically, but usually it is sufficient to employ some trial and error methodology. For each monomer we have to check their neighborhood once in the beginning and store all indices of monomers which lay inside some previously defined circle. If we choose the circle to be larger, we can let the monomers make many steps where we only have to take the monomers inside the circle into account, but there are more monomers inside that circle. An excessive circle-size will lead to including too many of the monomers, in the worst case some number comparable to N itself. In this case, the computation again has a complexity of $\mathcal{O}(N^2)$ and nothing is gained. Choosing the neighborhood to be close gives the benefit, that not many monomers are inside the neighborhood, resulting in few monomers to be checked every time, but forces us to update the lists more often because monomers will soon escape a circle which is too narrow. The updating cost of course is again of the order of $\mathrm{O}(N^2)$ so in this case, nothing has been gained, either. The optimum evidently lays somewhere in the middle. After some trial and error and comparing the computation times for different neighbourhood

sizes, we went with six full step size lengths, such that at least for six Monte Carlo moves, only the monomer-neighborhood has to be checked.

A.1.2. Pole Insertions

After having created the configurations, we need to tend to the throwing of poles. The realization of this is discussed in the following.

There are of course many ways to implement the insertion placing. One could for instance randomize the poles or systematically probe the space in grid-like fashion. that a pole lands inside. Furthermore, we could stick with the same monomer and sample over different orientations of the vector or we sample the same vector from every monomer, that is, effectively rotating the configuration. This is only a valid algorithm, if there is no special monomer in the ring, of course. In our case, all the monomers are equal due to which we resort to this latter method. After having determined the positions of the poles we have to determine, how many of them are on the inside of the circle and how many on the outside.

To do this we have to implement a counting algorithm which works reliably and fast; we used the algorithm described by [PF67]: first we perform a translation to place the pole in the origin. Then, each pair of neighboring monomers is checked for a crossing of one axis, say the y-axis. Then it is investigated whether the sign of the y-component changes between two successive crossings. Such a crossing is labelled *significant*. The part of the ring between two significant crossings of the same axis is referred to as a half-turn. The rest of the ring, i.e. the parts which do not make up half turns, are irrelevant. Every half turn is assigned a value $\pm\frac{1}{2}$, depending on whether it turns clockwise or counterclockwise. The orientation of the turn can be obtained when considering whether the crossing of the y axis has occurred on the upper or lower half plane and whether the x-component changed from $+$ to $-$ or vice versa. After assigning the values to each half-turn we can define the entanglement number q as the sum of all the half-turns' contributions. q can in principle detect multiple windings around a pole and differentiate between clockwise and counterclockwise entanglements. Since we are in two dimensions, our ring can not change orientation by rotating out of the plane along the x- or y-axis. Hence, the entanglement number will always be positive or always negative, depending on the counting direction of the monomers. Furthermore, our ring is self-avoiding which directly forbids the absolute value of the entanglement number to be higher than one; in fact its absolute value will always be either zero or one. In figure A.2 we see a listing of several instructive cases to illustrate the workings of the algorithm.

From assessing for each pole whether it is inside or outside the ring and counting either instance, we first determined the quantities $p_1(\text{in}|\mathbf{r})$ and $p_2(\text{in}|\mathbf{r}, \mathbf{D})$, respectively, before integrating out all but one of the variables. This is mentioned, because one could in principle obtain $p_2(D)$ in one step, sampling over both poles at the same time and averaging, but it is easier to check the plausibility of the code every step of the way instead. These steps are documented in the chapter A.2.

Here shall be briefly acknowledged that it is tempting to simply take a sample of linearly spaced r and ϕ to determine the vector which connects the reference monomer to the

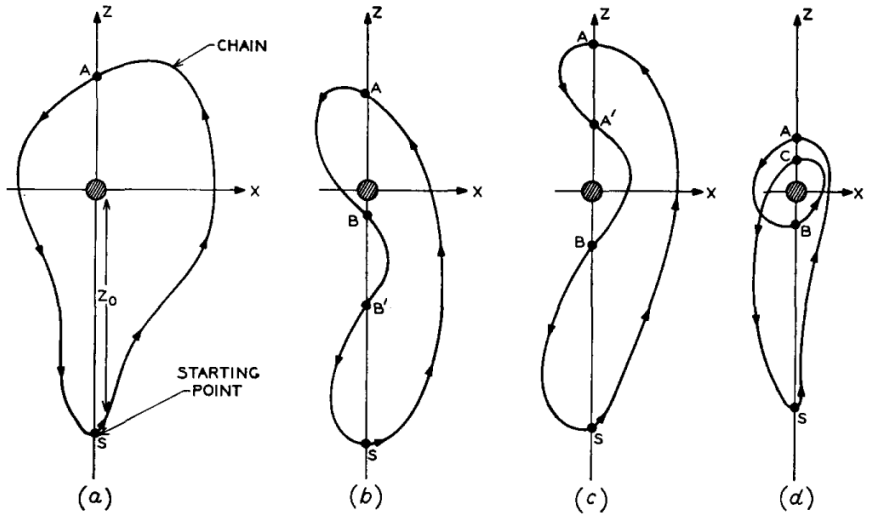

Figure A.2.: a) we see an entanglement with two significant crossings between points s and A, hence the entanglement is detected. In b) the section between the two crossings B and B' lays entirely inside the lower half-plane rendering the crossings insignificant. c) The contributions of the significant crossings between s and A and A' and B cancel each other out since one of them picks up a minus sign for having different orientation. d) Multiple windings are in principle detectable with this algorithm , but are insignificant here because we study a $2d$ self avoiding polymer which may not cross itself (reproduced from [PF67]).

pole $\mathbf{r} = \mathbf{r}(r, \phi)$ and simply loop over the two. However, if we fail to adapt the amount of values of ϕ with varying r, we do not probe space homogeneously which would lead to incorrect results.

After computationally obtaining the probability $p_2(\text{in}|\mathbf{r}, \mathbf{D})$, the variables other than D are integrated out one by one. First, since the system is rotationally invariant, one of the angular variables drops out and we have a vector probability effectively depending on magnitudes r, D and the angle between them ψ. First, ψ is integrated out, by sampling over ψ, determining the probabilities of both poles being on the inside of the ring and averaging over the latter. After that, we integrate over r in similar fashion. In the end we are simply left with $p_2(\text{in}|D)$ which is intimately related to the the central quantity $p_2(D) \coloneqq p_2(D|\text{in})$ of this thesis.

A.2. Sanity Checks

In this section we shall convince ourselves of the correctness of the algorithm by presenting some of the benchmark checks made on the way. We started out with the analytical results and checked the insertion algorithm against them, using a fixed circularly shaped ring monomer instead of the random configurations obtained by the Monte–Carlo method.

We begin by considering one insertion only. For the rigid circle the probability of the pole landing inside should follow relation (3.27). And indeed, as seen in figure A.3, the analytical expression agrees with the result of the simulation.

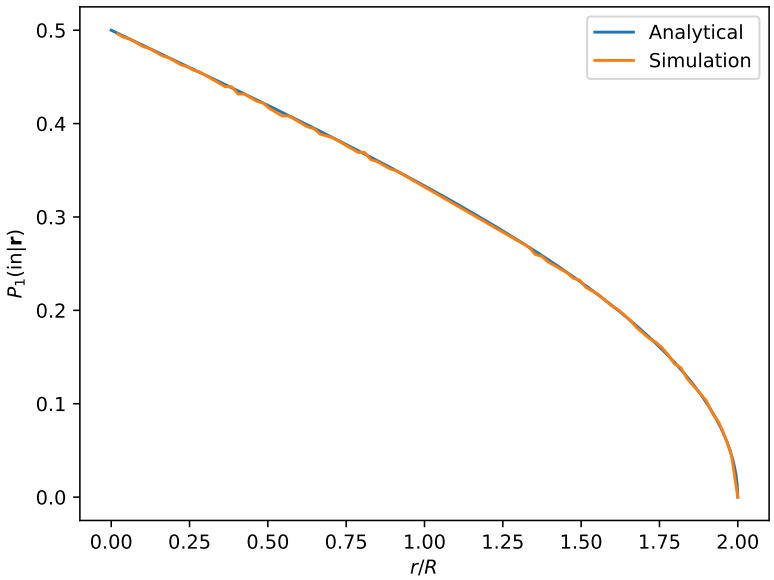

Figure A.3.: Comparison of the analytical calculation of the one-pole probability $p_1(\text{in}|\mathbf{r})$ with the result obtained via the algorithm.

Figure A.4 further shows that the counting algorithm works appropriately. To test the consistency of the one-pole and two-pole theory, we take the limit of $\psi = 0$ which should reduce the two-pole problem to a one-pole problem. Explicitly only considering the norm r of the first vector $\mathbf{r}$ and leaving $D = |\mathbf{D}|$ constant, produces an offset equal to the length of the second vector D. In figure A.4 we see exactly what was expected.

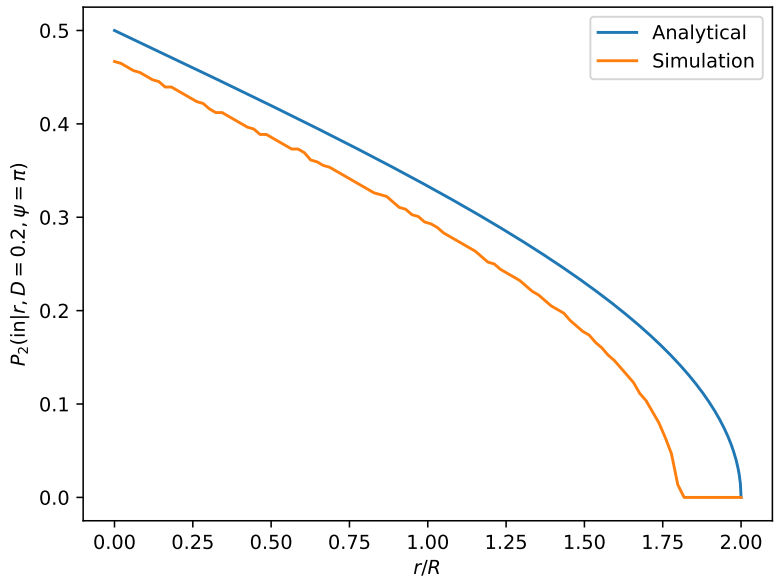

Figure A.4.: Comparison of the analytical one-insertion probability $P_1(\text{in}|\mathbf{r})$ with the two-insertion probability $P_2(\text{in}|\mathbf{r}, \mathbf{D})$ at $\psi = \pi$, both probabilities are for the rigid ring.

In figure 4.6 we see the total probability density obtained from the algorithm along the ψ axis for several fixed values r and D compared with the corresponding analytical results.

It is noteworthy that some of the figures display a certain amount of jaggedness. Especially in subfigure (a) of figure A.5 the deviations from the curve appear to be quite substantial. Of course these errors are due to discretization effects; with a finite amount of monomers where each of them acts as a pivot point for the vectors $\mathbf{r}$ and $\mathbf{D}$, the resolution is limited. We found that for high polymerization numbers the deviations tend to zero.

Digression: Error Estimation

For all practical matters it suffices to know that the deviations are due to discretization and are not due to erroneous sampling, it is insightful to analyze the errors in more depth. There are two candidates of discretization effects which might be responsible for the error. The first which comes to mind would account for the area and shape difference between a

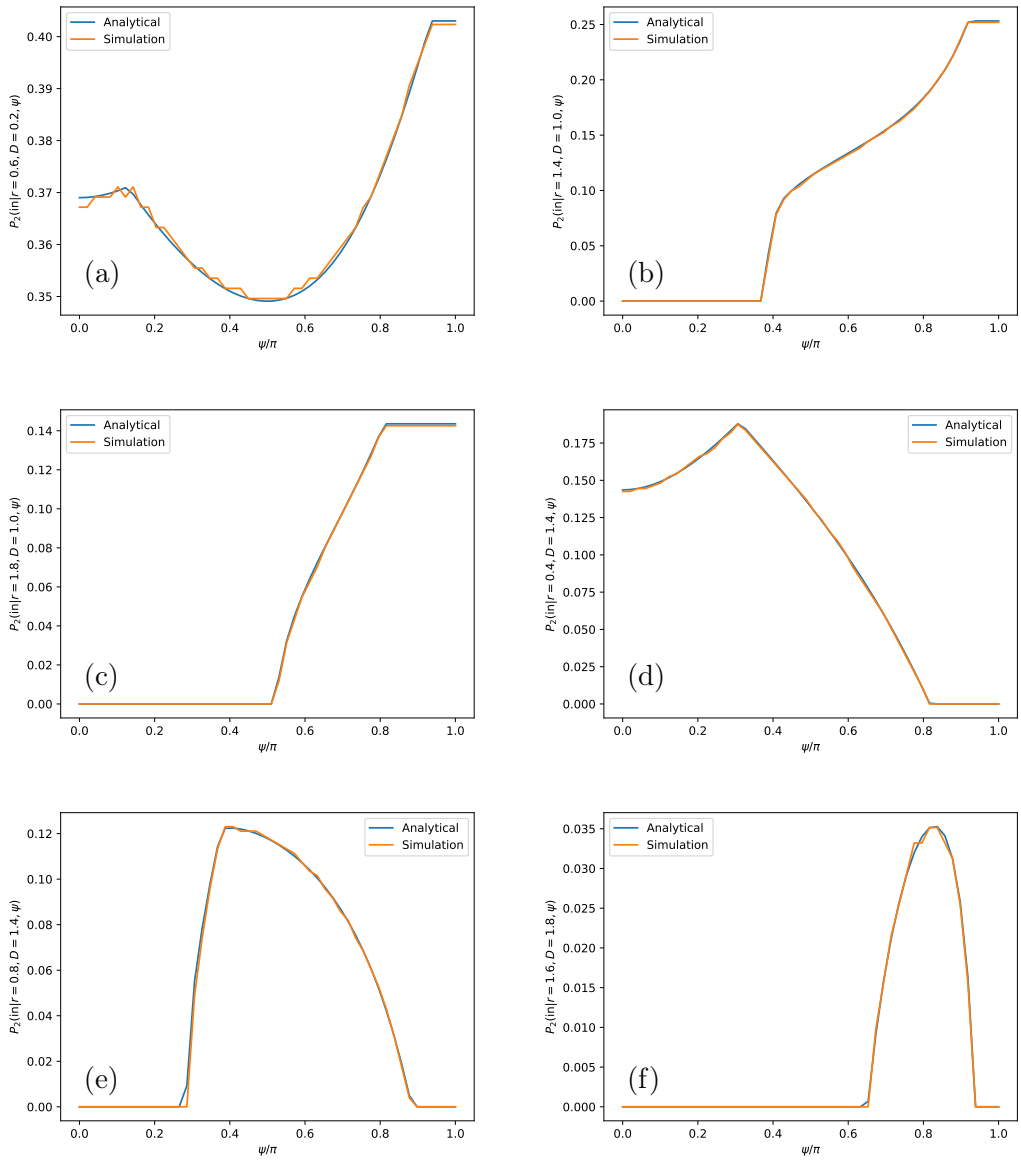

Figure A.5.: Comparing $P_2(\text{in}|r, D, \psi)$ obtained by the algorithm with the analytical results along the ψ-axis for a fixed r and D. The following values have been chosen:
(a): $r = 0.6R$, $D = 0.2R$, (b): $r = 0.6R$, $D = 0.2R$,
(c): $r = 1.8R$, $D = 1.0R$, (d): $r = 0.4R$, $D = 1.4R$
(e): $r = 0.8R$, $D = 1.4R$, (f): $r = 1.6R$, $D = 1.8R$

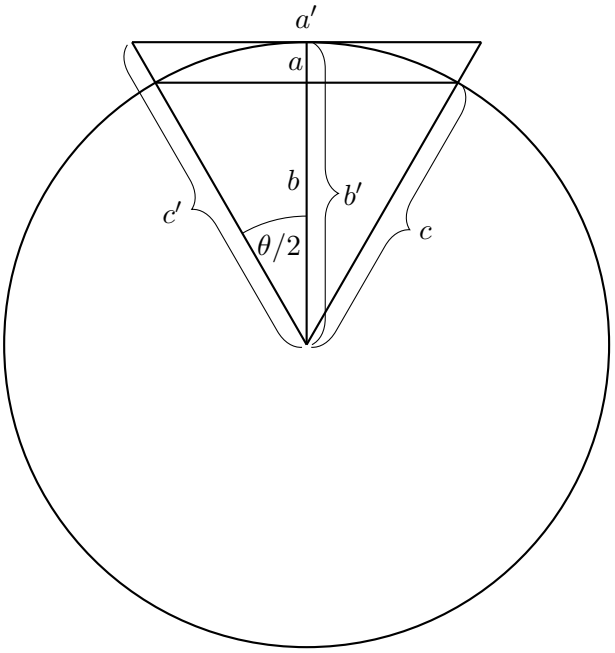

Figure A.6.: A circle with a triangular slice of an inner and outer polygon.

polygon and a circle; it is plausible to think that the straight lines in the polygon are the root cause for jaggedness, even if everything else was smooth. In figure A.6 we see a circle and one slice of the inner and outer equilateral polygons. We denote quantities belonging to the outer polygon with primed letters and the ones corresponding to the inner one with natural symbols. Now´, the area of the circle of course is between the two areas of the polygons.

Now if we assume that the fluctuation of the probability density can be roughly expressed as

$$\Delta p_{in} \sim 1 - \frac{A_{in}}{A_{circ}} \tag{A.1}$$

$$\Delta p_{out} \sim 1 - \frac{A_{circ}}{A_{out}}, \tag{A.2}$$

and from assuming that

$$\Delta p_{in} \sim \Delta p_{out} \tag{A.3}$$

follows

$$\Delta p \sim \left(1 - \frac{A_{in}}{A_{out}}\right) \tag{A.4}$$

where A_{in}, A_{out} and A_{circ} denote the areas of the inner and outer polygon and the circle, respectively. From figure A.6 we see that

$$\frac{A_{in}}{A_{out}} = \frac{a}{a'}\frac{c}{c'} = \cos^2\frac{\pi}{N} \tag{A.5}$$

and hence finally we get

$$\Delta p \sim 1 - \cos^2 \frac{\pi}{N}. \tag{A.6}$$

Equation (A.6) gives for polymerization number $N = 128$ that $\Delta p \sim 0.06\%$, however the observed deviations are of the order $\Delta p_obs \sim 0.5\%$. There is roughly an order of magnitude between the two values and we conclude that the above described effect can therefore not be the root cause of the observed deviations.

A second discretization error comes with the finite precision when determining how many instances of the vectors $\mathbf{r}$ and $\mathbf{r} + \mathbf{D}$ land inside. It is easier to think about this in terms of a rotational angle. Namely, it is equivalent changing the pivot points (monomers) of a constant vector and staying on the same pivot but rotating the vector. For N monomers the increments of the rotational angle θ of the total vector $\mathbf{r} + \mathbf{D}$ are $\Delta\theta = \frac{2\pi}{N}$. This defines a length scale $d = \sin\frac{\theta}{2}|\mathbf{r} + \mathbf{D}|$ which poses a limit to our resolution. That means, if we were probing not a circle but a complicated fractal structure, we would not be able to resolve the smaller length scales. The hypothesis is that for small changes in ψ which only varies the length of the vector $\mathbf{r} + \mathbf{D}$ marginally, the algorithm does not detect a change; it counts the same amount of throws to be inside and outside. As an example we take the simplest case of the two pole system,namely $\psi = 0$ where the problem is reduced to a one-pole problem. At $\psi = 0$ we know the probability of the pole landing inside according to equation (3.27). Performing the variation in ψ we obtain

$$\Delta p = \frac{1}{\pi}\Delta \arccos \frac{|\mathbf{r} + \mathbf{D}|}{2R} \tag{A.7}$$

$$\sim \Delta|\mathbf{r} + \mathbf{D}|, \tag{A.8}$$

where around $\psi = 0$ we can write

$$\Delta|\mathbf{r} + \mathbf{D}| = |\mathbf{r} + \mathbf{D}||_{\psi=\Delta\psi} \approx D + r - \frac{Dr}{2(D + r)}\Delta\psi^2 \tag{A.9}$$

and hence

$$\Delta p \sim \Delta\psi^2. \tag{A.10}$$

Since out probability change is for small changes proportional to the arclength of the inside portion of the pole-throwing circle with radius $|\mathbf{r} + \mathbf{D}|$ and center on our pivot point, we write $\Delta p \sim \Delta s$. By comparing the two length scales Δs and d, we get

$$\Delta s \sim d \tag{A.11}$$

$$\Delta\psi^2 \sim \sin\frac{\theta}{2} \tag{A.12}$$

$$\Delta\psi \sim \frac{1}{\sqrt{N}}, \tag{A.13}$$

where we used that $\frac{\theta}{2} = \frac{\pi}{N}$. Relation (A.11) tells us, that the true, analytical change in probability, becomes notable only if it changes the inside portion of the pole-throwing circle by an amount that is comparable to our resolution length scale d. So, for example,

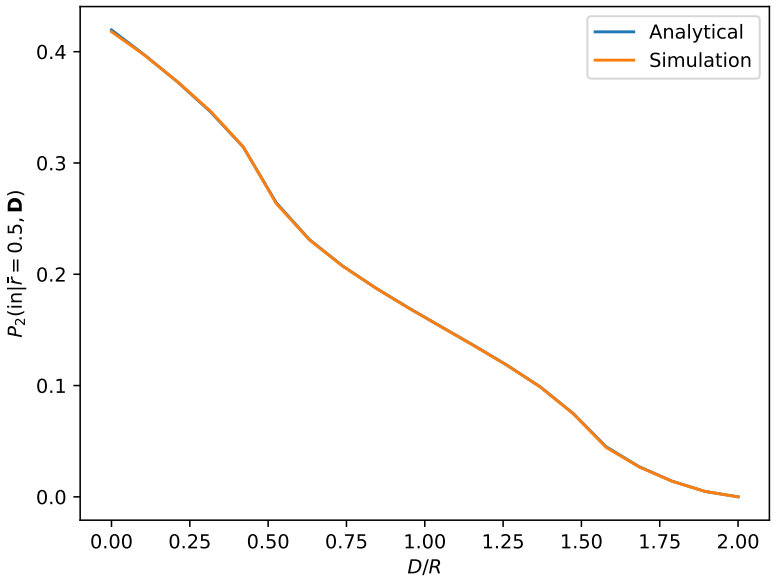

Figure A.7.: Vector probability $P_2(\text{in}|r, \mathbf{D})$ for fixed r. It has been integrated over ψ, therefore r is not denoted in bold face.

choosing $N = 100$ $\Delta\psi \sim \frac{1}{10} \sim \frac{\pi}{30}$. Therefore, if we divide the interval $[0, \pi]$ over which we evaluate ψ, then the evaluation of the probability density can be constant for an amount of subsequent values of the order $\mathcal{O}(3)$. This is comparable to the length of the intervals of constant value when we take $N = 100$, where 3-15 steps are the same. Of course this is an extraordinarily coarse analysis, but since it seems to roughly reproduce our observations, we shall be content with our result. **End of digression**

The above figures A.5 show that the first steps, throwing the poles and assessing whether they are inside the ring or outside, reproduces the analytical results in the zero temperature limit, that is the rigid ring. To obtain the desired quantity $p_2(D|\text{in})$, we have to perform several consecutive integrations correctly. In similar fashion as above, we compared the analytical integrations to the counting algorithms which approximate those integrations. Figure A.7 shows the results of the analytical integration over ψ and its algorithmic approximation. As we can see, the two curves overlap exactly, which further legitimizes the method at hand. Lastly, the integration over r has been carried out and again, the exact calculations are juxtaposed to the numerical method.

In figure A.8 we see the results. The analytically obtained curve is covered up by the numerical result, proving excellent correspondence. In the last check we perform the same integration as before but also include the Jacobi element D. It takes into account that a greater distance between two poles are favoured by geometry, similarly to what was already discussed in section 3.3. The set of all points which are at some equal distance

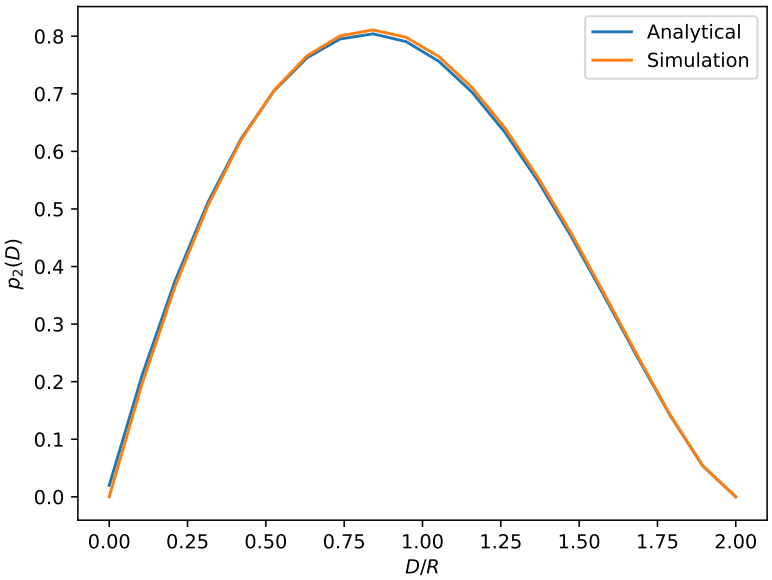

Figure A.8.: Comparison of the density $p_2(D)$ of the distance, once calculated analytically and once with the algorithm.

away from some central point resemble a circle. Since the circumference of a circle scales with its radius, the probability of landing a pole further away from the reference point increases with distance.

A.3. Further Results

In the following we present the lower N results for the corrected density approach. As one can clearly see, the model works still very well for $N = 64$, loses some of its precision for $N = 32$ and is not very good for $N = 16$.

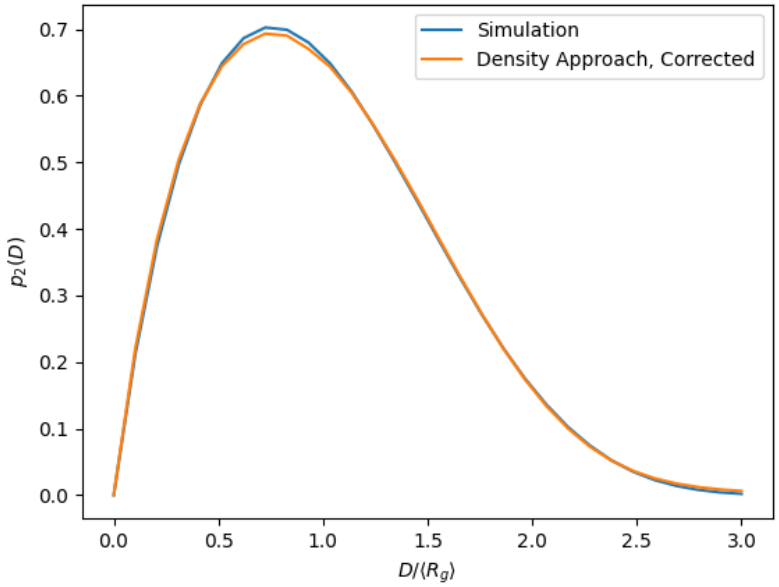

Figure A.9.: Corrected density approach for $N = 64$.

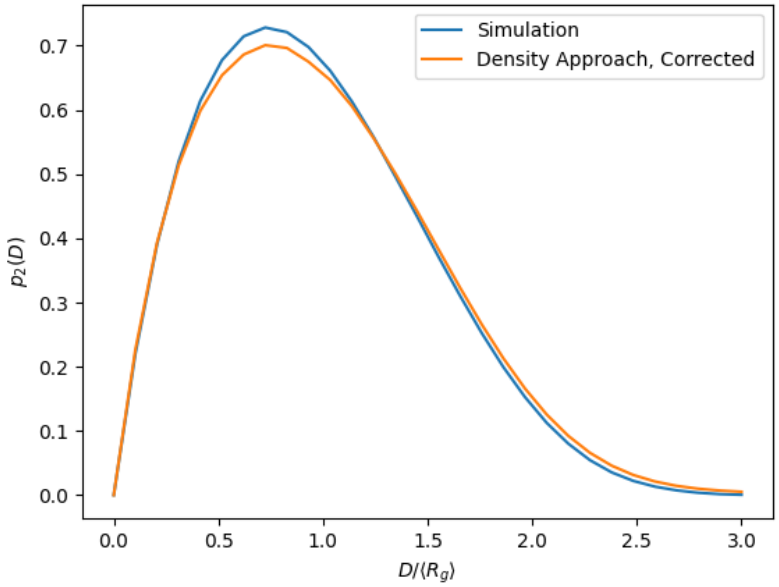

Figure A.10.: Corrected density approach for $N = 32$.

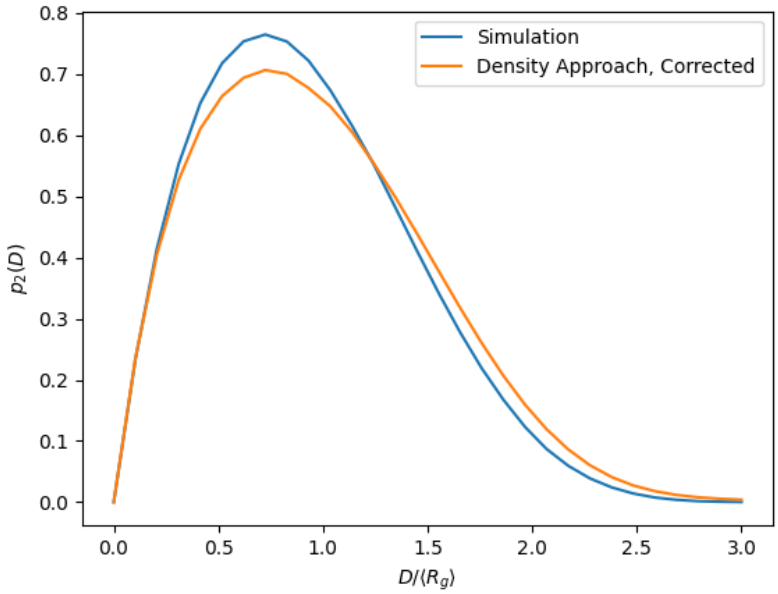

Figure A.11.: Corrected density approach for $N = 16$.